3-3-2020

Power Efficiency Enhancement and Linearization Techniques for Power Amplifiers in Wireless Communications

Haider Al-kanan
Portland State University

Recommended Citation

Power Efficiency Enhancement and Linearization Techniques for

Power Amplifiers in Wireless Communications

by

Haider Al-kanan

A dissertation submitted in partial fulfillment of the
requirements for the degree of

Doctor of Philosophy
in
Electrical and Computer Engineering

Dissertation Committee:
Fu Li, Chair
Xiaoyu Song
James Morris
Dacian Daescu

Portland State University
2020

Abstract

Wireless communication systems require Power Amplifiers (PAs) for signal transmissions. The trade-off between power efficiency and nonlinear distortion in PAs degrades the communication performance. Thus, power efficiency and nonlinearity are two main concerns of operating PAs in communication systems. Nonlinear behavioral models are typically used to quantify and mitigate the distortion effects of PAs on communication systems. This dissertation presents an estimation approach for modeling and linearizing the PA Amplitude-to-Amplitude (AM/AM) nonlinearity using the design specifications of PAs, such as gain, the third-order intercept point, and 1dB compression point. Furthermore, an enhanced approach for modeling solid-state power amplifiers is developed by modifying the Saleh empirical model.

The Envelope Tracking (ET) technique for PAs has been a popular power efficiency enhancement in modern cellular systems. However, the time-varying effects of the supply voltage impacts the PA linearity. Therefore, an accurate behavioral model for PA with ET has become an important research effort to characterize the effect of dynamic supply voltage on both the amplitude and phase nonlinearities. Furthermore, the empirical models of ET PAs are widely used to improve PAs linearity by using Digital Predistortion (DPD).

This dissertation develops an extended modeling approaches to characterize the AM/AM and Amplitude-to-Phase (AM/PM) conversions as well as account for the impact of the time-varying supply voltage on the ET PAs.

Memory effects, due to energy storage elements (e.g. capacitors and inductors) in ET PA circuits in addition to the temperature variation of integrated circuit, are modeled

using digital filters (finite impulse-response filters) in series with the static AM/AM and static AM/PM nonlinearities. A least-squares approach is mathematically derived for estimating the model coefficients of ET PAs.

The model identification of many coefficients requires high computational cost in Float Point Operations (FLOP$_S$), such as multipliers and adders. In addition, the computational cost in FLOPs of a complex number is equivalent to (2-6) times the cost of real numbers. The estimation complexity of the ET PAs model in this work requires around half the number of FLOP$_S$ compared to the state-of-the-art behavioral models. This is because the modeling approach in this work consists of real coefficients and a lower number of model parameters.

A DPD model is derived in this dissertation to compensate for both the AM/AM and AM/PM nonlinear distortions in ET PAs. A dual-input single-output function architecture is calculated for the DPD model to compensate for the nonlinearities in the AM/AM and AM/PM conversions contributed by the time-varying supply voltage in the ET system. Both the proposed AM/AM and AM/PM DPD models exhibit lower numbers of coefficients, which result in reduction of the identification complexity compared to the state-of-the-art DPD models. The proposed behavioral models of the ET PA and DPD are both evaluated in the time and frequency domains, as well as compared to the state-of-the-art models in terms of model accuracy and estimation complexity.

Acknowledgments

I would like to express my deepest gratitude to all the professors and classmates at Portland State University, who supported me during the entire study of pursing the PhD degree. I must admit that I would not have overcome the challenges without their support.

First of all, I would like to acknowledge the support of my advisor Prof. Fu Li for introducing me to the research field of communications, in addition to his guidance and the time of a regular meetings, valuable comments, and advice.

I am grateful to Prof. James Morris for reviewing parts of my dissertation. I also would like to extend my thanks to Prof. Xiaoyu Song and Prof. Dacian Daescu for serving on my committee and their valuable feedback.

Thanks to my fellow graduate students, Xianzhen Yang and Siyuan Yan, for their support and helping on the experimental set-up in the VIP Tektronix laboratory. I appreciate all members of our research group for the discussion and feedback. Thanks to the staff of writing center and library at Portland State University for the beneficial resources of improving this dissertation writing.

Finally, I would like to express deep appreciation and thanks to my parents, my wife Sarah, and my children, Rawan, Ayman, and Razan, for their encouragement and support during the entire study period.

Table of Contents

List of Tables

List of Figures

List of Abbreviations

ACEPR	adjacent-channel error power ratio
ACPR	adjacent-channel power ratio
ADS	advanced design system
AM/AM	amplitude-to-amplitude
AM/PM	amplitude-to-phase
AWG	arbitrary waveform generator
BM	binomial model
DISO	dual-input‑single-output
DPD	digital predistortion
DSP	digital signal processing
DUT	device under test
EM	envelope modulator
ET	envelope tracking
FIR	finite impulse response
FLOP	float point operation
IC	integrated circuit
IIR	infinite impulse response
IMD	intermodulation distortion
IP$_3$	third-order intercept point
I‑Q	in-phase-quadrature
LS	least-squares
LTI	linear time-invariant
LTE	long-term evolution
LUT	look-up-table
MBM	memory binomial model
MPM	memory polynomial model
MSE	mean squares errors
NMSE	normalized mean-square error

OFDM	orthogonal frequency-division multiplexing
PA	power amplifier
P_{1dB}	1dB compression point
PAPR	peak to average power ratio
PDF	probability density function
PSD	power spectral density
QAM	quadrature amplitude modulation
RF	radio-frequency
SISO	single-input single-output
SNR	signal-to-noise ratio
SSPA	solid-state power amplifier
TWTA	travelling-wave tube amplifier
VSG	vector signal generator
WCDMA	wideband code-division multiple access

Chapter 1

Introduction

1.1 Motivation

Improving power and spectral efficiencies in communication systems has become a major research effort to perform a reliable signal transmission. The application demand of high data-rate and multi-media transmissions in modern transceiver systems requires selecting components of energy-efficient and high linearity devices.

High linearity devices are extremely desirable in broadband communications because nonlinear distortion can degrade the overall spectral efficiency. Mixers and Power Amplifiers (PAs) are two major nonlinear devices in typical communication systems. This dissertation focuses specifically on power efficiency and linearity of PAs in communication systems because PAs exhibit more impact on signals transmission. In addition, PAs are one of the most power-hungry components in transceiver systems, which are required to amplify bandpass wireless signals as shown in Figure 1.1.
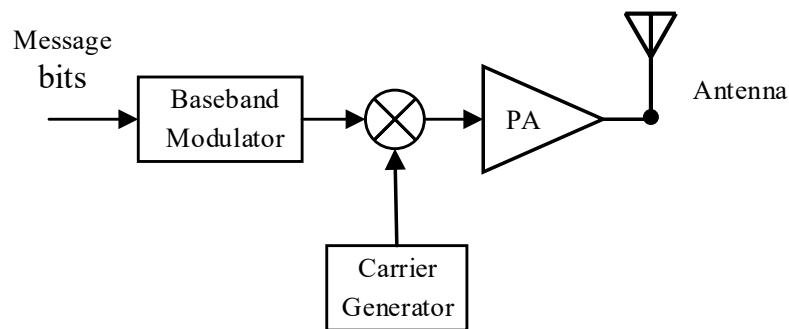
Figure 1.1 Simplified block diagram of wireless transmitter.

Low power efficiency and nonlinear distortion are the two common design challenges in PAs for wireless communications. Stand-alone linear PAs typically exhibit lower power efficiency due to the high-power dissipation in the circuit elements. For instance, the maximum power efficiency for a class-A RF PA is around 40%, which represents around 60% of the PA output power dissipated as heat. In addition, low power efficiency in PAs can degrade battery life in cellular hand-sets and minimize the transmitted power via the integrated circuit chip due to high heat dissipation [1]-[3]. Nonlinear distortion in RF PAs is another common problem that can significantly degrade signal-to-noise ratio, bit-error rate, and adjacent channel interferences in multi-band communication, due to both in-band and out-of-band spectral distortions [4]-[7].

Stand-alone RF PAs normally operate at maximum power efficiency in nonlinear regions when driven near the 1dB compression point [8]. The trade-off between power efficiency and linearity motivated researchers to develop several signal techniques for controlling the trade-off to improve the operational performance of PAs. The evolution of modern wireless signals makes the trade-off between power efficiency and linearity more complicated because of large amplitude fluctuations in modern modulation schemes. For example, operating PAs on signals of high Peak-to-Average Power Ratio (PAPR) can increase the trade-off challenges compared to the PA operation on small signals. In fact, the high dynamic amplitude range of the PA input signals (e.g. about 8 dB PAPR in Long-Term Evolution (LTE) downlink signals) causes a large fluctuation on Amplitude-to-Amplitude (AM/AM) conversion and dynamic transition between linear region and compression region (i.e. nonlinear region) [9]-[11].

The Envelope Tracking (ET) technique has become a very popular method for improving the power efficiency in modern wireless communications. The ET technique exhibits important advantages compared to the traditional efficiency enhancement techniques for PAs, such as Doherty and out-phasing approaches, which often exhibit limitations in bandwidth as well as challenges in efficient design of RF matching components and effect of load impedance [12]-[14].

Different ET systems have been developed over past decades to overcome the design challenges of high bandwidth and high PAPR on PAs in cellular wireless transmitters. The dynamic supply voltage in ET systems exhibits a significant impact on both the design characteristics and nonlinearity of RF PAs [15]-[16]. Therefore, various techniques have been developed in the literature of ET modeling to characterize the dynamic effect of the supply voltage on the PA nonlinearities. Empirical models are simplified approaches compared to circuit models for characterizing the hysteresis effects and nonlinear distortion in ET PAs [17]-[19]. PA empirical models can simplify modeling Digital Predistortions (DPDs) for efficiently mitigating the dynamic nonlinear distortion. For instance, Taylor and Volterra series are popular and accurate models for PAs and DPDs [20]-[23]. The drawbacks of high number of coefficients and high computational cost are extensively discussed in the state-of-the-art PA modeling.

This dissertation introduces empirical approaches for modeling both constant-supply PAs and ET PAs. The AM/AM behavioral model for a constant-supply voltage is calculated from the PA design parameters such as gain, IP_3, and the 1dB compression point. In addition, an extension of the Saleh behavioral model is developed for ET PAs to

characterize both amplitude and phase nonlinearities due to time-varying amplitude of the PA input signal.

The ET PA model can characterize the effect of the dynamic supply voltages on both amplitude and phase conversions. The memory effect due to the variation in the temperature of Integrated Circuit (IC) and energy storage elements in ET PA circuits (e.g. capacitors and inductors) have been an important aspect in wideband and multiband communications. Hence an approach of characterizing the impact of memory distortion on ET PA are presented in this work. An approach of linearizing ET PAs is introduced for mitigating the nonlinear distortion in both amplitude and phase of the PA output signal.

1.2 Dissertation Organization

This dissertation presents several modeling techniques for constant-supply PAs and ET PAs. In addition, linearization techniques using DPD are developed to improve the PA operational performance. Hence, this dissertation is organized as follows:

Chapter 1 begins with the research motivation for power efficiency and linearity challenges in communication systems. It is followed by research questions, the main contributions, and dissertation organization. Then, an overview of LTE statistical characteristics is demonstrated as a popular type of modern wireless signals to evaluate the power efficiency for typical PAs.

Chapter 2 describes the physical causes and effects of PA nonlinear distortion. It also demonstrates the distortion types in PAs, such as AM/AM distortion, AM/PM distortion, and memory effects. The AM/AM and AM/PM conversions in PAs are

represented using the state-of-the art mathematical models. An approach for estimating the AM/AM nonlinear distortion in PAs is calculated using the Saleh empirical function, based on PA manufacturing parameters, such as gain, IP_3, and the 1dB compression point.

Chapter 3 presents the ET technique for power efficiency enhancement in PAs. This include simulation results of different shaping functions. The ET system structure and effects of each design component is described for the required modeling task in the next chapter.

Chapter 4 begins with an overview of the behavioral modeling approach comparison with circuit models. Two different ET PA modeling approaches using single-input single-output and dual-input single-output are discussed, this examination is followed by examples of popular state-of-the-art behavioral modeling. Two behavioral modeling techniques are proposed in this chapter based on the Hammerstein theory and a new extension of the Saleh model. Model evaluations in both the time and the frequency domains are presented.

Chapter 5 presents a new linearization technique for constant-supply PAs using a DPD model, which is derived from the Saleh behavioral model. In addition, this chapter describes novel linearization techniques for the ET PAs using DPD. These linearization techniques consist of two independent functions: one model for mitigating the AM/AM distortion and another model for linearizing the AM/PM conversion. In addition, DPD model evaluation approaches are presented. Chapter 6 summarizes the dissertation's conclusions, list of publications, and future work.

1.3 Research Questions

The ongoing development of high-speed DSP systems facilitates signal processing techniques for improving the power efficiency and linearity of PA circuit. PA circuits are subject to design challenges of high-power efficiency and high linearity implementation, as were discussed in the introduction. This dissertation focuses on employing signal techniques to improve power efficiency using ET system and system level DPD model to improve the PA linearity.

Modeling of constant-supply and ET PAs as well as DPDs have gained significant interest in contemporary development of high efficiency and linearity wireless systems. This dissertation addresses the following important challenges:

1. How is the AM/AM nonlinear distortion modeled in PAs using the design manufacturing parameters such as gain, IP_3, and P_{1dB} ?

2. How is the AM/AM nonlinear distortion modeled in ET PA using a simple approach?

3. How is the AM/PM nonlinear distortion modeled in ET PA using a simple approach?

4. How are the long-term memory effects (i.e nonlinear dispersion) in both the AM/AM and AM/PM conversions are accurately modeled?

5. How can AM/AM nonlinear distortion in the ET PA be mitigated?

6. How can AM/PM nonlinear distortion in ET PA be mitigated?

7. How can the dynamic variation of the supply voltage in ET PAs and linearization techniques be accurately modeled?

1.4 Contributions

The key contributions in this dissertation are summarized as follows:

1. An estimation approach was calculated for the Saleh empirical model using the third-order intercept point (IP_3) and 1dB compression point [24], [25].

2. Model modification was developed to enhance the accuracy of the Saleh model for solid-state PAs.

3. An extended modeling approach was derived for the static AM/AM nonlinearity in ET PAs.

   The original Saleh AM/AM model is an empirical formula, which characterizes the nonlinearity for constant-supply PAs as a function of the signal input amplitude. In this dissertation, an extension of the Saleh AM/AM function was presented to model the ET dynamic supply voltage. The proposed Saleh extension increases the modeling accuracy, and quantifies the nonlinear distortion due to both the input signal and supply voltage [26].

4. A technique of extending the Saleh AM/PM function was developed.

   This work presents an extension to the static Saleh AM/PM function by including the effects of the phase variation caused by the supply voltage. The proposed model extension converts the behavioral modeling structure from Single-Input Single Output (SISO) to Dual-Input Single Output (DISO). An improvement in model accuracy was obtained by using this extension [27].

5. The dynamic modeling approach of the AM/PM conversion for long-term memory effects (i.e. dispersion effects) was calculated in this work.

Hysteresis effects in the AM/PM conversion are modeled using a simple digital filter, which is cascaded with the static AM/PM model. The digital filter is used to model hysteresis effects in the AM/PM conversion as a result of the energy-storage elements that cause different time-delays in the input signal [27].

6. A modeling approach for the AM/AM DPD in ET PA was developed.

Digital predistortion is an efficient approach for linearizing ET PAs. Thus, this dissertation presents a DISO function. The DISO function is calculated to compensate for the dynamic variation in the AM/AM nonlinearity due to the time-varying supply voltage [27].

7. Finally, this dissertation illustrates AM/PM DPD for the ET PA:

The AM/PM DPD function is typically used to compensate for the AM/PM distortion in an ET PA. We derived this model by inverting the PA phase function. In this approach, the proposed DPD model implements a $\mp 180^\circ$ phase shift to the PA phase to obtain a theoretical linear phase conversion from the combined DPD and PA model. The ET PA supply voltage is included in the DPD model to compensate for the output transistor drain/collector phase distortion [27].

1.5   Power Efficiency Characterization

Power efficiency is an important metric in the design of reliable wireless communications and calculating a link power budget. Power efficiency is defined as a ratio of the average output power delivered to the load and the DC power supplied to the PA [8] as:

$$\eta \% = \frac{\text{PA output power}}{\text{DC power delivered to PA}} * 100 \qquad (1.1)$$

In this equation, η is the percentage power efficiency. The DC power delivered to the PA (denominator of Equation 1.1) depends on conduction angle of the PA output transistor's drain/collector current flow from the power supply. In fact, the conduction angle is controlled by the DC bias voltage on the output transistor gate/base and specifies the operating class of the PA. For instance, class-A model assumes a 360° conduction angle, which corresponds to a theoretical maximum power efficiency of 50%. In a complementary-symmetry class-B operating mode, the conduction angle is 180°, which means the drain/collector current flows during the half cycle of the PA input signal (i.e complementary symmetry consists of two transistors) with around 78% maximum power efficiency. Therefore, the power efficiency depends on the PA circuit design and DC biasing conditions [1], [8]. Under these conditions, optimal power efficiency can be obtained when operating PAs in small amplitude signals. On the other hand, the biasing condition and conduction angle of the PA are dynamic and difficult to control when operating PAs at a high PAPR, because the transistor's gate/base is affected by the amplitude of the input signal [8].

Modern wireless signals (e.g. using Orthogonal Frequency Division Multiplexing (OFDM) modulation scheme) exhibit high variation in amplitude and phase [9], [11]. This variation has impact on the instantaneous power efficiency. For example, a time series power of the LTE (i.e. LTE_downlink uses OFDM modulation) signal in Figure 1.2 illustrates that the average power is 7.40 mw whereas the peak power is 29 mw.
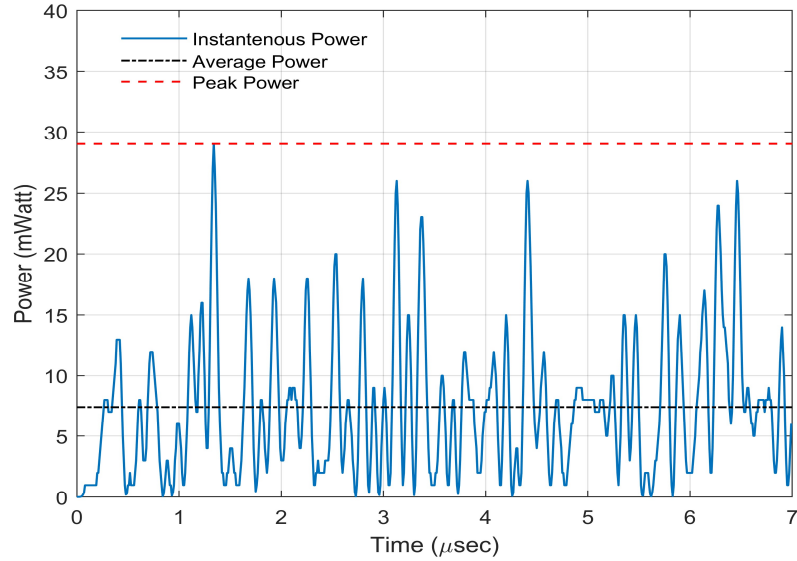
Figure 1.2 Power dynamic range of the LTE_downlink signal.

Thus, a power variation of about 21.6 mw is a significant variation in the power efficiency according to Equation 1.1. The instantaneous power in communications is a random quantity, which is statistically described by the Probability Density Function (PDF) [28]. Therefore, this causes the power efficiency to be a non-deterministic function because of signal-dependency.

The average power efficiency (as shown in Equation 1.2) is introduced in the literature as an adequate metric especially when operating PAs on signals of different PAPR (i.e. wide-range PDF).

$$\eta_{ave} = \frac{\mathrm{E}\left[P_{out}\right]}{\mathrm{E}\left[P_{DC}\right]} \qquad (1.2)$$

where η_{ave} is the average power efficiency, $\mathrm{E}[.]$ is the expected value, P_{out} is the output power, and P_{DC} is the DC power delivered to the load. The expected value "$\mathrm{E}[.]$" in

Equation 1.2 can be re-expressed using a mathematical integral over the PDF as illustrated in Equation 1.3.

$$\eta_{ave} = \frac{\displaystyle\int_0^{P_{out,max}} P_{out} f(P_{out}) dP_{out}}{\displaystyle\int_0^{P_{DC,max}} P_{DC} f(P_{out}) dP_{DC}} \tag{1.3}$$

where $f(.)$ is the PDF of the PA output signal. The PDF has a dominant effect on the average power efficiency in PAs. In fact, the PDF is a complicated random function in communication signals. Thus, an important parameter was introduced in the literature to account for the signal PDF characteristics by using the PAPR as shown below:

$$PAPR = \frac{max\left[P_{out}\right]}{E\left[P_{out}\right]} \tag{1.4}$$

where max $[P_{out}]$ is the peak output power. Substituting Equation 1.4 into Equation 1.2, results in the following:

$$\eta_{ave} = \frac{max[P_{out}]}{PAPR \times E[P_{DC}]} \tag{1.5}$$

Equation 1.5 illustrates an inversely proportional relationship between the power efficiency and PAPR. Figure 1.3 shows a histogram $f(P_{out})$ of the LTE_downlink signal and the instantaneous power efficiency (η) for a class-A PA. This indicates a low-power efficiency corresponding to the low signal amplitude, and high-power efficiency corresponding to the peak signal amplitude. Similarly, the power efficiency at average power is lower than the power efficiency at peak power. Therefore, operating PAs at high PAPR signals can

degrade gradually the average power efficiency, such as a common challenge in designing

high power efficiency PAs in OFDM signals [29].
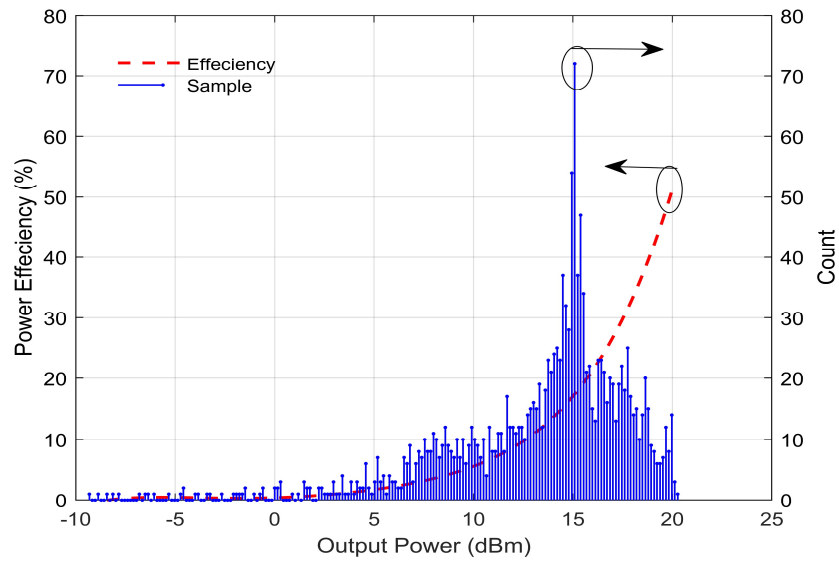
Figure 1.3 Histogram of LTE_downlink signal and power efficiency characteristics of a class-A
PA.

2.1   Overview

Nonlinear distortion in PAs is an ongoing design challenge in communication systems. Nonlinear distortion in PAs affects the reliability of data transmission and increases the chance of inter-symbol interference. In addition, the effects of PA distortion increase bit-error-rate and degrades signal-to-noise ratio on communication receiver [30]. This chapter describes and analyzes the main causes of nonlinearity and distortion effects on communication systems. PA distortions stem from different design aspects, such as:

1) Physical design topology (e.g. class-A, class-C, and class-D).

2) Circuit parasitic effects (e.g. mutual inductance, capacitance, and resistance).

3) Energy storage elements (e.g. charging and discharging of capacitors and inductors).

4) Nonlinear elements in transistors' junctions (e.g. PNP and NPN junctions).

Classifying and simplifying nonlinear distortion in PAs have become important tasks for supporting the developer implementing efficient empirical models and DPD of PAs.

Modeling techniques using circuit theory analysis have been used in the past. However, circuit approaches for modeling ET PAs are complicated due to the circuit complexity, as well as the challenges of quantifying the parasitic effects in circuit elements, such as electrical and magnetic coupling [31].

A signal modeling approach is used to simplify the modeling complexity. Hence, this work adopts a signal modeling approach for simplicity and flexibility of characterizing and analyzing different distortion effects in RF PAs. Various signal processing approaches have been developed in the modeling literature to quantify the distortion effects of PAs, but these models are classified into three main categories: memoryless or static, quasi-static, and memory models, as described in the next sections.

2.2   Static Amplitude-to-Amplitude Distortion

Static AM/AM distortion refers to the variation in the signal amplitude with respect to the instantaneous input amplitude of the PA. In other words, PAs typically output different scaled versions of the input amplitude, because of nonlinear gain with respect to the input amplitude. Memoryless models are often sufficient to characterize the static AM/AM conversion of the PA. Distortion effects due to the static AM/AM nonlinearity can be easily observed in the frequency domain (i.e. Intermodulation Distortion (IMD)) when the PA is excited by a two-tone signal [32], [33]. The static AM/AM distortion in the time domain results in signal smearing and clipping effects, as demonstrated in the simplified Figure 2.1.

The AM/AM conversion causes relatively high distortion effects compared to the other types of nonlinear distortions. In particular, odd-order IMDs exhibit higher impacts on baseband signals, and require sharp filtering techniques to eliminate this IMD.
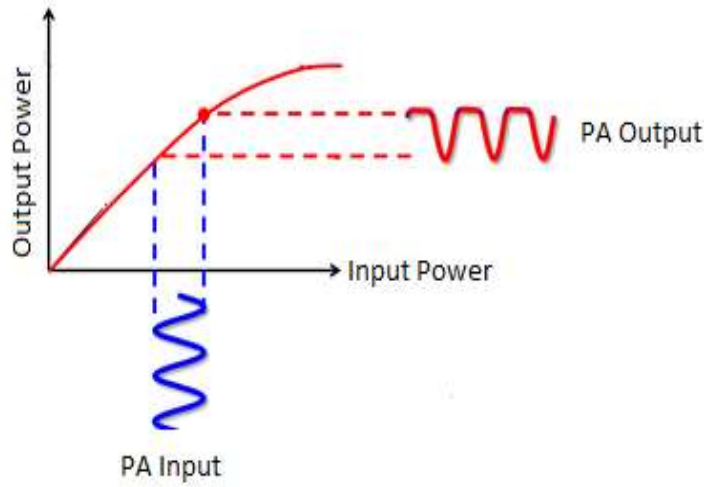
Figure 2.1 Effect of PA gain compression on signal envelope shape.

2.2.1 Taylor Model

The Taylor model is a popular empirical model for memoryless/static AM/AM conversion in PAs as in Equation 2.1. The Taylor coefficients are normally estimated using a least-squares method, or calculated directly from the specification parameters of the PA such as gain, intercept points, and 1dB compression points [34], [35]. The high orders of the Taylor model are often required in PA for optimal model accuracy, which is one of the model drawbacks. Thus, a low-order truncated Taylor model is commonly adopted to simplify the model complexity as follows:

$$v_o(t) = f(v_i(t)) = \sum_{n=1}^{N} c_n v_i^n(t) \tag{2.1}$$

where $v_i(t)$ is the input signal, $v_o(t)$ is the output signal, c_n are the Taylor coefficients (real numbers for the AM/AM model), and N is the Taylor truncated order. The Taylor nonlinear order N specifies the number of the modeled IMD in the PA.

A two-tone test is an experimental approach widely used to measure the AM/AM nonlinearity of the PA in the frequency domain, as illustrated below:

$$v_i(t) = A(\cos \omega_1 t + \cos \omega_2 t) \tag{2.2}$$

where A is the signal amplitude, ω_1 and ω_2 are the angular frequencies. Substituting Equation 2.2 into Equation 2.1, we obtain:

$$v_o(t) = c_1 A(\cos \omega_1 t + \cos \omega_2 t) + c_2 A^2 (\cos \omega_1 t + \cos \omega_2 t)^2 + c_3 A^3 (\cos \omega_1 t + \cos \omega_2 t)^3 + \ldots\ldots +$$
$$c_N A^N (\cos \omega_1 t + \cos \omega_2 t)^N \tag{2.3}$$

Equation 2.3 can be simplified using trigonometric identities to result in:

$$v_o(t) = c_2 A^2 + c_2 A^2 \cos(\omega_1 - \omega_2)t + (c_1 A + \frac{9}{4} c_3 A^3)\cos \omega_1 t + (c_1 A + \frac{9}{4} c_3 A^3)\cos \omega_2 t + \frac{3}{4} c_3 A^3 \cos(2\omega_1 - \omega_2)t$$
$$+ \frac{3}{4} c_3 A^3 \cos(2\omega_2 - \omega_1)t + c_2 A^2 \cos(2\omega_1 + \omega_2)t + \frac{1}{2} c_2 A^2 \cos 2\omega_1 t + \frac{1}{2} c_2 A^2 \cos 2\omega_2 t +$$
$$\frac{3}{4} c_3 A^3 \cos(2\omega_1 + \omega_2)t + \frac{3}{4} c_3 A^3 \cos(2\omega_2 + \omega_1)t + \frac{1}{4} c_3 A^3 \cos 3\omega_1 t + \frac{1}{4} c_3 A^3 \cos 3\omega_2 t + \ldots\ldots \tag{2.4}$$

Equation 2.4 characterizes the static AM/AM nonlinear distortion in PAs. In this expression, a mixture of the distortion harmonics is generated clearly in the PA output spectrum, in addition to the fundamental two tones at frequencies ω_1 and ω_2. The first term in the Taylor model ($c_2 A$) represents the DC component, which can be normally filtered-out using a simple DC-blocking capacitor on the PA output terminal. The other harmonics are classified according to their frequencies into even and odd IMDs as depicted in Figure 2.2 using a two-tone test of a narrow frequency spacing Δf. The third-order and fifth-order harmonics are relatively high in amplitude compared to the other odd-order IMD, as observed in practice using a two-tone test on RF PAs. In addition, these harmonics are closer to the fundamental frequencies and main concern in RF PAs.

The Taylor coefficient c_1 is the signal amplification factor, which is related to the power amplifier gain; the coefficient c_3 is a function of both gain and third-order intercept point (IP_3) [30]. Similarly, the higher-order coefficients (c_5, ..., c_k) are functions of the higher order intercept points and 1dB compression point. In fact, the higher the magnitude of the Taylor coefficient, the stronger the nonlinearity in PAs.

The Taylor model can be applied to a multi-tone signal for representing the cross-modulation distortion using a frequency mixture of multi-tone harmonics. The two-tone and multi-tone signals are widely used in signal processing to characterize the nonlinear distortion in a square-shaped baseband spectrum. This is because the multi-tone harmonics on the PA input result in a large amount of distinct in-band and out-of-band odd-order harmonic distortion [6]. Thus, a spectral regrowth in wireless communications is a result of out-of-band odd-order IMD.
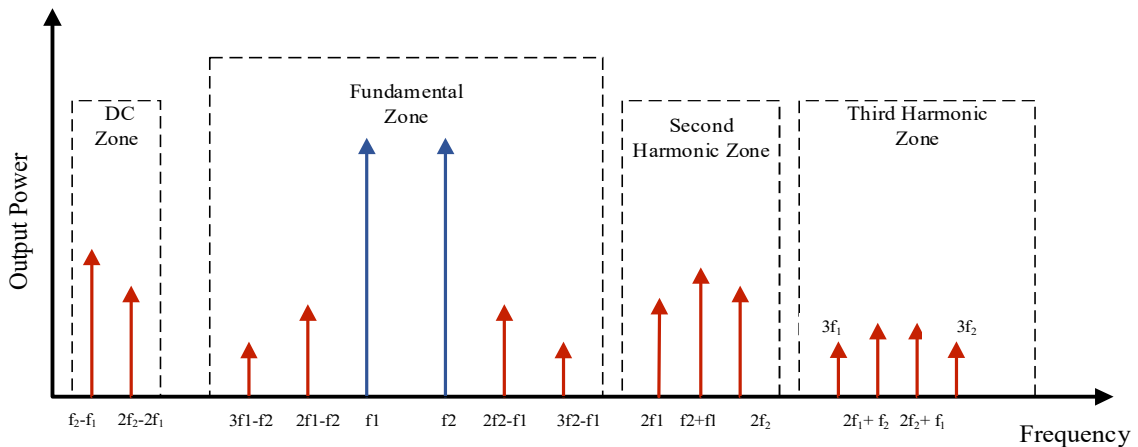
Figure 2.2 The two-tone intermodulation distortion due to AM/AM conversion.

2.2.2 Saleh Model

The Saleh AM/AM model is a popular empirical function for the memoryless nonlinearity of PAs. The Saleh model is a function of two parameters, α and β, which are positive and real numbers [10] specifying the gain and saturation amplitude of the PA. The baseband AM/AM conversion H[.] for the PA is given by:

$$y_s(t) = H[x(t)] \tag{2.5}$$

$$H[x(t)] = \frac{\alpha \cdot x(t)}{1 + \beta \cdot x^2(t)} \tag{2.6}$$

where $x(t)$ and $y_s(t)$ are the envelopes of the PA input and output baseband signals, respectively. Parameter α corresponds to the small signal gain of the PA, and parameter β adjusts the curvature smoothness of the compression region [7]. In fact, parameter β is mathematically related to the 1dB compression point, as demonstrated in this section [24].

The 1dB compression point in PAs is defined as a power level at which the small signal gain drops by 1dB. This can be expressed mathematically using:

$$20 \log |y_s(x_{1d})| = 20 \log |g \cdot x_{1d}| - 1 \tag{2.7}$$

Parameter g represents the small signal gain and x_{1d} reflects the input amplitude at the 1dB compression point. Substituting Equation 2.6 into Equation 2.7, and α into g, results in:

$$20 \log \left| \frac{\alpha \cdot x_{1d}}{1 + \beta \cdot x_{1d}^2} \right| = 20 \log |\alpha \cdot x_{1d}| - 1 \tag{2.8}$$

Using linear algebra on Equation 2.8, and simplifying the expression, results in

$$20 \log \left| \frac{\alpha . x_{1d}}{1 + \beta . x_{1d}^2} \right| = 20 \log \left| \frac{\alpha . x_{1d}}{10^{1/20}} \right| \tag{2.9}$$

Finally, the relationship between the Saleh parameter β and 1dB compression point is

$$x_{1d} = \sqrt{\frac{10^{(1/20)} - 1}{\beta}} \approx \frac{0.3493114}{\sqrt{\beta}} \approx \frac{1}{\sqrt{8\beta}} \tag{2.10}$$

Equation (2.10) is a new derived expression for the PA, which can be used to specify the linear operating region of the Saleh model [24]. This is because the 1dB compression point is a figure-of-merit widely used in PAs. The 1dB compression point refers to the PA maximum input amplitude to avoid signal clipping and high nonlinear distortion in the saturation region. In other words, the higher the amplitude of the 1dB compression point, the better and wider the linear region in PA and the smaller the value of the parameter β, because β is inversely proportional to the 1dB compression point, as shown in Figure 2.3. Hence, a minor change in the 1dB compression point can cause a large variation in the Saleh parameter β for any point below the 0.5 V in the 1dB compression point.
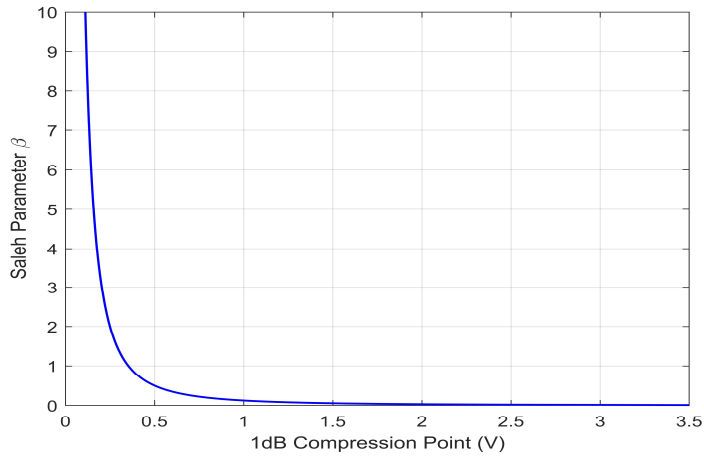
Figure 2.3 Estimation of the Saleh parameter β from the 1dB compression point.

19

2.2.2.1 Saleh Estimation Using IP3

      A least-squares method is a classical approach for estimating the Saleh behavioral model using discrete data points of the AM/AM conversion. The accuracy of the least-squares method depends on both the data number of samples and noise presented in the acquired data. This work presents a new estimation approach for the Saleh model using the design parameters of solid-state PAs. The presented approach is mathematically simpler than the least-squares and requires fewer measurements of the PA (gain and IP3). Alternatively, these parameters can be obtained easily from the manufacturing data sheets. The Taylor model is adopted in our derivation as follows:

$$y_T = c_1 x + c_3 x^3 + \ldots\ldots + c_n x^n \tag{2.11}$$

where x and y_T are envelopes of the baseband input and output signals, respectively, n is odd number for the nonlinear order of Taylor model. (c_1, c_3, ….. ,c_n) are the Taylor odd-order coefficients. The third-order intermodulation distortion (IM3) is a major concern in PAs, because the power of IM3 is relatively higher than any of the other higher odd-order IMDs as observed in measurement of a PA two-tone test. In addition, the IM3 distortions fall in-band and near the fundamental frequency in the spectrum domain. The higher-order IMDs can be eliminated using brick-wall band-pass filter. Similarly, the even-order coefficients of the Taylor model quantify the even-order IMDs, which are multiple frequencies of the fundamental frequency and can be easily filtered out.

The Taylor coefficients in Equation 2.11 are directly related to PA gain and intercept points. For simplicity, we consider only c_1 and c_3 coefficients as follows [30], [35]:

$$c_1 = 10^{\left(\frac{G}{20}\right)} \tag{2.12}$$

$$c_3 = \frac{-2}{3} 10^{\left(\frac{-IP_3}{10} + \frac{3G}{20}\right)} \tag{2.13}$$

where G is the power gain in dB and IP_3 is the output third-order intercept point in dBw. IP_3 represents the input power level at which the output power of the fundamental frequency intercepts with the output power of the third-order intermodulation (IM_3) frequency as depicted in Figure 2.4.

Third-order intercept points are popular technical specifications for PA linearity. The higher the value of IP_3, the better the gain linearity of PAs. The Saleh model is an odd-function which consists of odd-order Taylor expansion terms. Hence, the modeling approach in this work is calculated by minimizing the error objective function between the Saleh model and the third-order Taylor model in the linear region of PAs [24].
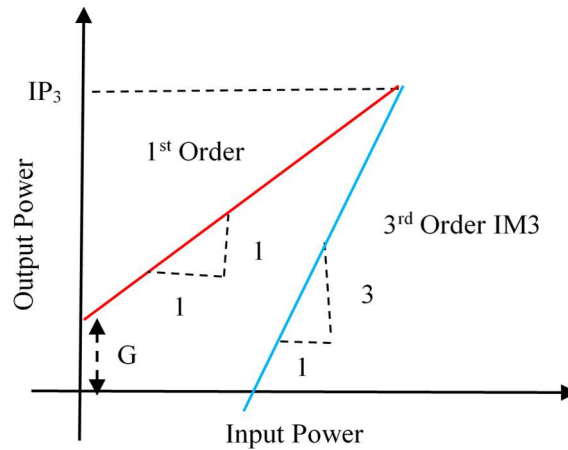
Figure 2.4 Graph illustrating the intercept point between the fundamental and third-order intermodulation distortion.

The objective function is written using the following mathematical notations:

$$\begin{cases} \text{Minimizing}\,[(y_T(x) - y_s(x))^2] \\ \qquad\qquad {}_{w.r.t\,(c_1,\;\;c_3)} \\ \\ x \in \mathbb{R}:\; 0 \le x \le x_{1dB} \end{cases} \tag{2.14}$$

where x_{1dB} is the input amplitude at 1dB compression point. The square-errors function (y_T - y_S)^2 is expressed as follows:

$$e^2(x) = \left((c_1 x + c_3 x^3) - \frac{\alpha\,x}{1 + \beta\,x^2} \right)^2_{x \in \left(0\,,\, 1/\sqrt{8\beta}\right)} \tag{2.15}$$

For simplicity, the square-errors $e^2(x)$ is computed over the amplitude range $(0\,,\,\sqrt{(1/8\beta)}\,)$ as derived from the 1dB compression point. Hence, the total square-errors e_T^2 represents the integral of Equation 2.15 over the defined input amplitude range

$$e_T^2 = \int_0^{1/\sqrt{8\beta}} \left(c_1 x + c_3 x^3 - \frac{\alpha x}{1 + \beta x^2} \right)^2 dx \tag{2.16}$$

The integral computation of Equation 2.16 is:

$$e_T^2 = \frac{(9\,\alpha^2 + 36 c_1 \alpha)(\tan^{-1}(1/2\sqrt{2})) - 2\alpha^2/\sqrt{2} - 9 c_1 \alpha\sqrt{2}}{18\beta\,\sqrt{\beta}} + \frac{c_3^2}{7168\beta^3\,\sqrt{2\beta}} +$$
$$\frac{c_1^2}{48\beta\,\sqrt{2\beta}} + \frac{640\sqrt{2}c_3\alpha(\tan^{-1}(1/2\sqrt{2}) - 23\sqrt{2}/96)) + c_1 c_3}{320\beta^2\,\sqrt{2\beta}} \tag{2.17}$$

The minimum square-errors of Equation 2.17 occurs when gradient operation in terms of the coefficients (c_1, c_3) approaches zero, and this can be written mathematically as

$$\nabla\left(e_T^2\right) = \left(\frac{\partial e_T^2}{\partial c_1}, \frac{\partial e_T^2}{\partial c_3} \right) = (0,0) \tag{2.18}$$

22

The gradient computation using Equation 2.17 and Equation 2.18 results in the following two equations:

$$\frac{\sqrt{2}c_1 - 1280\,\alpha\,(\tan^{-1}(1/2\sqrt{2}) - 23\sqrt{2}/96)}{640\,\beta^2\,\sqrt{\beta}} + \frac{\sqrt{2}c_3}{7168\,\beta^3\,\sqrt{\beta}} = 0 \qquad (2.19)$$

$$\frac{c_3}{320\,\beta^2\,\sqrt{2\beta}} + \frac{c_1 + 48\,\alpha\,\sqrt{2}\,(\tan^{-1}(1/2\sqrt{2}) - 2\sqrt{2})}{24\,\beta\,\sqrt{2\beta}} = 0 \qquad (2.20)$$

The instantaneous solution of Equation 2.19 and Equation 2.20 is:

$$\alpha = \frac{c_1}{1760 - 3660\sqrt{2}\,\tan^{-1}(1/2\sqrt{2})} \qquad (2.21)$$

$$\beta = \frac{-3c_3\,(183\sqrt{2}\,\tan^{-1}(1/2\sqrt{2}) - 88)}{56c_1\,(129\sqrt{2}\,\tan^{-1}(1/2\sqrt{2}) - 62)} \qquad (2.22)$$

Substituting Equation 2.12 into Equation 2.21 and simplifying both equations, results in the following:

$$\alpha = \frac{10^{\left(\frac{G}{20}\right)}}{1760 - 3660\sqrt{2}\,\tan^{-1}(1/2\sqrt{2})} \approx 1.003 \times 10^{\left(\frac{G}{20}\right)} \qquad (2.23)$$

$$\beta = \frac{-3\,c_3\,(183\sqrt{2}\,\tan^{-1}(1/2\sqrt{2}) - 88)}{56\,c_1\,(129\sqrt{2}\,\tan^{-1}(1/2\sqrt{2}) - 62)} \approx -1.137\,\frac{c_3}{c_1} \qquad (2.24)$$

Substituting Equation 2.12 and 2.13 into Equation 2.24, results in:

$$\beta = 0.758 \times 10^{\left(\frac{-IP_3}{10} + \frac{G}{10}\right)} \qquad (2.25)$$

Equation 2.23 and Equation 2.25 illustrate that the parameter α is directly proportional to the PA gain as expected from the formula of the Saleh model [24]. However, the parameter β is function of both gain and IP_3. In fact, the parameter β specifies the PA nonlinearity due to IM_3.

An experimental set-up using a commercial PA is implemented for data acquisition and verifying the estimation of the Saleh AM/AM model. A block diagram of the experiment is shown in Figure 2.5, which consists of the following measurement equipment: the Keysight E4438C signal generator, the Tektronix RSA 6120A spectrum analyzer, and commercial PA (ZFL-1000LN) from Mini-Circuit. A two-tone signal at 1 GHz with 50 KHz spacing was generated from the signal generator and applied to the PA input port. The AM/AM measurements of the PA were obtained by sweeping the power of the two-tone signal and recording the corresponding output power from the signal analyzer. The PA small signal gain is calculated at – 40 dBm input power as {Gain= -17.5 - (-40) = 22.5 dB}. The parameter IP_3 is calculated using the following Equation [30]:

$$IP_3 = P_o + \frac{\Delta P}{2} \tag{2.26}$$

where P_o is the output power of the fundamental tone, ΔP is the power difference between the fundamental and the third-order IMD as shown in Figure 2.6. Substituting P_o= -19.07 dBm and ($\Delta P = -19.07 + 69.7 = 50.63$ dBm) in Equation 2.26 and including both the cable and attenuator losses, results in IP_3=12.86 dBm.

The AM/AM measurements using the swept two-tone amplitude and the 3rd-order Taylor model as well as the curve of the Saleh model using this method are overlaid in Figure 2.7. The compared results show that both the Saleh model and 3rd-order Taylor model reflect

accurately the results obtained from the measurements for the amplitude range $(0, x_{1dB})$. However, the 3rd-order Taylor model decreases monotonically sharply after the saturation amplitude, because the Taylor coefficient c_3 is a relatively high negative value compared to the Taylor coefficient c_1. On the other hand, the slope of the Saleh model decreases smoothly at a slower rate after the 1dB compression point. This is because the output amplitude in the Saleh model is typically attenuated slowly by the denominator $(1+\beta x^2)$. Another accuracy evaluation is calculated using the square-errors function in Equation 2.27. A lower residual error can be observed in the Saleh model compared to the 3rd-order Taylor model in Figure 2.8.

$$e_T^2 = \sum_{n=1}^{K} \left(y_{md}(n) - y_{ms}(n) \right)^2 \tag{2.27}$$

where $y_{md}(n)$ is the modeled output amplitude, $y_{ms}(n)$ is the measured output amplitude, e_T^2 is the total residual square errors, and K is the number of samples.

Table (2.1) reports the modeling accuracy using the total square errors (e_T^2) and Mean Square Errors (MSE) between the measured and the output amplitude of the Saleh model as well as the 3rd-order Taylor model [24].

The accuracy results in Table (2.1) are calculated for model evaluation within the following amplitude ranges: (0) volt to the 1dB compression point, (0) volt to the saturation level of the Taylor model, and finally from (0) volt to the saturation region of the PA.
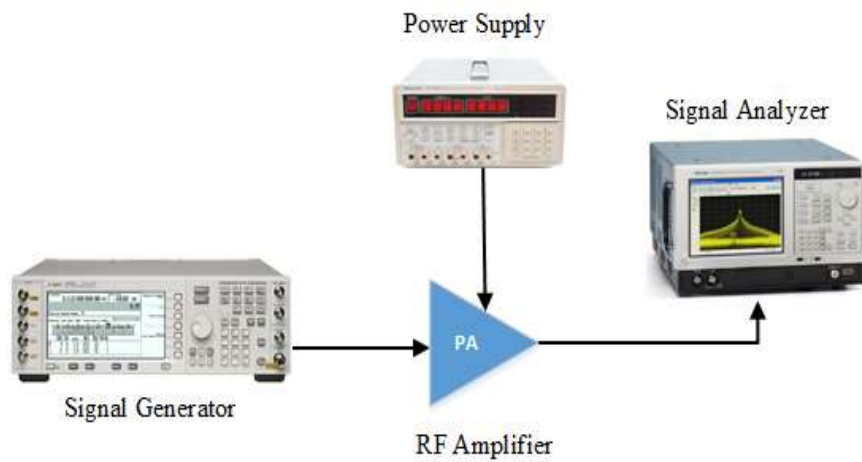
Figure 2.5 Measurement set-up for the PA experiment.
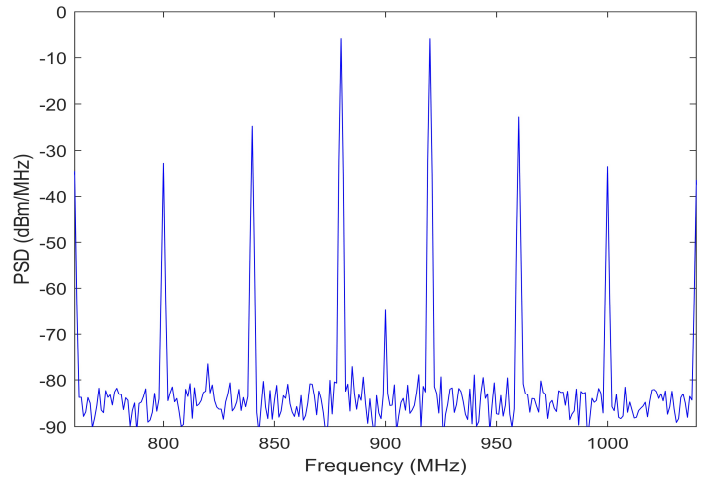
Figure 2.6 The measured two-tone intermodulation distortion on the output of the PA.
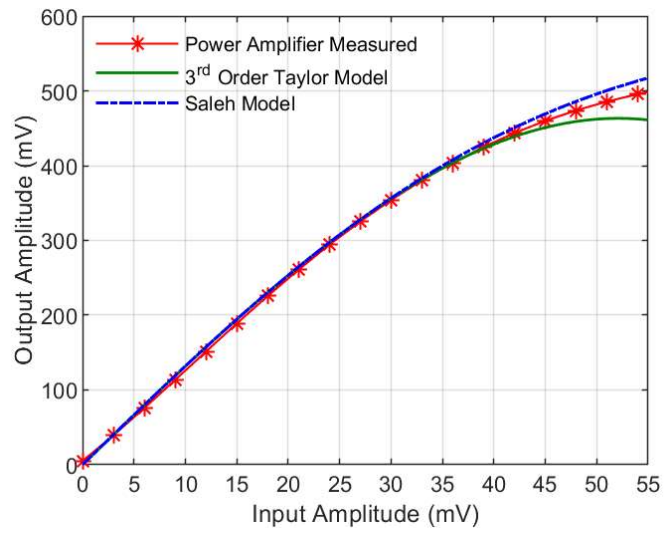
Figure 2.7 Measured and modeled AM/AM conversion for the PA.

Table (2.1) Accuracy comparison of the static AM/AM conversion in the Saleh and 3rd-order Taylor model.

Operating Amplitude Range	Saleh Model		Taylor Model	
	Total Squares Error (V^2)	MSE (dB)	Total Squares Error (V^2)	MSE (dB)
(0) volt to the amplitude at 1dB compression point (31mV).	$5.3757*10^{-4}$	-47.61	$5.2889*10^{-4}$	-47.68
(0) volt to the saturation of the Taylor model (52mV).	0.0022	-43.77	0.0031	-42.26
(0) volt to the saturation level of the power amplifier (120mV).	0.112	-26.46	39.05	-1.07
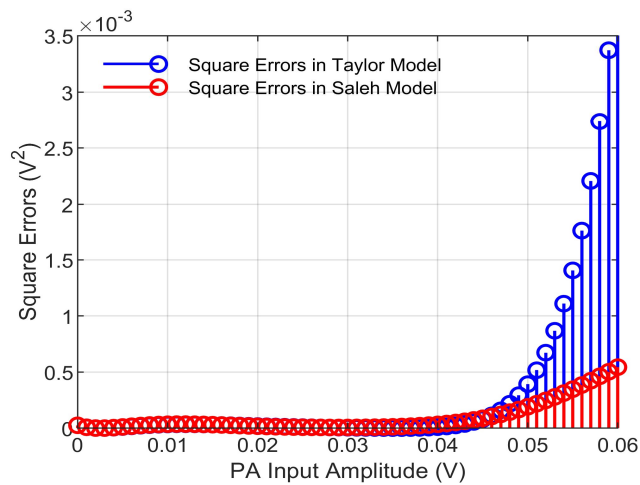
Figure 2.8 Residual errors between the PA measurements and the Saleh modeled amplitude.

2.2.2.2 Saleh Estimation Using 1dB Compression

The IP_3 is used to describe the IMDs contributed by the third-order nonlinear harmonics, which are major effects on the PA linearity. The 1dB compression point is another important parameter for quantifying the higher order IMDs of the static AM/AM nonlinearity in PAs [25]. Hence, a model estimation using both IP_3 and P_{1dB} is presented in this section for accuracy improvement in the Saleh AM/AM model $z_s(r) = \varepsilon\, r/(1 + \mu\, r^2)$ [25]. The 5th-order Taylor model is used in this derivation to quantify the dominant nonlinear effects.

$$z_T = c_1\, r + c_3\, r^3 + c_5\, r^5 \tag{2.28}$$

where r and z_T are the envelopes of the PA input and output signals, respectively. (c_1, c_3, c_5) are Taylor coefficients. The coefficients c_1 and c_3 are calculated from Equation 2.12 and Equation 2.13, respectively. The coefficient (c_5) is calculated approximately using the gain compression curve [34]

$$\frac{5}{8}\left(\frac{c_5}{c_1}\right) r_{1dB}^4 + \frac{3}{4}\left(\frac{c_3}{c_1}\right) r_{1dB}^2 + 0.109 = 0 \tag{2.29}$$

where c_1, c_3, and c_5 are Taylor coefficients, r_{1dB} is the input amplitude at the 1dB compression point. r_{1dB} is related to the power level using

$$r_{1dB}^2 = 2R \times 10^{\left(\frac{P_{1dB}}{10}\right)} \tag{2.30}$$

where R is the PA input resistant and P_{1dB} is the input power in dBw unit at the 1dB compression point [25].

For the sake of simplicity, Equation (2.29) can be re-expressed

$$c_5 = \frac{-6\,c_3}{5\,r_{1dB}^2} - \frac{0.174\,c_1}{r_{1dB}^4}$$

(2.31)

Substituting c_1, r_{1dB}^2, and c_3 in terms of Equation 2.12, Equation 2.13, and Equation 2.30, results in

$$c_5 = 0.4 \times 10^{\left(\frac{3G}{20}+\frac{-P_{1dB}}{10}+\frac{-IP_3}{10}\right)} - 0.043 \times 10^{\left(\frac{G-4\,P_{1dB}}{20}\right)}$$

(2.32)

The objective error function between the 5th-order Taylor model and the Saleh model is expressed mathematically in the amplitude range $(0\,,\,r_{1dB})$ as follows:

$$\begin{cases} \underset{w.r.t\,(c_1,\ c_3,\ c_5)}{\text{Minimizing}\,[(z_T(r)-z_s(r))^2]} \\[2mm] r \in \mathbb{R}:\ 0 \le r \le r_{1dB} \end{cases}$$

(2.33)

In Equation 2.33, we assume that the selected amplitude range represents the back-off operating region in PAs. In fact, the 1dB compression point is a design target specification in the RF applications of wireless communication. Substituting the Saleh and Taylor models' formulas into Equation 2.33, results in the following error objective functions [25]:

$$e^2(r) = \left((c_1\,r + c_3\,r^3 + c_5\,r^5) - \frac{\varepsilon\,r}{1+\mu\,r^2} \right)^2 \Bigg|_{r \in (0,\,1/\sqrt{8\mu})}$$

(2.34)

$$e_T^2 = \int_0^{1/\sqrt{8\mu}} \left(c_1\,r + c_3\,r^3 + c_5\,r^5 - \frac{\varepsilon\,r}{1+\mu\,r^2} \right)^2 dr$$

(2.35)

The integral operation in Equation 2.35 is mathematically complicated. Thus, we used MATLAB software to calculate this integral, as follows:

$$e_T^2 = \{(315\sqrt{2}c_5^2 + 6160\sqrt{2}c_3c_5\mu + 31680\sqrt{2}\,(c_3^2 + 2c_1c_5)\mu^2 - 227082240\sqrt{2}\mu^2(c_5 + \mu(c_1\mu - c_3))\varepsilon -$$
$$50462720\sqrt{2}\mu^4\varepsilon^2 + 709632\sqrt{2}\mu^2(c_1c_3\mu - c_5\varepsilon) + 4730880\sqrt{2}\mu^2(c_1^2\mu^2 +$$
$$2(c_5 - c_3\mu)\varepsilon) + 227082240\mu^2\varepsilon(4c_5 + \mu(-4c_3 + \mu(4c_1 + \varepsilon)))$$
$$\tan^{-1}(1/2\sqrt{2}))/(454164480\,\mu^{(11/2)})\} \tag{2.36}$$

The minimum square errors of Equation 2.36 occur when the gradient with respect to the

Taylor coefficients approaches zero [25], as described in the following expression:

$$\nabla(e_T^2) = \left(\frac{\partial e_T^2}{\partial c_1}, \frac{\partial e_T^2}{\partial c_3}, \frac{\partial e_T^2}{\partial c_5}\right) = (0, 0, 0) \tag{2.37}$$

The following three equations are obtained from calculating the gradient expression [25]:

$$(630\sqrt{2}c_5 + 6160\sqrt{2}\,c_3\,\mu + 63360\sqrt{2}\,c_1\,\mu^2 - 218330112\sqrt{2}\,\varepsilon\,\mu^2 + 908328960\,\varepsilon\,\mu^2$$
$$\tan^{-1}(1/2\sqrt{2}))/(454164480\,\mu^5\sqrt{\mu}) = 0 \tag{2.38}$$

$$(63360\sqrt{2}c_5\,\mu^2 + 709632\sqrt{2}\,c_3\,\mu^3 + 9461760\sqrt{2}\,c_1\,\mu^4 - 227082240\sqrt{2}\,\varepsilon\,\mu^4 + 908328960\,\varepsilon\,\mu^4$$
$$\tan^{-1}(1/2\sqrt{2}))/(454164480\,\mu^5\sqrt{\mu}) = 0 \tag{2.39}$$

$$(6160\sqrt{2}c_5\,\mu + 63360\sqrt{2}\,c_3\,\mu^2 + 709632\sqrt{2}\,c_1\,\mu^3 + 217620480\sqrt{2}\,\varepsilon\,\mu^3 - 908328960\,\varepsilon\,\mu^3$$
$$\tan^{-1}(1/2\sqrt{2}))/(454164480\,\mu^5\sqrt{\mu}) = 0 \tag{2.40}$$

By solving Equations 2.38 to 2.40 for (c_1, c_3, and c_5) in MATLAB, we obtain the

following relationships:

$$c_1 = 93093\,\varepsilon - 193698.75\sqrt{2}\,\varepsilon\,\tan^{-1}(1/2\sqrt{2}) \approx 0.99\,\varepsilon \tag{2.41}$$

$$c_3 = -3432912\,\varepsilon\,\mu + 7142940\sqrt{2}\,\varepsilon\,\mu\,\tan^{-1}(1/2\sqrt{2}) \approx -0.99\,\varepsilon\,\mu \tag{2.42}$$

$$c_5 = 24550310.4\,\varepsilon\,\mu^2 - 51082416\sqrt{2}\,\varepsilon\,\mu^2\,\tan^{-1}(1/2\sqrt{2}) \approx 0.82\,\varepsilon\,\mu^2 \tag{2.43}$$

We use a linear transformation on the Equations (2.41) - (2.43) to simplify these Equations and solve them using the least-squares method. In addition, a logarithmic transformation is used to form the following matrix equation [25]:

$$\begin{bmatrix} 1 & 0 \\ 1 & 1 \\ 1 & 2 \end{bmatrix} \begin{bmatrix} \log(\varepsilon) \\ \log(\mu) \end{bmatrix} = \begin{bmatrix} \log(1.01c_1) \\ \log(-1.01c_3) \\ \log(1.21c_5) \end{bmatrix} \tag{2.44}$$

Substituting Equations (2.12) - (2.13) into equation 2.44, results in

$$\begin{bmatrix} 1 & 0 \\ 1 & 1 \\ 1 & 2 \end{bmatrix} \begin{bmatrix} \log(\varepsilon) \\ \log(\mu) \end{bmatrix} = \begin{bmatrix} \dfrac{G}{20} + 0.004 \\[2mm] \dfrac{-IP_3}{10} + \dfrac{3G}{20} - 0.17 \\[2mm] \log \{0.48 \times 10^{\left(\frac{3G}{20} + \frac{-IP_3}{10} + \frac{-P_{1dB}}{10}\right)} - 0.048 \times 10^{\left(\frac{G}{20} + \frac{-P_{1dB}}{5}\right)}\} \end{bmatrix} \tag{2.45}$$

A matrix representation of Equation 2.45 is

$$\mathbf{KS = C} \tag{2.46}$$

The (2x1) column vector **S** is a logarithmic operation of the Saleh coefficients, the column vector **C** consists of (3x1) parameters of the PA: gain, IP_3, and P_{1dB}. **K** is a constants matrix of (3x2) elements. Using linear algebra on Equation 2.46 to separate the matrices, results in:

$$\mathbf{S = (K^T K)^{-1} K^T C} \tag{2.47}$$

By calculating the matrix pseudo-inverse on **K** and re-arranging the matrix as in Equation 2.47, we obtain the following:

$$
\begin{bmatrix} \log(\varepsilon) \\ \\ \log(\mu) \end{bmatrix} = \begin{bmatrix} 5/6 & -1/2 \\ 1/3 & 0 \\ -1/6 & 1/2 \end{bmatrix}^{T} \begin{bmatrix} \dfrac{G}{20}+0.004 \\ \\ \dfrac{-IP_3}{10}+\dfrac{3G}{20}-0.17 \\ \\ \log\left\{0.48\times 10^{\left(\frac{3G}{20}+\frac{-IP_3}{10}+\frac{-P_{1dB}}{10}\right)}-0.048\times 10^{\left(\frac{G}{20}+\frac{-P_{1dB}}{5}\right)}\right\} \end{bmatrix}
$$
(2.48)

Finally, Equation 2.48 is simplified as shown below to obtain a vector of the Saleh coefficients as a function of G, IP_3 and P_{1dB} [25].

$$
\begin{bmatrix} \varepsilon \\ \\ \\ \mu \end{bmatrix} = \begin{bmatrix} 10^{\left(\frac{11G}{120}+\frac{-4}{75}+\frac{-IP_3}{30}\right)}\left(0.48\times 10^{\left(\frac{3G}{20}+\frac{-IP_3}{10}+\frac{-P_{1dB}}{10}\right)}-0.048\times 10^{\left(\frac{G}{20}+\frac{-P_{1dB}}{5}\right)}\right)^{\frac{-1}{6}} \\ \\ 10^{-\left(\frac{G+0.008}{40}\right)}\left(0.48\times 10^{\left(\frac{3G}{20}+\frac{-IP_3}{10}+\frac{-P_{1dB}}{10}\right)}-0.048\times 10^{\left(\frac{G}{20}+\frac{-P_{1dB}}{5}\right)}\right)^{\frac{1}{2}} \end{bmatrix}
$$
(2.49)

The experimental measurement shown in Figure 2.9 is used to estimate the Saleh AM/AM model based on GaAs power amplifier ZFL-1000LN. The measured gain, third-order intercept, and 1dB compression point of the PA are G=22.45 dB, IP_3=12.81 dBm, and output P_{1dB}=2.25 dBm. The parameter IP_3 is measured using a two-tone test as described earlier in section 2.2.2.1. Gain and the 1dB compression point are both measured using a swept two-tone power on the input of PA as illustrated in Figure 2.10. Both the 5th-order Taylor model and Saleh model are calculated from the presented model equations using G, IP_3, and P_{1dB} of the PAs. Figure 2.11 illustrates the AM/AM measured results of the two-tone test as well as the 5th-order Taylor and Saleh model results of the PA in time domain. The results obtained exhibit significant model improvement in both the linear

region and near the compression region. The model evaluation in the frequency domain is illustrated in Figure 2.12 for both the PA measurement and spectrum estimation using the Saleh model. The Saleh model predicted the Power Spectral Density (PSD) well for both the in-band and spectrum regrowth regions. The model assessment using both the Normalized Mean Square Errors (NMSE) and Adjacent Channel Error Power Ratio (ACEPR) is calculated and presented in Table (2.2) for two different estimation approaches: gain and IP_3 in one scenario, and gain, IP_3, and the 1dB compression point in the second scenario [25].
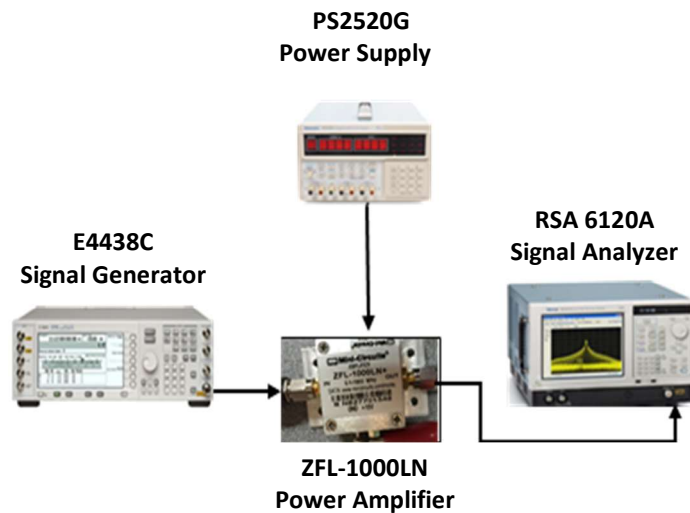
Figure 2.9   An experiment structure used for model evaluation of the PA.
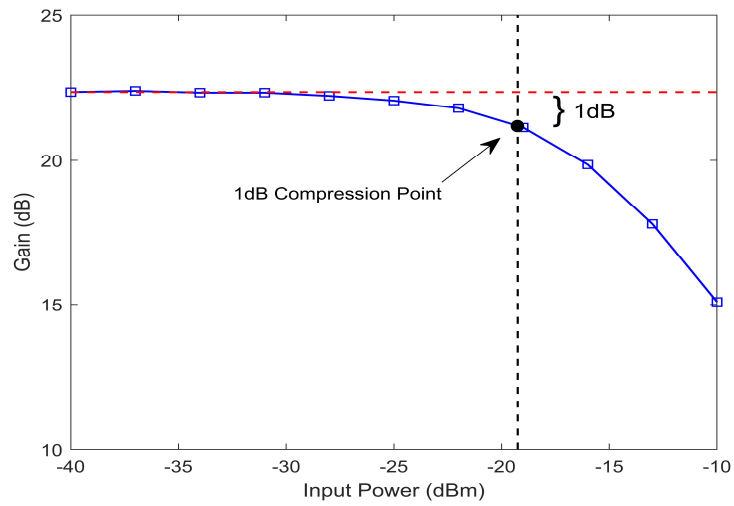
Figure 2.10 Measured gain compression curve for the PA.
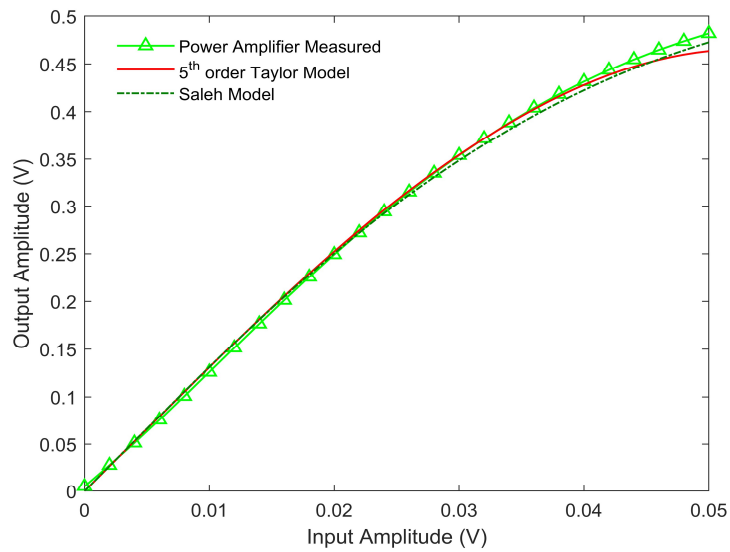
Figure 2.11 AM/AM measured and Saleh estimation using 1dB compression of the PA.
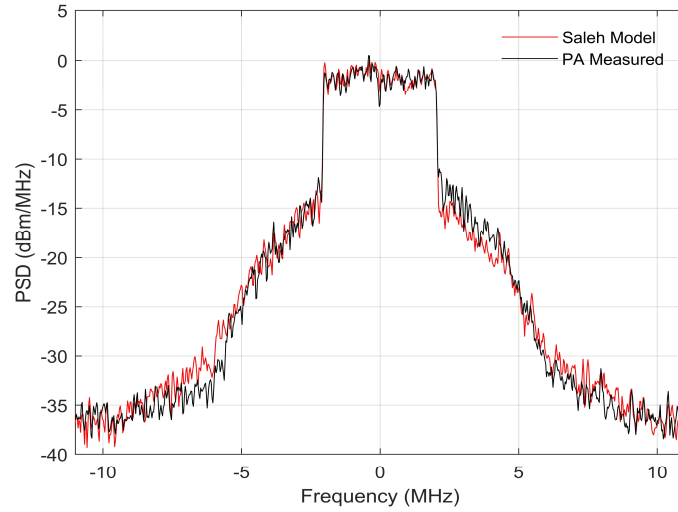
Figure 2.12   Power spectrum density of WCDMA signal of the PA measurement and modeled output signals.

Figures 2.13 and 2.14 depict significant relationships between the Saleh coefficients and PA specification parameters, IP_3 and P_{1dB}. These figures were obtained by sweeping the values of IP_3 and P_{1dB} and calculating the Saleh parameters ε and μ. A steady slope and increasing rate with respect to IP_3 and P_{1dB} are shown in these figures. In addition, the variation of the Saleh parameter μ exhibits a sharp slope with high sensitivity to the

Table (2.2) Assessment comparison between two different proposed estimation approaches of the Saleh model.

Estimation Approach	Model Parameters	NMSE (dB)	ACEPR (dB)
Scenario (1)	G, IP_3	-34.32	-42.52
Scenario (2)	G, IP_3, P_{1dB}	-35.85	-43.31

variation of the parameters IP_3 and P_{1dB}. This is because the parameter μ controls the

nonlinear characteristics of the Saleh behavioral model [25].
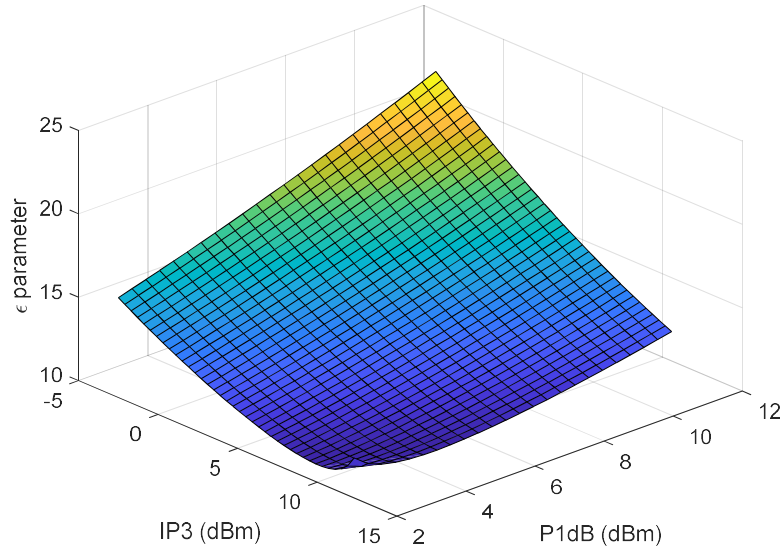
Figure 2.13 2D-mesh representation of the Saleh parameter ε versus IP_3 and P_{1dB}.
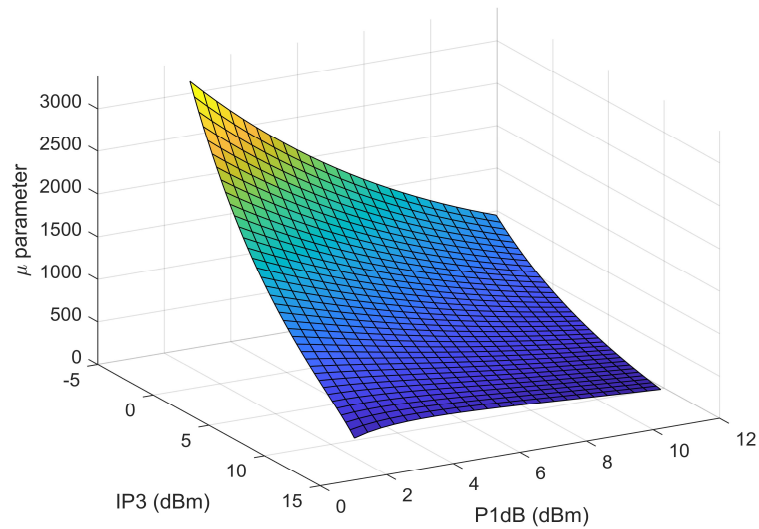
Figure 2.14 2D-mesh illustrating the variation of the Saleh parameter μ versus IP_3 and P_{1dB}.

2.2.2.3 Proposed Enhanced Saleh Model

The Saleh behavioral model was originally derived for Traveling Wave Tube Power Amplifiers (TWT-PAs). Due to the ongoing developments in the semiconductor industry, Solid-State Power Amplifiers (SSPAs) have become more popular devices in wireless communications. A new model enhancement is included to the Saleh AM/AM function for the applications of SSPAs. In particular, this enhancement is developed to improve the smoothness of the Saleh model near the saturation region. The new enhanced model consists of a 3-parameter rational function. The Saleh AM/AM model is expressed using the following notation:

$$F[u(t)] = \frac{\alpha \, u(t)}{1 + (\sqrt{\beta} \, u(t))^2} \tag{2.50}$$

where u(t) is the envelope of the PA input baseband signal. The Saleh model is an odd function {F[-u(t)] = -F[u(t)]}. The polynomial expansion of Equation 2.50 is

$$F[u(t)] = \sum_{k=0}^{\infty} (-1)^k \, \alpha \, \beta^k \, u^{(2k+1)}(t) \tag{2.51}$$

where k is an integer number {k = 0, 1, 2, 3, …. ∞}.

$$F[u(t)] = \alpha \, u(t) - \alpha \beta \, u^3(t) + \alpha \beta^2 \, u^5(t) + ...\infty \tag{2.52}$$

The polynomial expansion in Equation 2.52 consists of the nonlinear coefficients {α, $\alpha\beta$, … , $\alpha\beta^k$}. These coefficients are statistically magnitude dependent. On the other hand, the Taylor polynomial model consists of linearly independent variables as in Equation 2.53, which exhibits a higher degree of freedom in the model parameters fitting.

$$T[u(t)] = c_1 u(t) + c_3 u^3(t) + c_5 \, u^5(t) + ...\infty \tag{2.53}$$

38

The Taylor coefficients $\{c_1, c_3, \ldots, c_n\}$ are linear and often used independently in model estimation. In fact, the coefficients of the Taylor model exhibit device-related physical meaning, because each coefficient quantifies a specific order of IMD. In addition, the higher order IMDs affect the lower order IMDs in PAs, for example fifth-order intermodulation distortion (IM_5) affects the IM_3 [1], and the model coefficients are statistically quantified by the 1dB compression point. The model's high nonlinear slope and monotonically decreasing amplitude are the two weaknesses in the Saleh function for modeling SSPAs. This is because both the gain and saturation level are almost constants in SSPAs and they are specified by the supply voltage on the drain/collector of the PA. Hence, we propose a simple enhancement to overcome these limitations using the following new expression:

$$F_{es}[u(t)] = \frac{\alpha\, u(t) + \lambda\, u^2(t)}{1 + \beta\, u^2(t)} \tag{2.54}$$

where λ is a real positive number introduced here as a new parameter for controlling the amplitude roll-over near the saturation region. $F_{es}[.]$ is the enhanced Saleh model. The small signal gain of the enhanced Saleh model is equal to the linear gain (α) as illustrated in this derivation:

$$\lim_{u \to 0} \frac{\partial(F_{es}[u])}{\partial(u)} = \alpha \tag{2.55}$$

The new parameter λ forces Equation 2.54 to be non-monotonic and causes the model to become an asymptotically increasing function near saturation (the saturation level is approximated by λ/β) for a large signal magnitude. In addition, the polynomial expansion

39

of Equation 2.54 becomes a mixture of even and odd nonlinear IMD as illustrated below

$$F_{es}[u(t)] = \sum_{k=0}^{\infty} (-1)^k \, \beta^k \, u^{(2k)}(t)\{\alpha\, u(t) + \lambda\, u^2(t)\} \tag{2.56}$$

$$F_{es}[u(t)] = \alpha\, u(t) + \lambda\, u^2(t) - \alpha\beta\, u^3(t) - \lambda\beta\, u^4(t) + $$
$$\alpha\beta^2 u^5(t) + \lambda\beta^2\, u^6(t) - \alpha\beta^3 u^7(t) + \ldots\ldots \infty \tag{2.57}$$

The second order intermodulation distortion (IM2) is quantified by the parameter λ, and the higher even order terms are quantified by the nonlinear coefficients $\{\lambda, \lambda\,\beta, \ldots, \lambda\,\beta^k\}$. The proposed extension improves the model accuracy significantly [6], [7], and accounts for most the nonlinearity for AM/AM conversion of the PA. The enhanced Saleh model is numerically very stable compared to the truncated Taylor model of a high nonlinear order, because Equation 2.54 converges asymptotically to a constant value λ/β.

A two-tone experiment was implemented on SSPA GaAs from Mini-Circuit (ZFL-1000LN). A 100 discrete data points of the AM/AM conversion were acquired for the input and output amplitude measurements of the PA at 1 GHz center frequency.

The parameters of the enhanced Saleh model are calculated using a least-squares method, which is derived by substituting $z(t)=F_{es}[u(t)]$ in Equation 2.54 and re-arranging the parameters as follows:

$$z(t) = \alpha\, u(t) + \lambda\, u^2(t) - z(t)\,\beta\, u^2(t) \tag{2.58}$$

where $z(t)$ is the envelope of the PA baseband output signal. A matrix equation is formulated from the measured amplitude samples of $u(t)$ and $z(t)$ as illustrated below:

$$\begin{bmatrix} z(0) \\ z(1) \\ \vdots \\ z(n) \end{bmatrix} = \begin{bmatrix} u(0) & -z(0)\,u^2(0) & u^2(0) \\ u(1) & -z(1)\,u^2(1) & u^2(1) \\ \vdots & \vdots & \vdots \\ u(n) & -z(n)\,u^2(n) & u^2(n) \end{bmatrix} \begin{bmatrix} \alpha \\ \beta \\ \lambda \end{bmatrix} \tag{2.59}$$

A matrix notation is used in expressing Equation 2.59 as

$$\mathbf{z} = \mathbf{Uc} \tag{2.60}$$

where $\mathbf{z}$ is a column vector of $((n+1)\times 1)$ elements, $\mathbf{c}$ is a column vector of the model parameters (3×1), and $\mathbf{U}$ is a matrix consisting of $((n+1)\times 3)$ elements of the input and output samples. Finally, a vector of a model coefficients is calculated using a least-squares

$$\mathbf{c} = (\mathbf{U}^{\mathrm{T}}\mathbf{U})^{-1}\mathbf{U}^{\mathrm{T}}\mathbf{z} \tag{2.61}$$

where $(.)^{\mathrm{T}}$ denotes the operator of a matrix transposition. The calculated results of both the Saleh and enhanced Saleh AM/AM conversions are shown in Figure 2.15. The enhanced Saleh model shows an accuracy improvement in the back-off and saturation regions. The residual square-errors between the AM/AM measurements and the model conversions are overlaid on the same figure over a wide range of the input amplitude. The obtained model enhancement in NMSE is depicted in Table (2.3).

Table (2.3) The model assessment comparison between the Saleh and the enhanced Saleh model.

Model	Number of Coefficients	Intermodulation Distortion	NMSE (dB)
Saleh	2	odd terms	-28.32
Enhanced Saleh	3	odd and even terms	-31.85
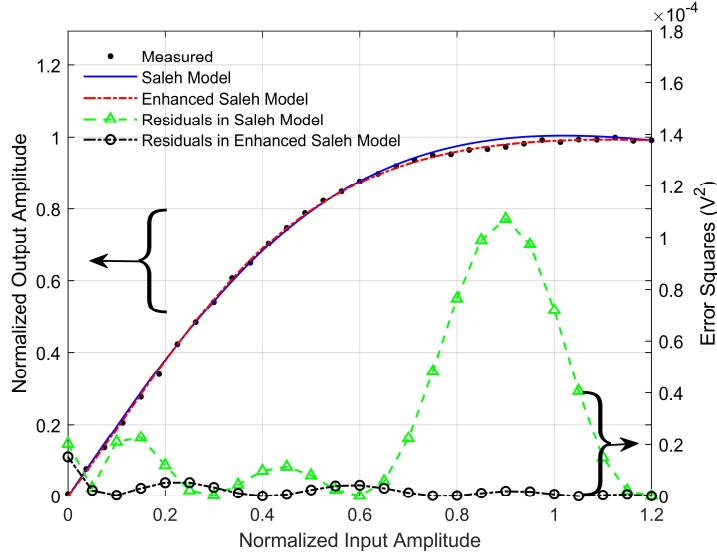
Figure 2.15 Measured and modeled AM/AM results of the PA, in addition to the residual errors of both Saleh and the enhanced Saleh model.

2.2.3   Other Static Models

Most published behavioral models of SSPAs exhibit limitations in characterizing the AM/AM nonlinearity near the saturation region. In fact, the roll-over from a linear to a saturation region (i.e model sharpness) is the main limitation in most behavioral models. For example, Rapp and Gharbani behavioral models are popular proposed models in the literature of SSPAs using different nonlinear functions. However, these models consist of complicated mathematical rational functions. This often leads to computation complexity in parameter calculations, such as using an iterative estimation method. In addition, these models are inappropriate for modeling digital predistortions in linearizing PAs. Polynomial-based behavioral models allow a flexible approach in parameter estimations and controlling the model accuracy. However, polynomial models are subject to challenges of under-fitting and over-fitting estimation.

2.3 Static Amplitude-to-Phase Distortion

The AM/PM distortion in PAs is a result of the nonlinear variation in time delay (i.e phase shift) between the PA input and output signals in terms of signal input amplitude. The physical origin of the AM/PM distortion is the nonlinear variation of the gate-source capacitance in terms of the input amplitude and drain-source capacitance in terms of the drain voltage magnitude. Theoretically, the AM/PM conversion is calculated mathematically from the in-phase and quadrature-phase components of input and output complex baseband signals as follows:

$$\theta(t) = \tan^{-1}\left(\frac{\Im\{z_{BB}(t)\}}{\Re\{z_{BB}(t)\}}\right) - \tan^{-1}\left(\frac{\Im\{x_{BB}(t)\}}{\Re\{x_{BB}(t)\}}\right) \qquad (2.62)$$

where $x_{BB}(t)$ and $z_{BB}(t)$ are the complex baseband input and output signals of the PA, respectively, and $\theta(t)$ is the AM/PM conversion. The static AM/AM and AM/PM conversions are shown in Figure 2.16. Gain compression and phase expansion at high input amplitude are two common nonlinear behaviors in PAs.

2.4 Quasi-Static Modeling Technique

PAs are analog devices, which normally operate in RF bandpass signals (carrier up-converted time continuous signals). A system level in a digital baseband is the most often-used PA empirical modeling [30]-[31]. A quasi-static modeling approach is a widely used to characterize both the static AM/AM and static AM/PM conversions for short-term memory nonlinear systems. Hence, quasi-static modeling approaches are adequate for

narrow-band wireless communications, and other applications where the long-term memory effect exhibits lower impact on the signal distortion.

Quasi-static modeling approaches for PAs and DPDs are typically calculated using a least-squares method on a complex baseband input and output signals. The baseband empirical models can be converted to RF bandpass models by using carrier up-conversion. Carrier up-conversion is a complex multiplication, which exhibits no impact on the AM/AM and AM/PM nonlinear functions. Similarly, carrier down-conversion is another complex multiplication, which is independent of the applied modeling technique in RF power representation of communication signals.

This section describes a common computation of a quasi-static model using the first kernel of the Volterra series, and the conversion between the baseband and bandpass representation.
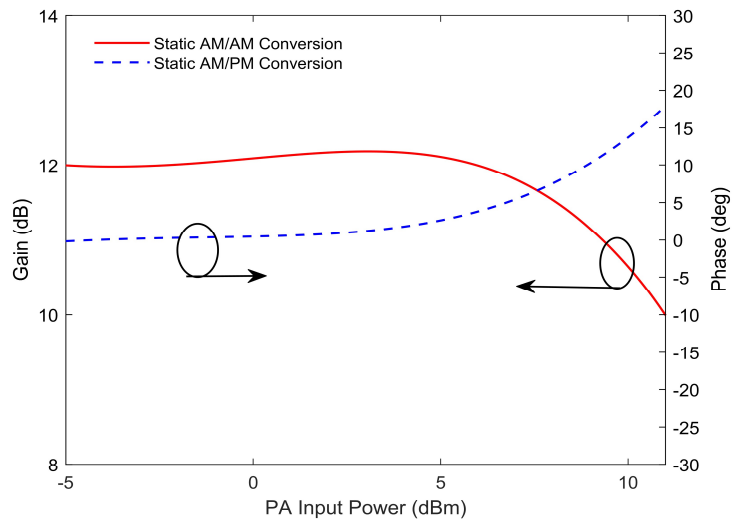
Figure 2.16 Typical static AM/AM and AM/PM conversions in PAs.

$$x_{RF}(t) = \Re\left\{x_{BB}(t)e^{j\omega_c t}\right\}$$ (2.63)

where $x_{RF}(t)$ is the PA bandpass input signal, $x_{BB}(t)$ is a complex baseband input signal, and ω_c is a carrier frequency for up-conversion. The operator $\Re\{\}$ refers to the real part of a complex term. Substituting the magnitude and phase of $x_{BB}(t)$ in Equation 2.63, results in:

$$x_{RF}(t) = \Re\left\{|x_{BB}(t)|e^{\angle x_{BB}(t)}e^{j\omega_c t}\right\}$$ (2.64)

$$x_{RF}(t) = |x_{BB}(t)|\cos(\omega_c t + \angle x_{BB}(t))$$ (2.65)

where $|x_{BB}(t)| = \sqrt{\left\{\Re\{x_{BB}(t)\}\right\}^2 + \left\{\Im\{x_{BB}(t)\}\right\}^2}$, and $\angle x_{BB}(t) = \tan^{-1}\left\{\dfrac{\Re\{x_{BB}(t)\}}{\Im\{x_{BB}(t)\}}\right\}$

The PA bandpass output signal $y_{RF}(t)$ is calculated using a simplified Volterra series in $x_{RF}(t)$

$$y_{RF}(t) = \Re\left\{\sum_{k=1}^{\infty}C_k\left|x_{BB}(t)e^{j\omega_c t}\right|^{k-1}\left\{x_{BB}(t)e^{j\omega_c t}\right\}\right\}$$ (2.66)

where C_k denotes the complex coefficients of the Volterra series. Substituting a polar representation on $x_{BB}(t)$ using magnitude and phase notation in Equation 2.66, results in the following:

$$y_{RF}(t) = \Re\left\{\sum_{k=1}^{\infty}C_k\left|x_{BB}(t)\right|^{k-1}\left|x_{BB}(t)\right|e^{j(\omega_c t + \angle x_{BB}(t))}\right\}$$ (2.67)

$$y_{RF}(t) = \Re\left\{f(|x_{BB}|)e^{j(\omega_c t + \angle x_{BB}(t) + g(|x_{BB}|))}\right\}$$ (2.68)

$$y_{RF}(t) = f(|x_{BB}|)\cos(\omega_c t + \angle x_{BB}(t) + g(|x_{BB}|))$$ (2.69)

where $f(.)$ refers to the AM/AM conversion, and $g(.)$ refers to the AM/PM conversion. The $f(.)$ and $g(.)$ are expressed, respectively as follows:

$$f\left(\left|x_{BB}(t)\right|\right) = \left|\sum_{k=1}^{\infty} C_k \left|x_{BB}(t)\right|^{k-1} \left|x_{BB}(t)\right|\right|$$ (2.70)

$$g\left(\left|x_{BB}(t)\right|\right) = \tan^{-1}\left\{\frac{\Re\left\{\sum_{k=1}^{\infty} C_k \left|x_{BB}(t)\right|^{k-1} \left|x_{BB}(t)\right|\right\}}{\Im\left\{\sum_{k=1}^{\infty} C_k \left|x_{BB}(t)\right|^{k-1} \left|x_{BB}(t)\right|\right\}}\right\}$$ (2.71)

A truncated nonlinear order can be chosen in the Volterra series instead of an infinite order in Equation 2.70 and Equation 2.71. The AM/AM and AM/PM nonlinear distortions are often represented using a signal constellation diagram of baseband input and output symbols. The AM/AM and AM/PM is another way of representing a complex signals error, which causes imbalance between the In-phase (I) and Quadrature-phase (Q) components of the baseband signal as shown in Figure 2.17.
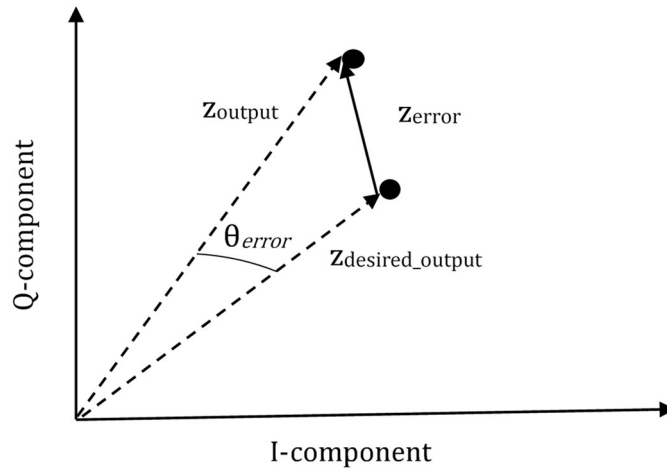
Figure 2.17 Impact of AM/AM and AM/PM distortions on baseband symbol's magnitude and phase.

2.5.   Dynamic AM/AM and AM/PM Distortion

Memory effects (i.e. time-delays) in RF PAs represent the variation of the nonlinear gain due to the frequencies of the PA input signal, the supply voltage, and chip temperature. Thus, PAs exhibit dispersion behavior in both AM/AM and AM/PM conversions (i.e. dynamic effect in the AM/AM and AM/PM conversions). Most of the memory effect is a result of many energy storage elements in the PA circuit, such as capacitors and inductors as simplified in Figures 2.18, 2.19. Hysteresis effects are normally classified according to the physical origin into electrical memory and thermal memory effects [1], [36]. RF matching and DC circuit biasing are two major causes of electrical memory. The thermal memory effect is a result of the dynamic variation in the IC chip temperature of PAs.

Memory effects of short-time constants cause static AM/PM distortions. On the other hand, the memory effects of long-time constants cause dispersion effects in both the
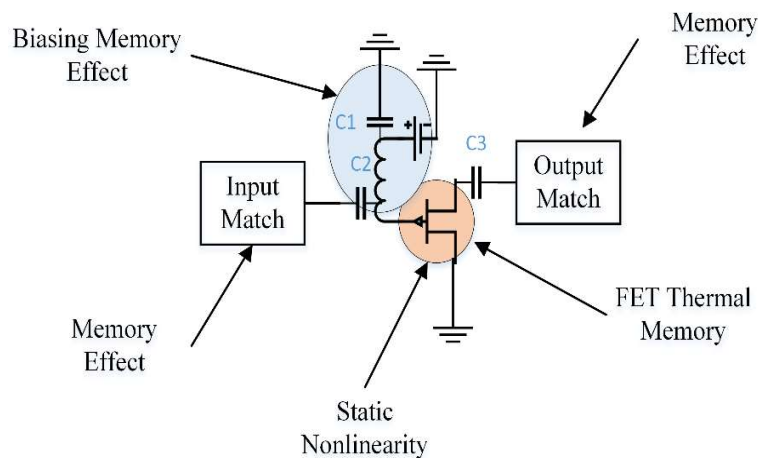
Figure 2.18 Simplified circuit illustrates the main memory components in PAs.

AM/AM and AM/PM distortions as shown in Figure 2.20. Therefore, the static AM/AM and static AM/PM conversions are one-to-one functions, and the dynamic AM/AM and AM/PM conversions are two-to-one functions due the effect of the memory distortion. The dynamic AM/AM conversion represents the combined impact of the static nonlinearity and memory effect as described by Equation 2.72. Similarly, the dynamic AM/PM conversion is described by Equation 2.73.

$$v_{out}(t) = A\left(v_{in}(t), \Delta t\right) \tag{2.72}$$

$$\psi(t) = \theta\left(v_{in}(t), \Delta t\right) \tag{2.73}$$

where $v_{in}(t)$ is the PA input amplitude, Δt is the delay variation due to the memory effect, $A(.)$ is the AM/AM function, and $v_{out}(t)$ is the PA output amplitude. $\psi(t)$ is the dynamic output phase, and $\theta(.)$ is the AM/PM function.

The effects of nonlinear dispersion represented by Equations 2.72 and 2.73 cause uncertainty and difficulty in predicting the PA output response. In other words, the PA output deviates from the static AM/AM and static AM/PM conversions as illustrated in Figure 2.20. This figure shows that the maximum nonlinear spread corresponds to the lower input amplitude. The memory effect can contribute to the spectral regrowth in the frequency domain, but it is very minor, especially in narrow-band wireless communications.
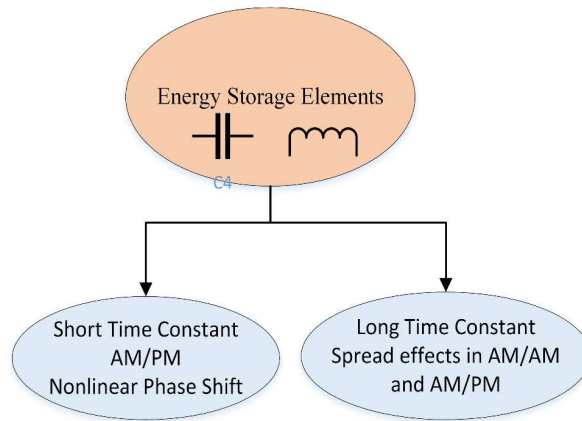
Figure 2.19 Modeling characteristics of memory effects in PAs.
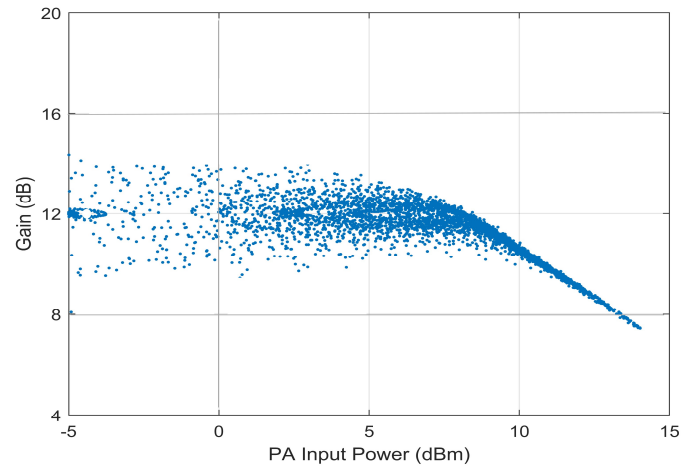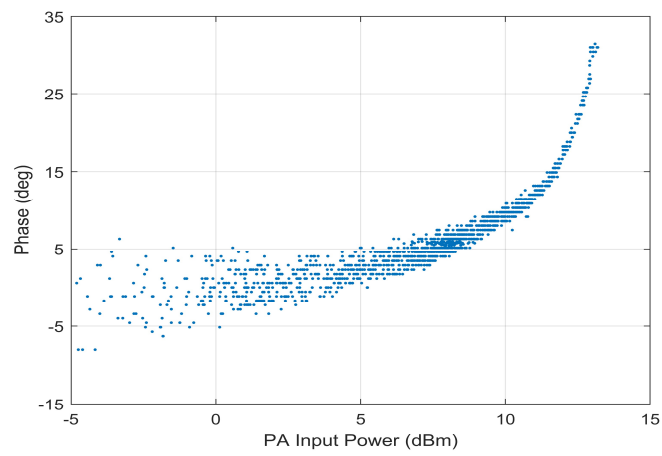
Figure 2.20 Dispersion effects in AM/AM and AM/PM conversions due to memory effects. (a) Dynamic AM/AM conversion. (b) Dynamic AM/PM conversion.

Chapter 3

Envelope Tracking System

3.1   Introduction

Controlling the power efficiency in PAs is a challenging task, because power efficiency is subject to the design aspects of PAs and applications (e.g. power efficiency degradation when operating the PAs on high PAPR signals). In general, the concept of enhancing power efficiency depends on minimizing the DC-supply power in PAs according to Equation 1.1. In other words, power efficiency enhancement techniques are developed to reduce the power losses in the PA circuit [8]. Several design approaches were presented in the literature for power efficiency enhancement. Examples of popular architectures include Doherty power amplifiers, envelope elimination and restoration amplifiers, and out-phasing power amplifiers [3]. Some of these techniques are complicated, and other techniques suffer from limitations in signal bandwidth, RF mismatch challenges, and high nonlinear distortion [12]-[14].

ET techniques gained significant interest in the recent research because of important advantages they perform to control the trade-off between the power efficiency and linearity, as well as the design flexibility in a multi-band wireless communication system. The implementation approach of ET is adopted in modern wireless cellular (e.g. Apple and Samsung electronics have used ET ICs in modern cellular handsets [37]). Various design improvements have been included recently to operate and linearize PAs in high bandwidth wireless communications and high PAPR signals for future wireless generations [10], [28].

51

The ET systems and digital predistortion are implemented using a combination of analog circuits and DSP systems. In this work, we use an ET experimental set-up consists of measurement equipment for evaluating both the modeling and linearization approaches. The typical ET PA structure, component functionality, and limitation challenges of each component are described in the next sections.

3.2 Envelope Tracking Architecture

The DC-supply voltage must be maintained close to or higher than the maximum required amplitude to avoid signal clipping near the saturation amplitude in normal operation of fixed-biased PAs. Hence, an ET system is an additional component for controlling the supply voltage in PAs. The supply voltage in the ET case varies dynamically along with the PA input amplitude. In other words, the primary concept in an ET system is to operate the PA at high efficiency by driving the operating region near the compression region, because the power efficiency is maximum in the compression region as presented in Chapter 1 [8], [38], [39].

An average ET system is another modified approach of the ET, which performs discrete-level ET instead of continuous tracking for wideband applications [17]. The ET system architecture consists of the following three main components: envelope detector, shaping function, and envelope modulator, as shown in Figure 3.1.
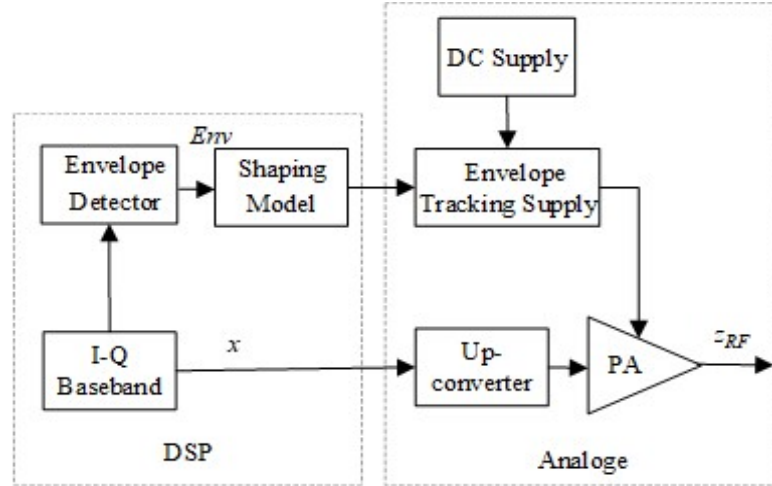
Figure 3.1 ET system architecture for power efficiency enhancement.

3.2.1 Envelope Detector

Envelope detectors are simple mathematical operations to which perform the following signal computation on the PA baseband input as:

$$\text{Env(t)} = \sqrt{I(t)^2 + Q(t)^2} \tag{3.1}$$

where Env(t) is the envelope signal magnitude, I(t) and Q(t) are the in-phase and quadrature-phase components of the PA input baseband signal.

3.2.2 Envelope Shaping Model

The shaping model is a mapping function between the instantaneous envelope amplitude and the required supply voltage to the PA drain/collector. The shaping function is the key element in ET system, and it controls the PA characteristics, such as power efficiency and linearity. Shaping functions have been recently deployed as an alternative

approach for linearizing the AM/AM characteristics of the ET PA [40]-[41]; however, shaping function-based linearization often leads to degradation in power efficiency, because of the existing trade-off between the power efficiency and linearity. Shaping functions are often combined with a hardware envelope modulator (e.g. Nujira ET commercial modulator) [8].

Discrete-level and slew-rate shaping functions have been utilized for dual-band and multiband wireless communication. Iso-gain shaping functions have been developed for linearity enhancement in PAs [40]-[42], and detroughing shaping functions are empirical models for high-power efficiency as described in Chapter 4. The detroughing is an exponential function consisting of two parameters, one parameter for setting the PA minimum supply voltage to avoid gain collapse, and the second parameter to set the maximum required supply voltage to the collector/drain [43].

A linear mapping between the envelope amplitude and supply voltage is another simple model in the implementation of ET systems. However, a problem of gain collapse often occurs at a low input amplitude [21]. Figure 3.2 illustrates different detroughing and linear shaping functions. Figure 3.3 shows an example of the supply voltage required for a PA using linear and detroughing shaping function scenarios. The detroughing shaping functions maintain a minimum of 1 volt on the PA drain/collector at lower input amplitudes, whereas the linear shaping drops near zero volts for a low input signal [43]. This research deploys a detroughing shaping function in software to achieve high power efficiency in the PA.
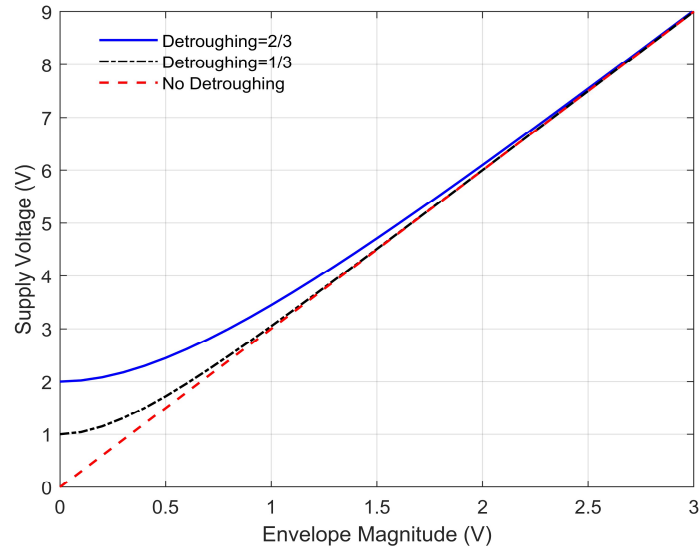
Figure 3.2 Linear and detroughing supply shaping functions using different shaping ratios.
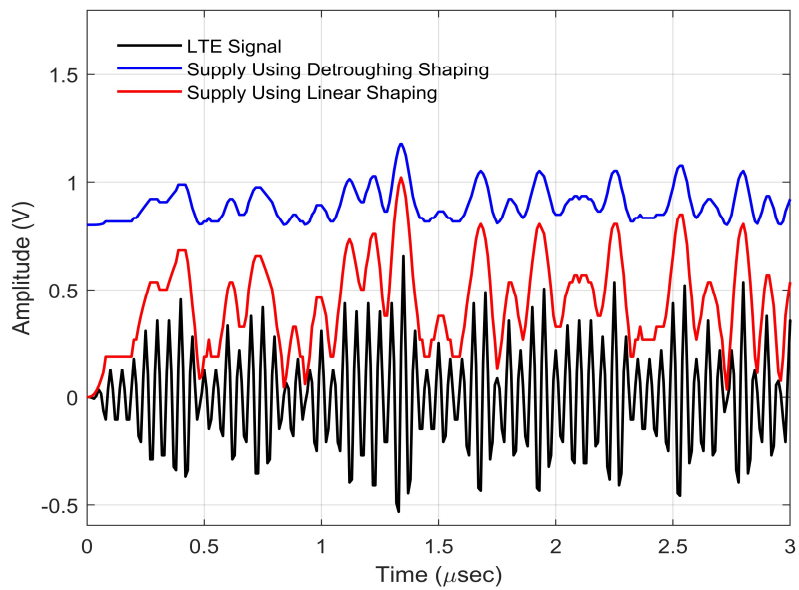
Figure 3.3 Dynamic Power supply voltage using two different shaping functions, detroughing and linear in the envelope tracking system.

3.2.3 Envelope Modulator

Envelope Modulator (EM) is an analog circuit device that is deployed to supply dynamic current to the PA transistor drain/collector. The EM is used to adjust the flow of the DC-supply current with respect to the amplitude of the shaped envelope voltage. The EM devices can be more complicated in high bandwidth and power applications, therefore, several state-of-the-art implementation techniques of EM have been proposed in the literature, such as DC/DC converters, hybrid envelope amplifiers, and envelope amplifiers.

The power efficiency of EM can affect the overall power efficiency of an ET PA. The overall power efficiency degrades when using low power efficiency EM devices. In addition, the linearity of ET systems can also be affected by the modulator distortion effects [17]. The high PAPR and bandwidth limitation in wireless signals are other design challenges in EM, because the envelope signals are normally several times higher in bandwidth than the baseband signal as demonstrated in the ET PA literature [42].

3.3 Power Efficiency Enhancement

Maximum power efficiency occurs near the compression region in constant-supply PAs [44]. Furthermore, the AM/AM conversion and compression region are affected by the variable-supply voltage scenario [19]. Therefore, the power efficiency is expressed as a function of the output amplitude and the supply voltage as depicted in Equation 3.2.

The supply voltage in the ET case is controlled by the envelope shaping function and the power efficiency function changes with respect to the supply variable and the PA input amplitude, as shown in Figure 3.4. The maximum power efficiency is obtained for a certain value of the output power and the supply voltage. In other words, the efficiency

must be optimized over two independent variables: PA output voltage (v_o) and the supply voltage (v_s).

$$\eta = E_f(v_o, v_s) \tag{3.2}$$

The power efficiency is a statistically non-deterministic function, because it depends on the output power, which is a random in communication signals as depicted in Equation 1.4. Thus, the maximum power efficiency can be derived analytically as follows:

1) Sweeping a tow-tone amplitude on the PA input for a specific DC supply.

2) Calculating the PA efficiency at each input amplitude.

3) Changing the DC supply voltage on the PA drain/collector.

4) Repeating step 1 and 2 for each supply voltage point.

5) Interpolating the results in step 4 to obtain the power efficiency versus the output power for each supply voltage (see Figure 3.4).

6) Specifying the optimal power efficiency with respect to the output power on each curve.

7) Interpolating the results in step 6 to obtain mapping between the output power and the required supply voltage for a maximum power efficiency.

The above approach normally results in an arbitrary function; therefore, the implementation using a look-up-table shaping function is a popular design structure in the ET system. The required dc-supply voltage is 4.5 V (black solid line in Figure 3.4) for a PA output peak power 25 dBm. This shows poor power efficiency corresponds to the low signal output power (less than 10 dBm), whereas in the ET case (dash and black line), the power efficiency is around 15% higher for a certain output power range.

The detroughing shaping function is another alternative approach for achieving high power efficiency using empirical functions instead of LUTs. Detroughing shaping is straightforward method, which requires adjustment of the detroughing ratio according to the specific PA knee voltage (V_{min}) and the maximum supply voltage (V_{max}) for the desired PA output power.
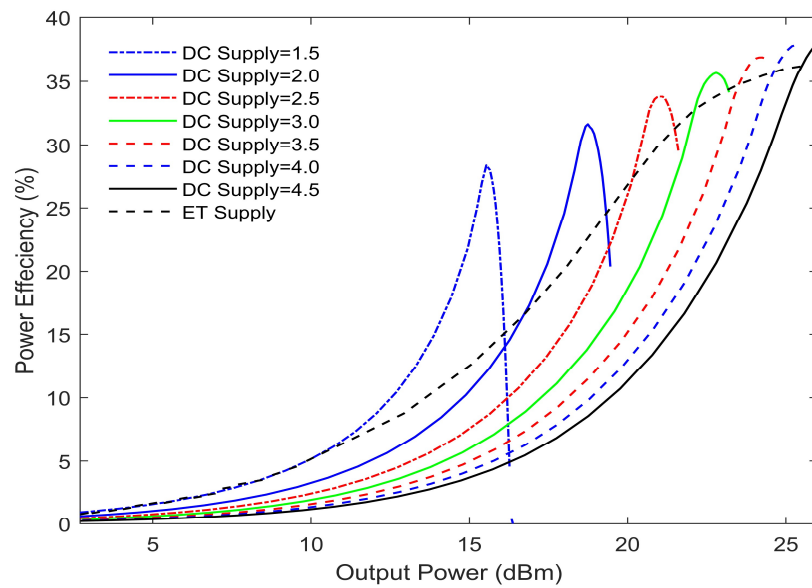
Figure 3.4 Power efficiencies at different supply voltages.

Chapter 4

Modeling Techniques for Envelope Tracking Power Amplifiers

4.1   Introduction

An accurate modeling of PA is required for predicting the nonlinear distortion effects in communication systems. PA models are used extensively to predict spectral distortion emissions due to nonlinear distortion. In particular, spectral emissions in wireless communications must comply with the telecommunication standards, such as lower channel interference in the adjacent channels [35]. Circuit model approaches for ET PA are complicated due to the complexity of ET operation. In addition to the computational complexity, a detailed design aspect of the circuit structure must be known before conducting any circuit analysis method.

Empirical and behavioral models are other low-complexity techniques, which are often deployed to estimate the nonlinear distortion effects in PAs. Behavioral models are basically mathematical functions, which express the statistical relationship between the PA output signal and both the input signal and variable supply voltage [1]. Behavioral models are often called black-boxes with input and output ports as shown in Figure 4.1. The main advantages of the behavioral models include a low computational-complexity, without a prior knowledge of the PA circuit topology or design. Finally, behavioral models can simplify the PA linearization models in the areas of DPDs.

Behavioral models are classified according to memory effects into statics, quasi-statics, and dynamics. Static models refer to only memoryless AM/AM conversions. The quasi-static models refer to modeling both memoryless AM/AM and AM/PM conversions.

Finally, the dynamic models consider both the memory AM/AM and memory AM/PM conversions. This dissertation uses the dynamic behavioral approach for better accuracy in modeling the ET PA.
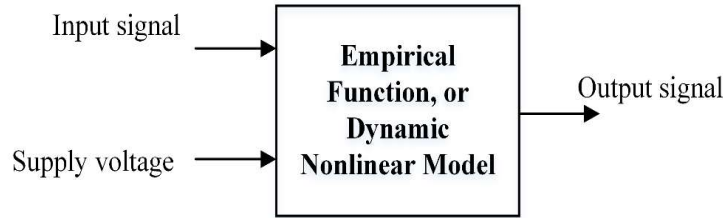
Figure 4.1 Black-box representation for behavioral modeling of ET PAs.

4.2   Literature Reviews on Modeling ET PAs

The internal circuit structure of the PAs is very complicated, because it consists of many linear and nonlinear discrete elements. In addition, the circuit parasitic effect and transistors' junctions pose additional challenges when operating PA under specific signals.

As we discussed in the previous chapters, the amount of nonlinearity and memory effects in PAs are device and signal dependent. For example, signal bandwidth and PAPR have significant effects on both the circuit capacitance and inductance. Therefore, several different behavioral techniques have been presented in literature to address the distortion effects in PAs [45].

Behavioral models based on polynomial and binomial series are the most widely presented and studied kernels in the modeling literature, including the Taylor series, binomial series, Volterra series, and other modified special cases of Volterra models. These

models provide high flexibility in selecting nonlinear orders for the model optimal accuracy. Other PA models are calculated using a specific mathematical formula, such as the Cann model, the Saleh model, and the Ghorbani model. These models require fewer parameters when compared to the typical series expansion; however, the models' accuracies are limited for a specific PA due a fixed number of coefficients and function structures.

Artificial neural networks and Bayesian estimation are also presented in the modeling literature concerning PAs [46]. However, these models exhibit high computation and number of coefficients similar to the Volterra and polynomial series. In fact, memory polynomial series exhibit lower computational-complexity than the neural networks. Furthermore, polynomial coefficients can be calculated easily using a least-squares method, and can be built easily in a DSP using blocks of product and summation functions. On the other hand, neural networks require several nonlinear functions (e.g. sigmoid decision) in addition to many blocks of products and summation operations.

Most of the presented behavioral models in the literature are implemented in a time domain using PA measurement or simulation data. However, the recent X-parameters technique was proposed by Agilent technologies to model the PA circuit in a frequency domain [47]. The X-parameters are super-set equations of S-parameters which are widely used in RF circuit design for PA input and output matching.

An overview of the state-of-the-art ET PA models' structure and computational cost are presented in the next sections.

4.3   Dual-Input Behavioral Models

The supply voltage exhibits significant effects on the PA characteristics, including gain and saturation amplitude. In addition, the variable supply voltage on the drain/collector can affect both the linearity and efficiency of the PAs as described earlier in Chapter 3.

Figure 4.2 illustrates 2D-plot variation of the PA output amplitude versus both the magnitude of the input signal using two-tone signal and variable supply voltage. In other words, the ET technique is a special case of a stand-alone PA with a variable supply. For that reason, two types of behavioral models are proposed in ET PA modeling literature: SISO and DISO. The SISO model structure characterizes the nonlinear distortion in both AM/AM and AM/PM conversions as a function of one independent variable, the input signal.

The DISO models characterize the nonlinear distortion in both AM/AM and AM/PM conversions as functions of two independent variables: input signal and supply voltage [8], [21], [22]. A simple architecture of ET PA in Figure 4.3 illustrates two reference planes describing the modeling difference between SISO and DISO architectures.

The effect of the dynamic supply voltage on the PA nonlinearity has been widely discussed and investigated in the ET PA modeling literature [19], [29]. The DISO modeling approaches have become very popular and accurate modeling techniques account for a time-varying envelope signal, especially in a slew-rate ET scenario using a modified envelope waveform. Therefore, a DISO modeling approach is adopted in this research for modeling the ET PAs. The accuracy and complexity trade-off between the DISO and SISO

models are important properties for designing an efficient DPD technique for linearizing

ET PAs.
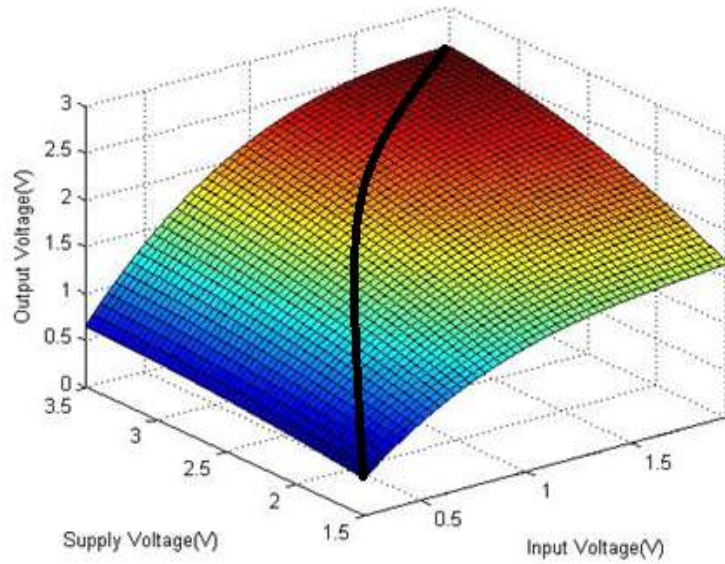
Figure 4.2 PA output voltages versus the swept amplitude of the input and supply voltages. The black curve represents the output voltage of ET case.
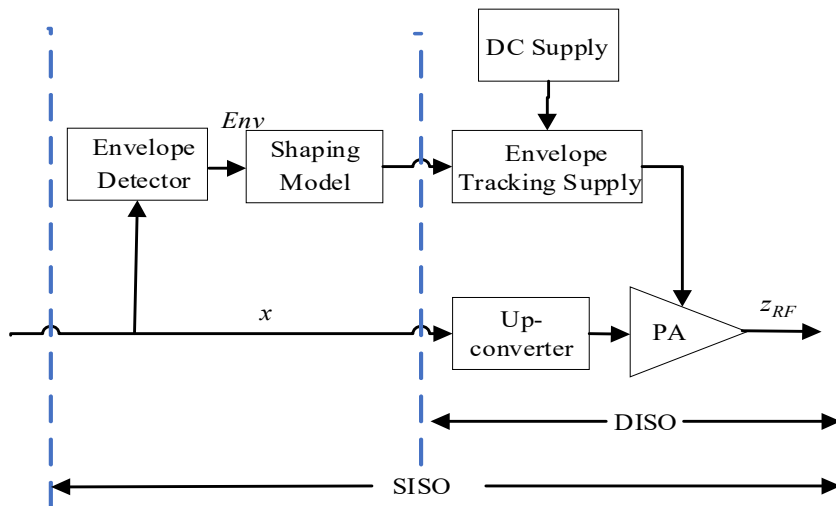
Figure 4.3 DISO and SISO output reference planes for modeling the ET PA.

4.3.1 Two-Dimensional Look-up-Tables

Look-up-Tables (LUTs) are extensively used in signal theory for approximating any arbitrary function. LUT technique is used to map data between input and output pairs [39], [48]. Two independent LUTs are required for quasi-static modeling: one LUT for static AM/AM and another LUT for static AM/PM. LUTs are typically implemented independently in software/hardware circuits. Although LUTs are considered simple modeling approaches, it is difficult to use LUTs for modeling and memory behavior effects in ET PA.

The 2D-LUT modeling approach was recently proposed for modeling the ET PA. In this approach, the PA's gain and phase are modeled independently, such that the output signal is a function of both the input and supply voltage. In fact, this technique is based on

a two-directions search method (i.e. x-y plane) in estimating the PA output values [39]. The quasi-static LUT model representation is

$$z = x. G\{|x|, v_{en}\} e^{j\{\theta(|x|, v_{en})\}}$$
(4.1)

where x and z are the ET PA complex input and output signals, respectively. $G(.)$ and $\theta(.)$ are the gain and phase functions, respectively, of the instantaneous input amplitude and the supply voltage.

The 2D-LUT is a computationally less expensive approach for modeling and digital predistortion of ET PAs. However, LUTs often use approximation of linear interpolation, significantly degrading the ET PAs model smoothness and accuracy. Figure 4.4 shows an implementation structure of a 2D-LUT model in both AM/AM and AM/PM conversions. The steps of interpolation approximation in the 2D-LUT model specify the size of the LUT model, which might significantly reduce the modeling accuracy. Hence, a large size memory chip is required to store many data samples for achieving high resolution interpolation.
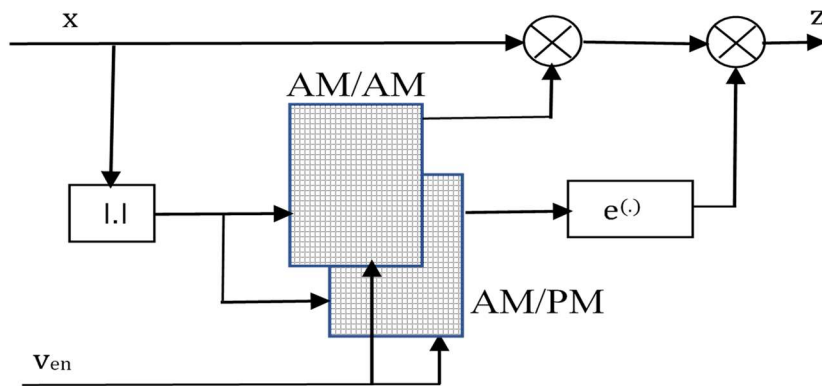
Figure 4.4 The 2D-LUT modeling structure for the ET PA using a DISO approach.

4.3.2 Cann Model

The Cann model is an empirical function which was proposed by A. Cann in 1980. It is a memoryless AM/AM behavioral function for a constant-supply SSPA. The expression of the Cann model is

$$y_{RF}(t) = \frac{g \cdot x_{RF}(t)}{\left(1 + \left(\frac{g \cdot x_{RF}(t)}{L}\right)^s\right)^{\frac{1}{s}}} \qquad (4.2)$$

where $x_{RF}(t)$ is the PA input amplitude, $y_{RF}(t)$ is the PA output amplitude, g is the small signal gain, L is the saturation level, and s is the model sharpness. An extension of the Cann model was proposed in [21], [29] for the ET PA by expressing the model parameters as a function of the supply voltage

$$y_{RF}(t) = \frac{g(v_d) x_{RF}(t)}{\left(1 + \left(\frac{g(v_d) x_{RF}(t)}{L(v_d)}\right)^{s(v_d)}\right)^{\frac{1}{s(v_d)}}} \qquad (4.3)$$

where V_d is the drain/collector voltage of the PA. The parameters of the Cann model are typically calculated using a two-tone test by sweeping the supply voltage. Nonlinear least-squares method can also be used for estimating the model parameters [8]. The complexity for parameter estimation and the difficulty of inverting the model function are two disadvantages of the Cann model for ET PAs.

4.3.3 Binomial Model

Binomial Models (BM) are power series, sum of two independent variables [21] as in Equation 4.4. The expansion of the binomial series represents a sum product of one

66

variable with increasing order and another variable with decreasing order as illustrated in the following expansion:

$$(x+y)^n = \sum_{k=0}^{\infty} \binom{n}{k} x^{n-k} y^k$$

$$= \binom{n}{0} x^n y^0 + \binom{n}{1} x^{n-1} y^1 + \binom{n}{2} x^{n-2} y^2 + \ldots + \binom{n}{n-1} x^1 y^{n-1} + \binom{n}{n} x^0 y^n$$

(4.4)

where x and y are the two independent variables, n is the order of the sum terms. The binomial model in Equation 4.4 is a static. Therefore, a new dimension variable (m) can be included to model the memory behavior effect for ET PAs [21] as in:

$$z_{BB}(n) = \sum_{k=0}^{N} \sum_{j=0}^{k} \sum_{m=0}^{M} a_{k,m} \, x^{k-j}(n-m) \, v_{ven}^{j}(n-m)$$

(4.5)

where x and v_{en} are the complex baseband input and envelope signals, respectively, z is the PA complex baseband output, $a_{k,m}$ are the model coefficients, N is the maximum nonlinear order, and M is the memory depth. Equation 4.5 can be expressed in a matrix form as follows:

$$z = Ba$$

(4.6)

where $z=[z(0),z(1),\ldots\ldots.z(L)]^T$ is an $(L+1)\times 1$ vector representing the (L+1) samples of the output signal, $a = [a_{00}, a_{01}, \ldots, a_{0M}, \ldots\ldots, a_{N0}, \ldots\ldots, a_{NM}]^T$ is a $((N+1)(M+1))\times 1$ vector of the model coefficients and **B** is a model matrix formulated as

$$B = [x^N(n) v_{en}^0(n), \ldots, x^N(n-M) v_{en}^0(n-M), \ldots, x^{N-1}(n) v_{en}^1(n), \ldots, x^0(n-M) v_{en}^N(n-M)]$$

The BM number of coefficients are

$$N_{coef} = \frac{(M+1)(N+1)(N+2)}{2} - M \qquad (4.7)$$

4.3.4 Volterra Model

The Volterra model is a multi-dimensional polynomial series, which can model complicated nonlinear system with memory effects. However, the accuracy of the Volterra model degrades when modeling strong nonlinear memory effects, as described in the state-of-the-art model evaluation [20]. The Volterra kernels are combinations of the Taylor series and multi-dimensional convolutions. Thus, the model output is a power series expansion of the input sample and the time delayed input samples at different nonlinear orders, as illustrated

$$y(n) = \sum_{m=0}^{M} h_1.x(n-m) + \sum_{m_1=0}^{M} \sum_{m_2=0}^{M} \sum_{m_3=0}^{M} h_3(m_1, m_2, m_3)x(n-m_1)x(n-m_2)x(n-m_3)$$

$$(4.8)$$

$$+ \sum_{m_1=0}^{M} \sum_{m_2=0}^{M} \sum_{m_3=0}^{M} \sum_{m_4=0}^{M} \sum_{m_5=0}^{M} h_5(m_1, m_2, m_3, m_4, m_5).\prod_{i=1}^{5} x(n-m_i) + ...$$

where $x(n)$ and $y(n)$ are the input and output signals, respectively, and h_1, h_3, h_5 are the coefficients of Volterra kernels. M is the model memory depth. The number of Volterra coefficients grows exponentially as the model's nonlinear order and memory depth increases. The high correlation among Volterra coefficients is a common problem in Volterra series, which causes high redundancy and numerical instability in coefficients estimation. Thus, Volterra series is not a practical modeling approach for PAs and DPDs.

4.3.5 Dual-Input Memory Polynomial Model

The Memory Polynomial Model (MPM) was derived from the first order Volterra kernel for simplicity purposes, since Volterra models are computationally expensive. MPMs have become a very popular and widely deployed modeling approach for PAs. The Dual-Input Memory Polynomial Model (2D-MPM) is an extended version of the MPM for ET PAs of two independent variables.

The 2D-MPM is similar to MBM in Equation 4.5. However, the MBM consists of one nonlinear order, whereas the 2D-MPM consists of two nonlinear orders. Another difference between the 2D-MPM and MBM is the kernel structure, which exhibits high impact on the model accuracy [49]. The 2D-MPM expression for ET PA is

$$z_{BB}(n) = \sum_{j=1}^{N}\sum_{k=0}^{L}\sum_{m=0}^{M} c_{k,j,m}\, x(n\text{-}m)\big|x(n\text{-}m)\big|^{j-1}\, v_{en}^{\,k}(n\text{-}m) \tag{4.9}$$

where $x(n)$ and $v_{en}(n)$ are the complex baseband input and modulated supply voltage, respectively. $z_{BB}(n)$ is the PA complex baseband output, $c_{k,j,m}$ are the model coefficients, N is the maximum nonlinear order of the variable x, L is the maximum nonlinear order of the variable v_{en}, and M is the memory depth. The matrix form of Equation 4.9 is

$$\mathbf{z} = \mathbf{Pc} \tag{4.10}$$

where $\mathbf{z}=[z(0),z(1),\ldots\ldots.z(L)]^{T}$ is an $(L+1)\times 1$ is a vector representing the $(L+1)$ samples of the output signal, $\mathbf{c} = [c_{0,1,0}, c_{1,1,0},\ldots, c_{L,N,M}]$ is a $(L(N+1)\,(M+1))\times 1$ vector of the model coefficients, and $\mathbf{P}$ is a model matrix which is formulated

$$\mathbf{P} = [x(n),\ldots, x(n\text{-}M),\ldots, x(n)\big|x^{N\text{-}1}(n)\big|v_{en}^{0}(n),\ldots, x(n\text{-}M)\big|x^{N\text{-}1}(n\text{-}M)\big|v_{en}^{L}(n\text{-}M)] \tag{4.11}$$

The 2D-MPM number of coefficients is

$$N_{PM} = (N)(L+1)(M+1) \qquad (4.12)$$

4.3.5.1 Complexity of Power Series Models

Most of the power series models consist of a kernels structure, allowing efficient implementation using DSP. The series number of coefficients is often used for evaluating the model complexity. The high number of coefficients in power series models leads to a higher number of Float Point Operation (FLOP) in system implementation. Furthermore, the required number of the model parameters depends specifically on the nonlinearity of PAs (e.g. weak nonlinearity normally leads to a lower number of coefficients compared to the strong nonlinearity PAs). The power series kernels structure, such as binomial and polynomial terms can also impact the model accuracy when used for the ET modeling case. The high PAPR in OFDM signals can increase the nonlinear distortion in PAs, because the high PAPR signals can derive PAs to the compression region, thus a power series of high order is typically needed to characterize the strong nonlinearity in PAs. The slew-rate and discrete shaping function in ET system can increase both the distortion effect and modeling complexity [48], [50]. Here we compare the accuracy and complexity using the state-of-the-art series kernels in evaluating model accuracy with respect to the model number of coefficients. A dual-input static (memoryless) representation for ET PA is used for the model evaluation. Table (4.1) presents the model structure and the required number of coefficients for binomial, 2D-polynomial, and 2D-Taylor models of the state-of-the-art behavioral modeling of the ET PAs [49].

Table (4.1) Comparison in series kernels and number of coefficients for dual-input behavioral models.

Model	Model Formula	Model Number of Coefficients
Binomial	$z_{BB}(n) = \sum_{k=0}^{N} \sum_{j=0}^{k} c_{k,j}\, x^{k-j}(n)\, v_{en}^{\ j}(n)$	$\dfrac{(N+1)(N+2)}{2}$
2-D Polynomial	$z_{BB}(n) = \sum_{j=1}^{N} \sum_{k=0}^{L} c_{k,j}\, x(n)\big|x(n)\big|^{j-1}\, v_{en}^{\ k}(n)$	$(N)(L+1)$
2-D Taylor	$z_{BB}(n) = \sum_{k=0}^{N} \sum_{j=0}^{L} c_{k,j}\, x^{k}(n)\, v_{en}^{\ j}(n)$	$(N+1)(L+1)$

4.3.5.2 Evaluation of Model Estimation

Each estimation method using the least-squares exhibits bias and variance in data modeling. Bias and variance are two important criteria for evaluating the estimator performance. A model of low variance and small bias is desired for optimal accuracy. The estimator bias and variance are highly affected by the model kernels structure and the total number of data samples used in the estimation. For instance, series expansion, such as MPM and BM show lower model accuracy for predicting the dynamic nonlinearity at low number model coefficients. On the other hand, overfitting is another problem when using a large number of model coefficients. The noise in data modeling and memory effects increases the model estimation errors at high nonlinear orders.

71

The underfitting is another problem in estimating MPM and MBM when the model prediction fails to capture all the nonlinear features of the measurement data. The underfitting is often occur when a low number of coefficients are used in model estimation, therefore, this can degrade the model performance in capturing all the nonlinear features of PAs.

In the statistical theory, the problem of underfitting and overfitting is subject to the existing trade-off between the bias and variance in the estimator. While low variance and high bias is a common problem of underfitting estimation, the drawback of the overfitting estimation includes the high variance and low bias. Thus, it is important to adjust the trade-off between the bias and variance for high accuracy model prediction. It was shown in the literature each model reaches optimal accuracy at a certain number of coefficients.

4.4   Experimental Results

The measurement architecture of ET system was implemented as shown in Figure 4.5. This set-up consists of the Keysight E4438C Vector Signal Generator (VSG), which was fed to the ZFL-1000LN RF power amplifier, and the Keysight 33522B Arbitrary Waveform Generator (AWG), which was fed to the envelope modulator (THS3120). Both the RF signal generator and the waveform generator were connected and controlled by MATLAB software from a desktop computer [49].

The PA was driven by 10,000 symbols of LTE-downlink baseband signal from a signal generator. A detroughing shaping function was coded in MATLAB, before it was fed to AWG. The output signal of the PA was demodulated using a Tektronix signal analyzer and exported to MATLAB in a complex discrete baseband format. The acquired

data of the PA input, envelope waveform, and output signals are synchronized in MATLAB using a cross-correlation function.

A DC power supply with a current meter was used to feed supply voltage to both the main PA and the envelope amplifier. The PA supply current was 60 mA without using the envelope modulator, and it was dropped to 50 mA when the envelope modulator was applied; hence the reduction in power dissipation due to the ET system is

$$P_{enh} = I_{enh} \times V_{DC} \qquad (4.13)$$

$$P_{enh} = (60 - 50) \times 15 = 150\,\text{mw}$$

where P_{enh} represents the power enhancement due to the ET system, I_{enh} is the drain current reduction, and V_{DC} is the power supply voltage. The power efficiency enhancement using the ET system is

$$\eta_{enh} = \frac{P_{enh}}{P_{DC}} = \frac{150}{15 \times 60} = 16\%$$
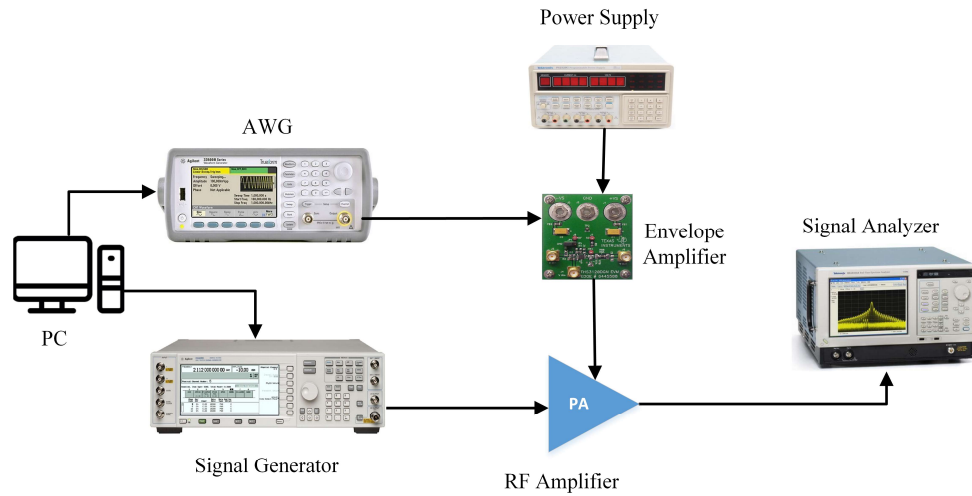
Figure 4.5 Measurement set-up used for the ET PA.

Three different state-of-the-art power series models, binomial, 2D-polynomial, and 2D-Taylor series, are evaluated for accuracy and complexity using the measurement data acquired from the experiment on the ET PAs. The model coefficients are calculated using the least-squares method as in Equations (4.14) and (4.15) for binomial and 2D-polynomial models, respectively.

$$\mathbf{a} = (\mathbf{B^H B})^{-1} \mathbf{B^H z} \tag{4.14}$$

$$\mathbf{c} = (\mathbf{P^H P})^{-1} \mathbf{P^H z} \tag{4.15}$$

where $\mathbf{(.)^H}$ denotes the Hermitian matrix. The measured and modeled AM/AM conversions of the 2D-Taylor, binomial, and 2D-polynomial models are illustrated in Figure 4.6. These results show that both 2D-Taylor and binomial models are slightly offset from the measurement data point at the lower input amplitude region. On the other hand, the 2D-
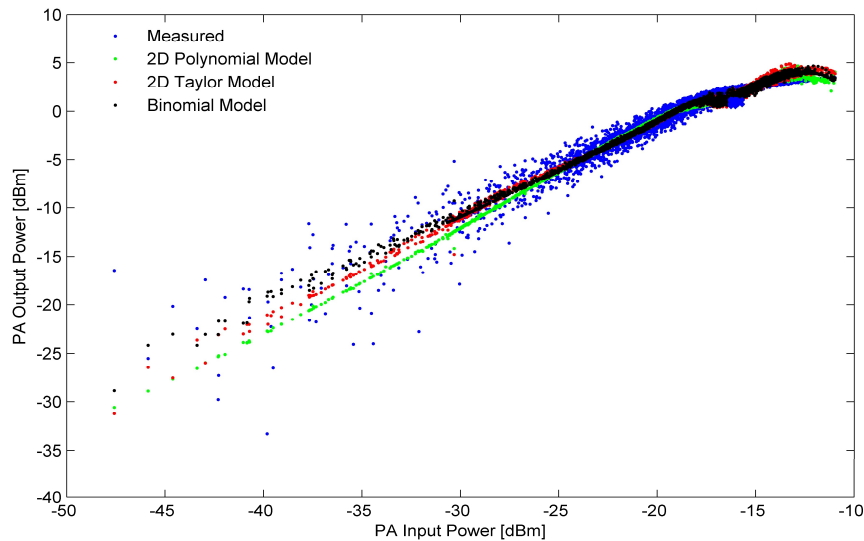
Figure 4.6 Measured and modeled AM/AM conversions of ET PA using different modeling approaches.

polynomial model shows better model accuracy and is symmetrical in the regions close to the mean of the measurement points.

The calculated NMSE and ACEPR for different model nonlinear orders are shown in Table (4.2). The optimal model accuracy in NMSE and ACEPR occurs at different nonlinear orders of each model as illustrated in Figure 4.7. The calculated results show a round 2 dB NMSE improvement in the 2D-polynomial compared to the binomial model. Therefore, the kernel type of 2D-polynomial $\{x[n]|x[n]|^{j-1}[n]v_{env}^{k}[n]\}$ reflects well with the nonlinear characteristics of the ET PAs, and better accuracy than the Taylor kernel type $\{x^{j}[n]v_{env}^{k}[n]\}$ [49].

Table (4.2) Accuracy comparison results of the behavioral modeling versus model number of coefficients.

Model	Nonlinear Order	Number of Coefficients	NMSE (dB)	ACEPR (dB)
Binomial	Q=3	10	-31.5	-40.2
	Q=4	15	-32.2	-40.5
	Q=5	21	-33.3	-41.8
	Q=6	28	-33.7	-42.4
2D-Polynomial	N=5, M=1	10	-33.5	-41.8
	N=5, M=2	15	-34.3	-42.6
	N=7, M=2	21	-34.6	-42.9
	N=7, M=3	28	-35.4	-43.7
2D-Taylor	N=4, M=1	10	-32.3	-41.1
	N=4, M=2	15	-32.6	-41.4
	N=6, M=2	21	-34.2	-42.7
	N=6, M=3	28	-34.5	-43.2

4.5 Digital Predistortion Results

Three different static models of DPD using 2D-Taylor, binomial, and 2D-polynomial series are calculated using an indirect-learning approach, as depicted in Figure 4.8. This figure shows that the DPD identification block is supplied by the same signal measurement from the PA input, output, and envelope signals. A least-squares method is used to calculate the model coefficients as follows:

$$\mathbf{d} = (\mathbf{W}^H \mathbf{W})^{-1} \mathbf{W}^H \mathbf{q} \tag{4.16}$$

where **d** is a column vector of the DPD coefficients, **q** is a column vector of the PA input signal, and **W** is the model matrix, which is formulated from the PA output and supply voltage. The DPD evaluation in ACPR and number of coefficients for BM, 2D-PM, and 2D-TP are depicted in Table (4.3).

The DPD comparison results in PSD using three-different linearization approaches are shown in Figure 4.9 for the same model number of coefficients. This figure shows that the 2D-polynomial model exhibits a better linearization capability for mitigating the nonlinear distortion in the ET PA than the 2D-Taylor and binomial models.
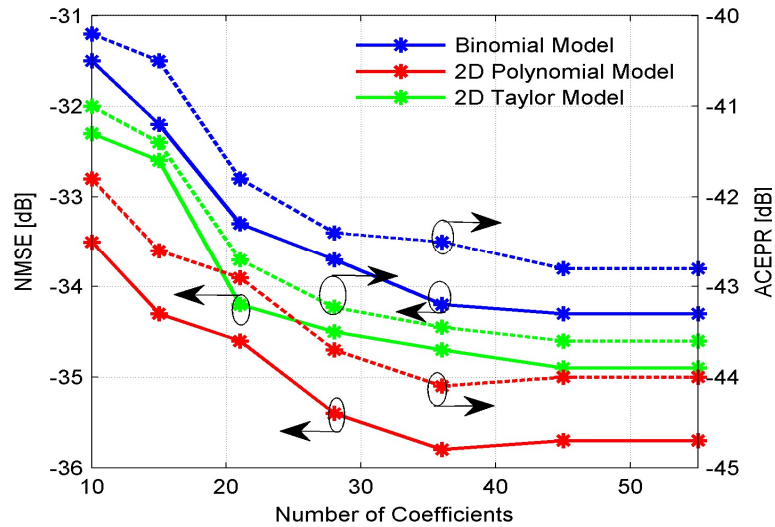
Figure 4.7 Comparison of the modeling accuracies in NMSE (continuous traces) and ACEPR (dotted traces) versus model number of coefficients.
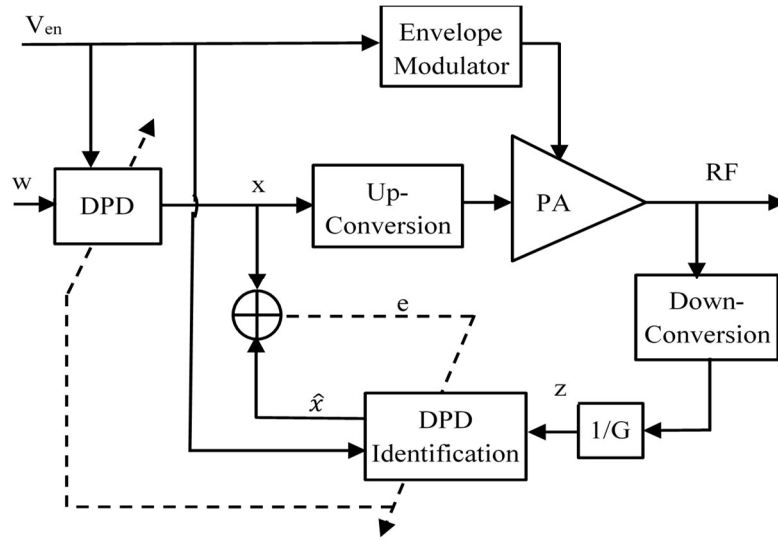
Figure 4.8 Indirect learning approach for modeling the 2D-DPD.

Table (4.3) NMSE and ACPR comparison results for different DPD models.

Case	Nonlinear Order	Model Number of Coefficients	NMSE (dB)	ACPR(dB) -/+4MHz
PA Input	*	*	*	-58.3/-57.2
PA Output	*	*	*	-23.1/-24.7
PA with BM DPD	Q=6	28	-29.5	-43.2/-41.6
PA with 2D-PM DPD	N=7, M=3	28	-31.6	-48.4/-47.8
PA with 2D-TP DPD	N=6, M=3	28	-30.3	-45.1/-44.6
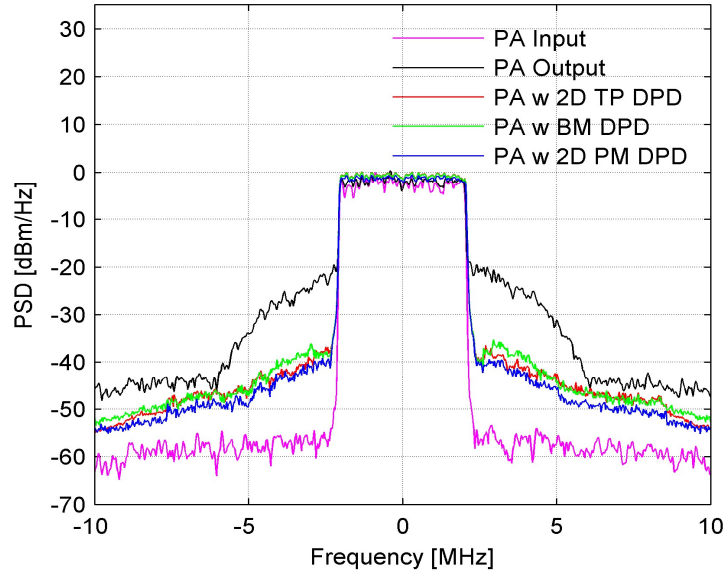
Figure 4.9 Normalized power spectrum density using static 2D-DPD models.

4.6 Dual-Input Modeling Approach

An evaluation comparison for the state-of-the-art behavioral models have been presented in the previous section. In this section, an approach for modeling and digital predistortion of the ET PA is develops using behavioral modeling of a higher accuracy and lower number of coefficients.

Both AM/AM and AM/PM conversions cause statistically independent nonlinear distortion behavior in PAs, as described earlier in Chapter 2. Hence this work proposes a new approach for optimizing the model accuracy of the AM/AM and AM/PM conversions independently and then combining these models using a complex polar representation. The modulated supply voltage of ET PA is another important effect which is considered in modeling the AM/AM and AM/PM conversions. The proposed approach in this section takes into account the dynamic variation in both the AM/AM and AM/PM nonlinearities

due to the memory effects, as discussed earlier in Section 2.5. A complex representation of the ET PA output in terms of both AM/AM and AM/PM functions is

$$z = f_{AM}(x, v_{en})e^{j(f_{PM}(x,v_{en})+\angle x)} \tag{4.17}$$

where x is the ET PA complex input signal, v_{en} is the modulated supply voltage, and z is the ET PA output signal in a complex baseband form, which is acquired from the PA after RF signal down-conversion as shown in Figure 4.10. $f_{AM}(.)$ and $f_{PM}(.)$ are the AM/AM and AM/PM functions, respectively. The operator $\angle(.)$ denotes the phase of a complex variable x. Equation 4.17 can be expressed in terms of magnitude and phase variables, respectively as follows:

$$y_d = |z| = f_{AM}(x, v_{en}) \tag{4.18}$$

$$\theta_d = f_{PM}(x, v_{en}) \tag{4.19}$$

where y_d is the magnitude of the output signal z, and θ_d is the ET PA phase deviation, as a function of x and v_{en}. A simplified block diagram in Figure 4.11 shows a block diagram of the overall model architecture using independent AM/AM and AM/PM nonlinear functions. The AM/AM and AM/PM blocks are two independent behavioral models for ET PA.
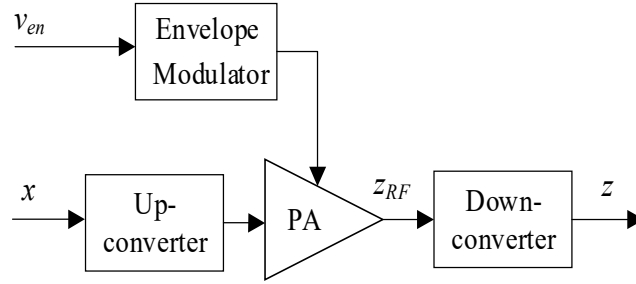
Figure 4.10 Block diagram of the baseband equivalent three-port representation for PA.
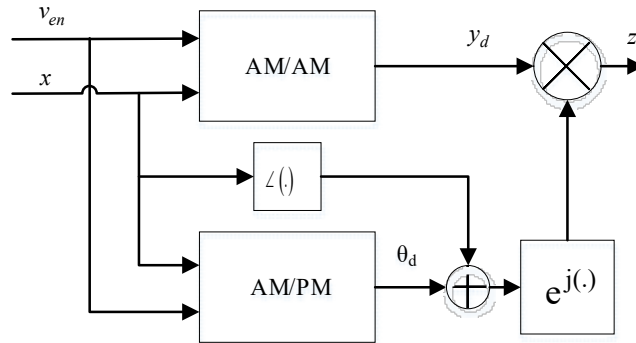
Figure 4.11 System architecture of the proposed model for the ET PA.

4.7   Extended Saleh AM/AM Model

The Saleh model was proposed in 1981 to characterize the static AM/AM and AM/PM nonlinear conversions for TWT PA using two independent functions. The Saleh model is a simple empirical SISO function of two parameters [51]. The Saleh AM/AM model for a constant-supply PA is

$$y = \frac{|x| \alpha}{1 + |x|^2 \beta} \qquad (4.20)$$

where x is the complex baseband input signal, y is the equivalent-baseband output amplitude, α and β are the model parameters, which can be calculated using a linear regression or nonlinear estimation on x and y data obtained from PA simulation or measurements. The Saleh model parameters α and β specify the PA's gain and saturation level.

The saturation voltage of the Saleh model is calculated by taking the derivative of Equation 4.20

$$argmax_{x}\left\{\frac{\alpha x}{1+\beta x^2}\right\} \Rightarrow \frac{d}{dx}\left\{\frac{\alpha x}{1+\beta x^2}\right\} = 0 \tag{4.21}$$

Solving Equation 4.21, results in the maximum input amplitude as

$$x_{max} = \frac{1}{\sqrt{\beta}} \tag{4.22}$$

Substituting Equation 4.22 into Equation 4.20, results in

$$y_{max} = \frac{\alpha}{2\sqrt{\beta}} \tag{4.23}$$

where y_{max} is the output saturation amplitude. The parameter α is proportional to the PA small signal gain, and the parameter β is inversely proportional to the PA saturation level.

The accuracy limitation of the Saleh model near the saturation region and SISO model structure makes the model inappropriate for ET PAs. Hence, this dissertation presents two extensions to optimize the accuracy of the Saleh model for modeling ET PAs while maintaining the model simplicity. The first proposed extension consists of model conversion from SISO to DISO structure. The hysteresis effects in amplitude and phase

conversions are modeled using the second extension. [27].

The coefficients of the Saleh model control the shape of a static AM/AM curve, which depends on the PA specifications, such as gain, saturation level, and supply voltage, and other factors, including the PA topology, transistor type, and operating frequency range. The coefficients of the Saleh model are used in the literature as a function of two independent variables, input amplitude and operating frequency for modeling a frequency dependent nonlinearity [51].

The PA characteristics in the AM/AM and AM/PM nonlinearities change significantly with respect to the supply voltage, causing a significant variation in the magnitude of the Saleh coefficients. Hence, a new relationship of the Saleh coefficients with respect to the supply voltage is described in this chapter.

A two-tone test was implemented by sweeping the amplitude of the two-tone for each supply voltage. The AM/AM and AM/PM Saleh functions are calculated using the nonlinear least-squares method in MATLAB. Figure 4.12 and Figure 4.13 show the variations in the slope and saturation level of the Saleh model for different supply voltage. Therefore, the Saleh parameters are supply voltage- and input signal amplitude- dependent. Thus, the Saleh parameters are functions of the modulated supply voltage for the ET PA case [27].
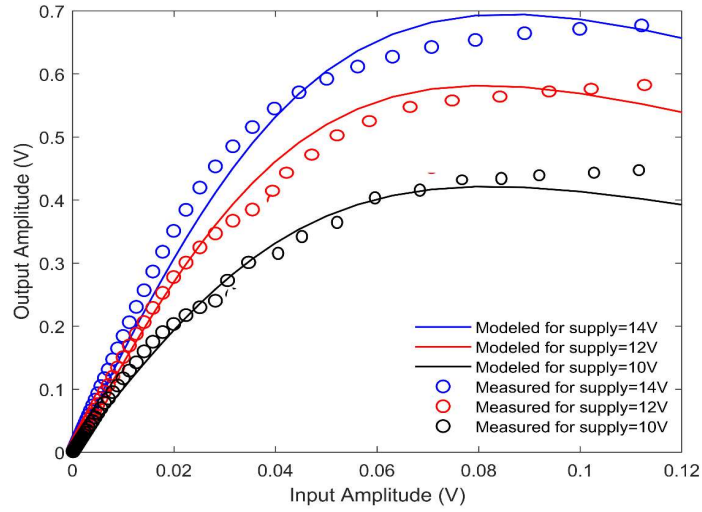
Figure 4.12 PA measured and modeled results of the AM/AM conversion for different supply voltages.
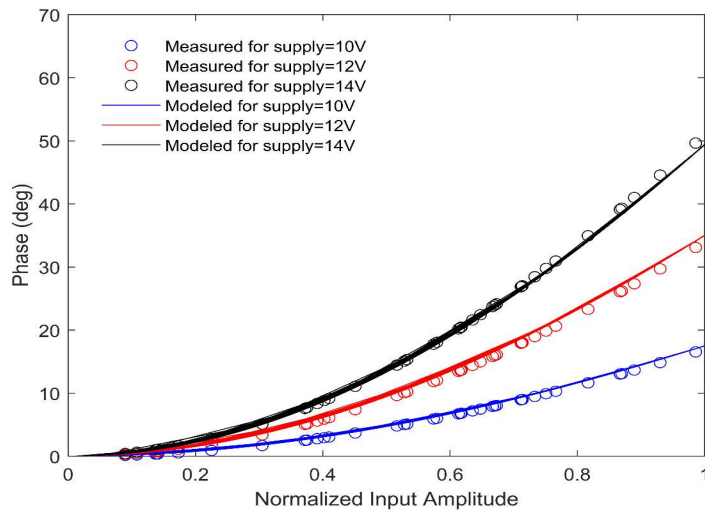
Figure 4.13 PA measured and modeled results of the AM/PM conversion for different supply voltages.

The extended static Saleh model is proposed by using Equation 4.20, with the parameters α and β replaced in terms of the supply voltage for the envelope tracking case as

$$y = \frac{|x|\,\alpha(v_{en})}{1 + |x|^2\,\beta(v_{en})} \tag{4.24}$$

where $\alpha(v_{en})$ and $\beta(v_{en})$ are the Saleh model coefficients as functions of the EM input voltage v_{en}. A truncated Taylor series is used to model the coefficients $\alpha(v_{en})$ and $\beta(v_{en})$ with respect to the supply voltage [26], [27]

$$\alpha(v_{en}) = \sum_{i=1}^{N_A} \alpha_i v_{en}^i \tag{4.25}$$

$$\beta(v_{en}) = \sum_{i=1}^{N_B} \beta_i v_{en}^i \tag{4.26}$$

where N_A and N_B are the maximum orders of the truncated Taylor series. By substituting Equation 4.25 and Equation 4.26 into Equation 4.24, results in a static dual-input single-output AM/AM function that can be expressed [26]

$$y(x, v_{en}) = \frac{|x|\sum_{i=1}^{N_A} \alpha_i v_{en}^i}{1 + |x|^2 \sum_{i=1}^{N_B} \beta_i v_{en}^i} \tag{4.27}$$

Equation 4.27 can be represented in a matrix form to simplify the calculation

$$y(x, v_{en}) = \frac{\boldsymbol{\alpha} \mathbf{v}_{\boldsymbol{\alpha}}^{\mathrm{T}} |x|}{1 + \boldsymbol{\beta} \mathbf{v}_{\boldsymbol{\beta}}^{\mathrm{T}} |x|^2} \tag{4.28}$$

where $\boldsymbol{\alpha} = \begin{bmatrix} \alpha_1, & \alpha_2, & \dots, & \alpha_{N_A} \end{bmatrix}$ and $\boldsymbol{\beta} = \begin{bmatrix} \beta_1, & \beta_2, & \dots, & \beta_{N_B} \end{bmatrix}$ are vectors of the ET PA model coefficients. $\mathbf{v_\alpha}$ and $\mathbf{v_\beta}$ are vectors of the variable supply voltage

$$\mathbf{v_\alpha}[N_s] = \begin{bmatrix} v_{en}^1(N_s) & v_{en}^2(N_s) & \dots & v_{en}^{N_A}(N_s) \end{bmatrix} \tag{4.29}$$

$$\mathbf{v_\beta}[N_s] = \begin{bmatrix} v_{en}^1(N_s) & v_{en}^2(N_s) & \dots & v_{en}^{N_B}(N_s) \end{bmatrix} \tag{4.30}$$

The extended model in Equation 4.28 can be deployed with any ET PA topology, because the Taylor series is a generic form of any analytical function. Furthermore, the Taylor series theoretically converges to the optimal accuracy when the nonlinear order approaches infinity. The extended static Saleh model consists of (N_A+N_B) total number of coefficients.

4.7.1 Estimation of Saleh Coefficients

The coefficients of the extended Saleh model in Equation 4.28 can be calculated using a surface fitting on the data set x, y, and v_{en}. A new method to extract the model coefficients is proposed by using linear algebra on Equation 4.28 to yield

$$y = \boldsymbol{\alpha} \, \mathbf{v_\alpha^T} \, |x| - y \, \boldsymbol{\beta} \, \mathbf{v_\beta^T} \, |x|^2 \tag{4.31}$$

By substituting time index of all the variables in Equation 4.31, and re-formulating the following matrix [26]:

$$
\begin{bmatrix} y(1) \\ y(2) \\ \vdots \\ \vdots \\ \vdots \\ y(N_s) \end{bmatrix} =
\begin{bmatrix} |x(1)| \, \mathbf{v_\alpha}[1] & -y(1)|x(1)|^2 \, \mathbf{v_\beta}[1] \\ |x(2)| \, \mathbf{v_\alpha}[2] & -y(2)|x(2)|^2 \, \mathbf{v_\beta}[2] \\ \vdots & \vdots \\ \vdots & \vdots \\ \vdots & \vdots \\ |x(N_s)| \, \mathbf{v_\alpha}[N_s] & -y(N_s)|x(N_s)|^2 \, \mathbf{v_\beta}[N_s] \end{bmatrix}
\begin{bmatrix} \alpha_1 \\ \vdots \\ \alpha_{N_A} \\ \beta_1 \\ \vdots \\ \beta_{N_B} \end{bmatrix} \tag{4.32}
$$

The matrix equation 4.32 can be re-written as

$$\mathbf{Y} = \mathbf{UC} \qquad (4.33)$$

where $\mathbf{Y}$ is $(N_s \times 1)$ a column vector of the ET PA output magnitude samples, $\mathbf{U}$ is $(N_s \times (N_A + N_B))$ model matrix, and $\mathbf{C}$ is a $((N_A + N_B) \times 1)$ column vector of the model coefficients. The extended Saleh coefficients are calculated by inverting Equation 4.33 in the sense of a minimum square errors

$$\mathbf{C} = (\mathbf{U}^T\mathbf{U})^{-1}\mathbf{U}^T\mathbf{Y} \qquad (4.34)$$

Matrix decomposition techniques, such as Singular Value Decomposition (SVD) and Cholesky decomposition, can be applied to calculate the pseudo-inverse of the matrix $\mathbf{U}$ in Equation 4.34. However, the pseudo-matrix inverse in Equation 4.34 is computationally efficient compared to SVD and Cholesky decomposition, because the model matrix $\mathbf{U}$ has a larger number of rows than the number of columns.

The simulation results of the dynamic AM/AM conversion in Figure 4.14 show accuracy improvement in the extended Saleh model compared to the original Saleh model. The curve of the extended Saleh model is close to the statistical mean of the dynamic simulated data in the region of a lower input power compared to the Saleh curve.

4.8. Hammerstein Theory

The Hammerstein approach is a simplified mathematical structure and a special modeling approach of a Volterra series. It is a widely used technique to approximate the nonlinear functions exhibiting memory effects. The Hammerstein model structure consists of cascading two models, memoryless nonlinear model (to account for static nonlinearity)

followed by a linear filter (to account for memory effect) as shown in Figure 4.15. In the Hammerstein approach, the static nonlinearity and memory system are independently calculated. The Hammerstein technique reduces the parameters' redundancy compared to the Volterra model. This advantage is important for adjusting the model complexity and accuracy.
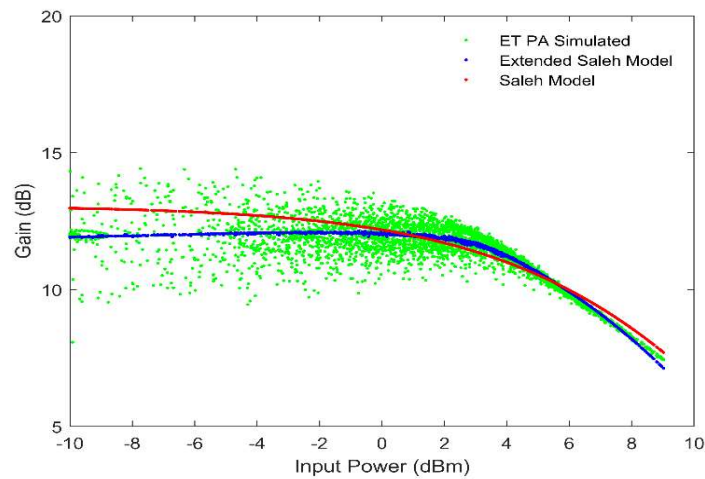
Figure 4.14 PA simulated and modeled gain using both the Saleh model and the extended Saleh approaches.
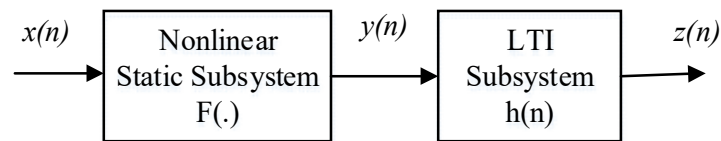
Figure 4.15 The Hammerstein modeling structure for nonlinear system with memory effects.

4.9. Dynamic Saleh AM/AM Model

Energy-storage elements in the ET PA circuit and variation level of the supply voltage cause major nonlinear dispersion effect (i.e. model uncertainty) in the PA model. Therefore, static nonlinear models are not capable of characterizing memory effect in the ET circuit. Dynamic nonlinear models are often required for accurately predicting circuit response [27], [52]-[54]. This phenomenon of hysteresis effect is a well-studied and described in the literature of behavioral models.

The hysteresis effect in ET PA is often modeled using the Hammerstein approach. Therefore, the residuals (i.e memory effect) between the output of the static extended Saleh model and the actual output of the PA are modeled in this work using a Finite Impulse Response (FIR) filter [26].

The FIR filter is cascaded in series with the static nonlinear model to make the model time-dependent as well. The output of the complete dynamic Saleh AM/AM model can be expressed as:

$$y_d(n) = \sum_{k=0}^{M_{AM}} h(k) y(n-k) \tag{4.35}$$

where y(n) is the output of the extended Saleh model, $h(k)$ is the filter impulse response, M_{AM} is the AM/AM memory depth, and $y_d(n)$ is the dynamic AM/AM model output. A least-squares method is a simple approach for calculating the FIR filter's coefficients using

$$\mathbf{h} = (\mathbf{Y}_s^T \mathbf{Y}_s)^{-1} \mathbf{Y}_s^T \mathbf{y_d} \tag{4.36}$$

where $\mathbf{h}$ is a vector of the FIR filter coefficients, $\mathbf{y_d}$ is a vector of the dynamic ET PA magnitude output samples, and $\mathbf{Y}$s is a matrix generated from the extended Saleh AM/AM output [26], [27].

4.10 Modeling of AM/PM using 2D-Polynomial.

The AM/PM conversion is a nonlinear time-dependent function as described earlier in Section 2.5. Therefore, the 2D-MPM is used here to model the dynamic AM/PM conversion in ET PA. The 2D-MPM uses the input signal and supply voltage as two independent variables

$$q(n) = \sum_{k=0}^{L}\sum_{j=0}^{N}\sum_{m=0}^{M} P_{(k,j,m)} x^{j}(n-m) v_{en}^{k}(n-m) \tag{4.37}$$

where L and N are the maximum orders of the baseband input and envelope variables, respectively, M is the memory depth and, $q(n)$ is a complex output of the dynamic AM/PM conversion. $P_{(k,j,m)}$ are the model coefficients, which can be calculated from the ET PA input and output data using the following least-squares equation:

$$\mathbf{P} = (\mathbf{A}^{\mathrm{T}}\mathbf{A})^{-1}\mathbf{A}^{\mathrm{T}}\mathbf{Q} \tag{4.38}$$

where $\mathbf{A}$ is a matrix, which is generated from the polynomial terms in Equation 4.37, $\mathbf{Q}$ is a vector of a complex output samples, and $\mathbf{P}$ is a vector consists of the MPM coefficients. The dynamic AM/PM conversion (ψ) can be calculated as shown in Equation 4.39. Finally, the complete model architecture based on the presented extensions is shown in Figure 4.16.

$$\psi(n) = \tan^{-1}\left(\frac{\Re(q(n))}{\Im(q(n))}\right) \qquad (4.39)$$
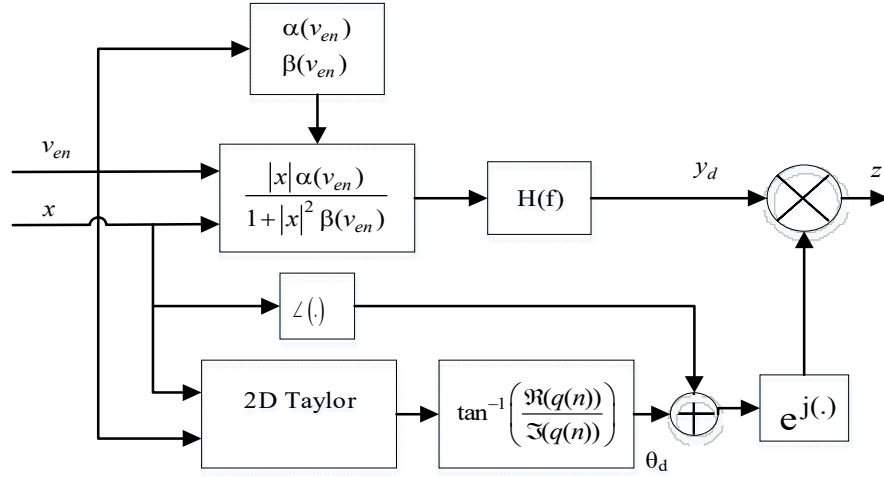
Figure 4.16 The proposed extended Saleh model architecture used for the envelope tracking power amplifier.

4.11 Model Evaluation of ET PA

The modeling accuracy is typically evaluated in the time domain using the NMSE, and in the frequency domain using the ACEPR, figures-of-merit widely used in the state-of-the-art assessment of the PA behavioral models [55]-[57]. Both the NMSE and ACERP are expressed as follows:

$$\text{NMSE}_{\text{dB}} = 10\log_{10}\left(\frac{\sum_{n=1}^{N}\left|y_{meas}(n) - y_{model}(n)\right|^2}{\sum_{n=1}^{N}\left|y_{meas}(n)\right|^2}\right) \qquad (4.40)$$

where $y_{meas}(n)$ and $y_{model}(n)$ are the complex baseband output measured and modeled signals, respectively. N is the signal number of symbols. ACEPR refers to the model accuracy in the frequency domain, which is defined as:

$$\text{ACEPR} = 10\log_{10}\left(\frac{\displaystyle\int_{f_{s,L}}^{f_{p,L}} \left|E\left(f\right)\right|^2 df + \int_{f_{s,U}}^{f_{p,U}} \left|E\left(f\right)\right|^2 df}{\displaystyle\int_{f_{s,ch}}^{f_{p,ch}} \left|Z_s\left(f\right)\right|^2 df}\right) \tag{4.41}$$

where $E(f)$ is the frequency domain error signal of (y_{meas} - y_{model}), $Z_s(f)$ is the Fourier transform of the measured ET PA output signal. $f_{s,L}$ and $f_{p,L}$ are the start and stop frequencies, respectively, of the lower adjacent channel. $f_{s,U}$ and $f_{p,U}$ are the start and stop frequencies, respectively, of the upper adjacent channel. $f_{s,ch}$ and $f_{p,ch}$ are the start and stop frequencies, respectively, of the desired channel.

4.11.1 Simulation Set-up

A simulation circuit of the ET PA was designed using Advanced Design System (ADS) software. The circuit schematic is shown in Figure 4.17. The ET PA in this simulation was designed using GaAs field-effect transistor from the ADS library, RF input and output matching circuits, and mathematical components for the shaping and envelope models. The PA was excited by LTE-downlink signal, which was acquired from the Keysight signal generator. The envelope tracking branch in Figure 4.17 consists of an envelope detector and shaping function to perform the following calculations:

$$Env(n) = \sqrt{\mathrm{I}(n)^2 + \mathrm{Q}(n)^2} \tag{4.42}$$

$$v_{en}(n) = v_{dd,\max}\left(\left|Env(n)\right| + k.e^{\left(\frac{\left|Env(n)\right|}{-k}\right)} \right) \tag{4.43}$$

where I(n) and Q(n) are the in-phase and quadrature-phase baseband components of LTE signal, $Env(n)$ is the envelope waveform, $v_{dd,max}$ is the maximum supply voltage, k is the detroughing ratio, which is equal to $\frac{v_{dd,min}}{v_{dd,max}}$, and $v_{dd,min}$ is the minimum voltage required to operate the RF PA. The time series data of the ET PA signal, output signal, and envelope voltage are exported to MATLAB for model computation and validation [26].
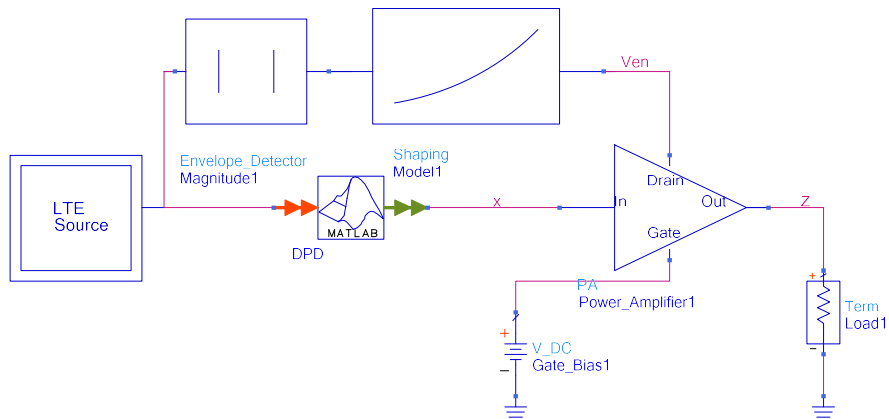
Figure 4.17 Circuit schematic used for the ET PA simulations in the ADS.

4.11.2 Modeling Results

The coefficients of the extended Saleh model are calculated using a least-squares as described earlier in Section 4.7, based on data acquired from ADS simulation. Figure 4.18 illustrates the results of both the ADS simulation and extended Saleh model in the AM/AM and AM/PM conversions [26].
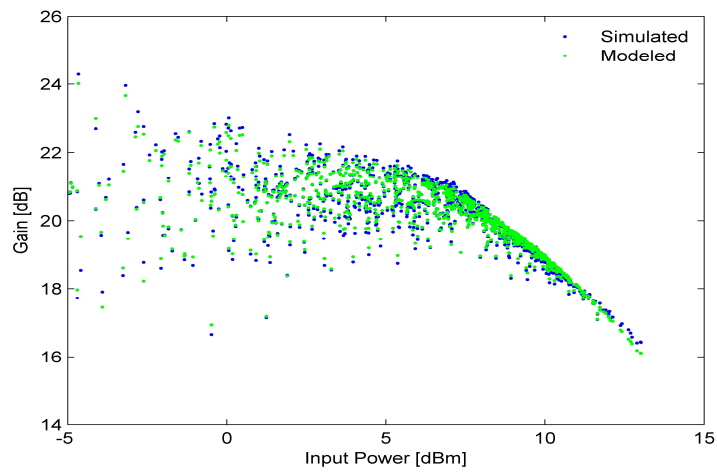
(a)
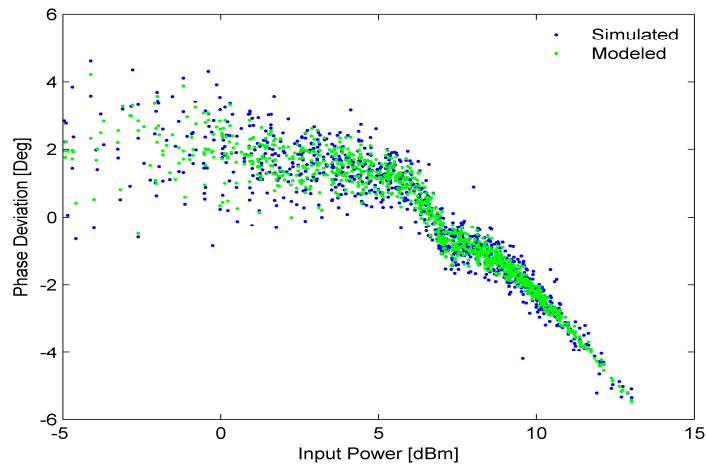
(b)

Figure 4.18 Gain and phase deviation of the ET PA simulated in the ADS and the proposed extended Saleh model. (a) Gain. (b) Phase.

The obtained simulation results show that the modeled data points matched well with the dynamic nonlinearity in both amplitude and phase conversions. In addition, the PSD in Figure 4.19 shows an adequate modeled spectrum for both in-band and out-of-band regions of the simulated signal in the frequency domain [26].

Figure 4.20 illustrates the performance of the model accuracy in NMSE and ACEPR versus the swept values of nonlinear orders and memory depth. The calculated NMSE and ACEPR of the extended Saleh model are shown in Table (4.4), for different nonlinear orders N_A and N_B [26].
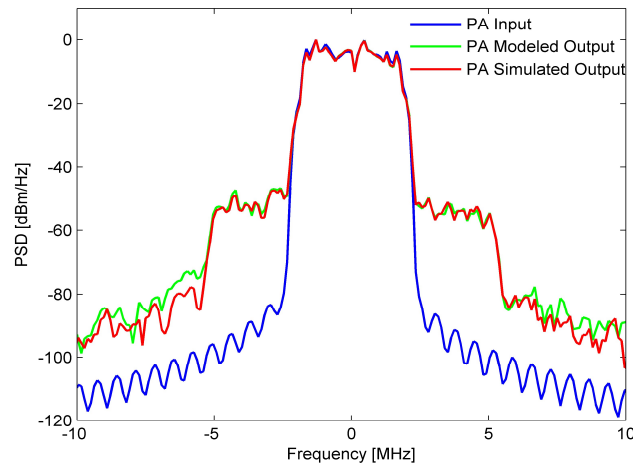
Figure 4.19 Power spectral density of the ET PA simulated in the ADS and the proposed extended Saleh model.

The NMSE and ACEPR are calculated for the swept memory depth of the H(f) filter from 1 to 60 coefficients as shown in Figure 4.20. The optimal model accuracy is -44.6 dB in NMSE and -53.7 dB in ACEPR, which occurs at the maximum modeled nonlinear order. Finally, NMSE and ACEPR results for different nonlinear order (N) and (Q) of the Taylor polynomial are depicted in Figure 4.21 [26].

Table (4.4) Accuracy evaluation of the extended Saleh model using NMSE and ACEPR.

Nonlinear Orders	Number of Static AM/AM Coefficients	NMSE (dB)	ACEPR (dB)
$N_A=1$, $N_B=1$	2	-32.56	-41.32
$N_A=2$, $N_B=1$	3	-36.19	-45.31
$N_A=3$, $N_B=1$	4	-36.24	-45.62
$N_A=3$, $N_B=2$	5	-36.31	-46.01
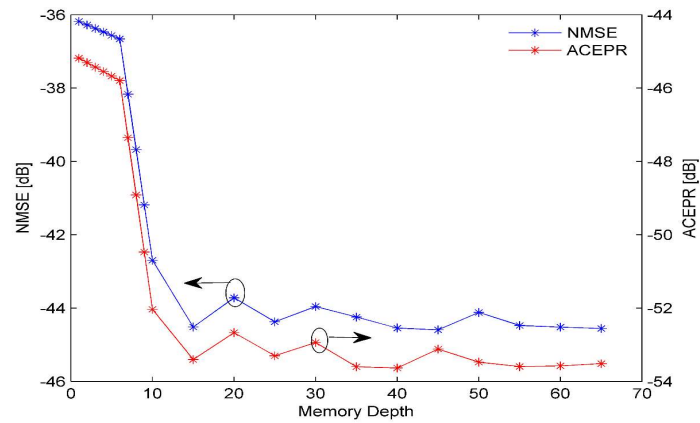
Figure 4.20 Modeling accuracy results in NMSE and ACEPR versus the AM/AM model memory depth.
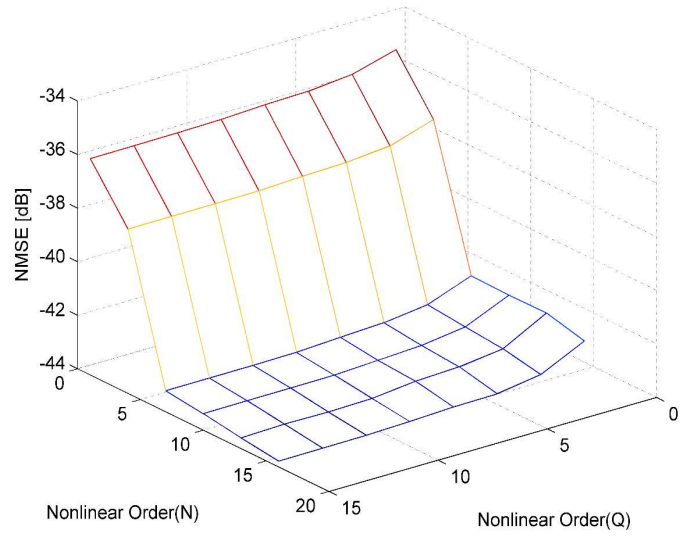
(a)
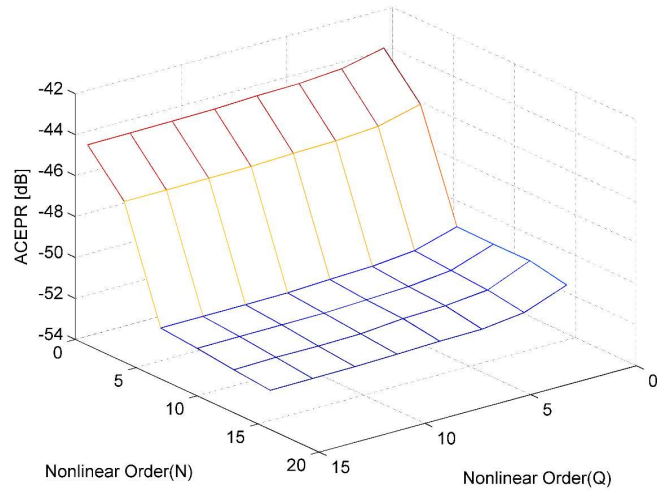
(b)

Figure 4.21 NMSE and ACEPR in terms of the nonlinear orders N and Q of the AM/PM Taylor model. (a) NMSE.   (b) ACEPR.

4.12   Proposed Model for ET PAs

The 2D-Taylor polynomial model for the AM/PM conversion in Section 4.10 exhibits a high modeling accuracy; however, the 2D-polynomial model is computationally expensive due to a high number of coefficients. Therefore, an approach for modeling the AM/PM conversion using the Hammerstein structure is proposed in this section. The Hammerstein approach for the AM/PM modeling consists of a static dual-input Saleh model in cascade with a simple digital filer (FIR filter) to account for a long-memory effect in the dynamic AM/PM nonlinearity modeling [27]. The dual-input Saleh model is an extended version of a constant-supply Saleh AM/PM model as described in Section 4.12.1. The IIR filter can also be used to model the memory effect in PAs. However, the FIR filter exhibits advantages over the IIR filter such as the stability and simplicity of the filter implementation.

A complete structure of the proposed model is shown in Figure 4.22, the upper block branch represents the dynamic effect of the AM/AM conversion, and the lower block branch represents the dynamic AM/PM conversion. A complex exponential operator is used to combine these two branches using a mathematical complex multiplier block [27].
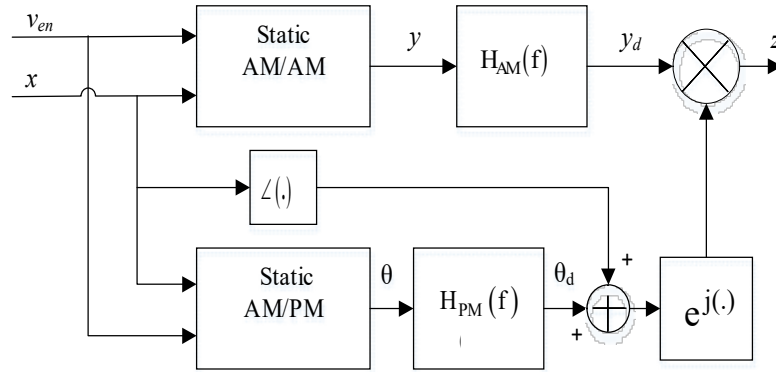
Figure 4.22 Block diagram of the three-port dynamic Saleh model architecture.

4.12.1 Extended Saleh AM/PM Model

The extended Saleh AM/PM model is proposed to model the AM/PM conversion as described in variable supply PA. The advantage of this approach is to reduce the complexity of the AM/PM model compared to the 2D-MPM model in the previous approach. This modeling approach is derived from the original Saleh AM/PM model for the constant-supply case [51]

$$\theta = \frac{|x|^2 \lambda}{1 + |x|^2 \gamma} \qquad (4.44)$$

where λ and γ are the Saleh model AM/PM parameters, x is the complex baseband input signal, and θ is the output phase. The phase of the ET PA varies dynamically along the supply voltage as demonstrated in Figure 4.13. Therefore, the dependency of the ET PA phase with respect to the supply voltage is modeled by expressing the Saleh parameters as function of the modulated supply voltage using a Taylor polynomial [27].

$$\theta(x, v_{en}) = \frac{|x|^2 \lambda(v_{en})}{1 + |x|^2 \gamma(v_{en})} \tag{4.45}$$

where $\lambda(v_{en})$ and $\gamma(v_{en})$ are the Saleh coefficients as functions of the envelope modulator voltage v_{en}. Polynomial functions are used to model these coefficients with respect to the supply voltage [27]

$$\lambda(v_{en}) = \sum_{i=1}^{P_a} \lambda_i v_{en}^i \tag{4.46}$$

$$\gamma(v_{en}) = \sum_{i=1}^{P_b} \gamma_i v_{en}^i \tag{4.47}$$

where P_a and P_b are the maximum polynomial orders in the envelope amplitude variable v_{en}. By substituting Equation (4.46) and (4.47) into Equation (4.45), results in a static DISO Saleh AM/PM function as [27]

$$\theta(x, v_{en}) = \frac{|x|^2 \sum_{j=1}^{P_a} \lambda_j v_{en}^j}{1 + |x|^2 \sum_{j=1}^{P_b} \gamma_j v_{en}^j} \tag{4.48}$$

The polynomial functions in Equation (4.48) can be expressed in vector forms as

$$\theta = \frac{|x|^2 \boldsymbol{\lambda} \mathbf{v}_\lambda^{\mathrm{T}}}{1 + |x|^2 \boldsymbol{\gamma} \mathbf{v}_\gamma^{\mathrm{T}}} \tag{4.49}$$

where $\boldsymbol{\lambda} = \begin{bmatrix} \lambda_1, \lambda_2, \ldots, \lambda_{P_a} \end{bmatrix}$ and $\boldsymbol{\gamma} = \begin{bmatrix} \gamma_1, \gamma_2, \ldots, \gamma_{P_b} \end{bmatrix}$ are model coefficients, $\mathbf{v}_\lambda$ and $\mathbf{v}_\gamma$ are vectors of the envelope amplitude using different polynomial orders

$$\mathbf{v}_\lambda = [v_{en}^1, v_{en}^2, \ldots, v_{en}^{P_a}] \tag{4.50}$$

$$\mathbf{v}_{\gamma} = \left[v_{en}^{1}, v_{en}^{2}, \ldots, v_{en}^{P_b} \right] \qquad (4.51)$$

The simulation results showed that the proposed extension results in an adequate accuracy and matched well with the PA AM/PM conversion, as compared to the original Saleh model, which is depicted in Figure 4.23.
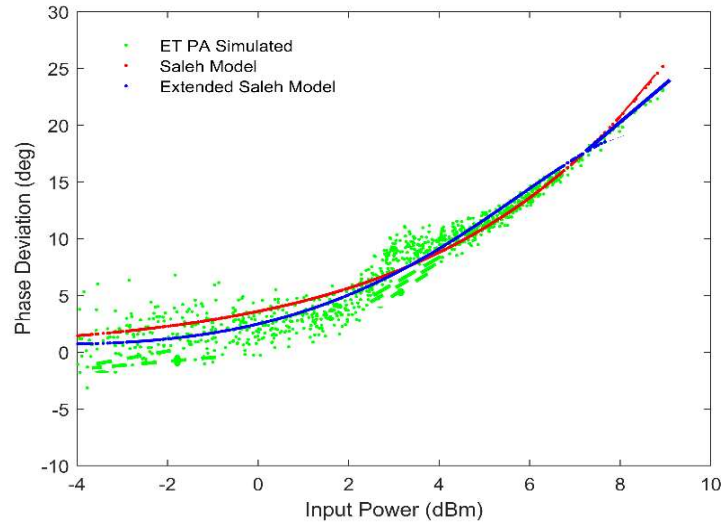
Figure 4.23 Simulated and modeled phase deviation of ET PA.

4.12.1.1. Estimation of Model Coefficients

The extended Saleh AM/PM model in Equation 4.49 can be re-expressed as:

$$\theta = |x|^{2} \, \boldsymbol{\lambda} \mathbf{v}_{\lambda}^{\mathrm{T}} - \theta \, |x|^{2} \, \boldsymbol{\gamma} \mathbf{v}_{\gamma}^{\mathrm{T}} \qquad (4.52)$$

Applying the signal time samples on Equation 4.52, results in the following matrix equation [27]:

$$
\begin{bmatrix} \theta(1) \\ \theta(2) \\ \vdots \\ \vdots \\ \vdots \\ \theta(k) \end{bmatrix} = \begin{bmatrix} |x(1)|^2\, \mathbf{v}_\lambda[1], & -\theta(1)|x(1)|^2\, \mathbf{v}_\gamma[1] \\ |x(2)|^2\, \mathbf{v}_\lambda[2], & -\theta(2)|x(2)|^2\, \mathbf{v}_\gamma[2] \\ \vdots & \vdots \\ \vdots & \vdots \\ \vdots & \vdots \\ |x(k)|^2\, \mathbf{v}_\lambda[k], & -\theta(k)|x(k)|^2\, \mathbf{v}_\gamma[k] \end{bmatrix} \begin{bmatrix} \lambda_1 \\ \vdots \\ \lambda_{P_a} \\ \gamma_1 \\ \vdots \\ \gamma_{P_b} \end{bmatrix} \tag{4.53}
$$

where k is the signal number of samples, $\mathbf{v}_\lambda$ and $\mathbf{v}_\gamma$ are row vectors that are expressed as

$$
\mathbf{v}_\lambda[k] = \left[v_{en}^1(k), \quad v_{en}^2(k), \quad \dots \quad , v_{en}^{P_a}(k) \right] \tag{4.54}
$$

$$
\mathbf{v}_\gamma[k] = \left[v_{en}^1(k), \quad v_{en}^2(k), \quad \dots \quad , v_{en}^{P_b}(k) \right] \tag{4.55}
$$

Equation (4.53) is expressed using a matrix notation form

$$
\boldsymbol{\theta} = \mathbf{Q}\mathbf{L} \tag{4.56}
$$

where $\boldsymbol{\theta}$ is a ($k \times 1$) column vector of the ET PA output phase samples, $\mathbf{Q}$ is a matrix of $k \times (P_a + P_b)$ samples, and $\mathbf{L}$ is a vector of $(P_a + P_b) \times 1$ model coefficients. The vector $\mathbf{L}$ is calculated by inverting (4.56) in the sense of a least-squares error

$$
\mathbf{L} = (\mathbf{Q}^T\mathbf{Q})^{-1}\mathbf{Q}^T\boldsymbol{\theta} \tag{4.57}
$$

The residuals from the extended Saleh model in Equation 4.49 is modeled using the FIR filter in series with the static model based on the Hammerstein approach. The FIR filter is used to model the spreading effects in the AM/PM due to the long-memory effect. FIR is a simple digital filter, which is always stable [27]. The FIR filter output is a convolution operation between the static model and the filter impulse response

$$\theta_d(n) = \sum_{k=0}^{M_{PM}} f(k)\theta(n-k) \tag{4.58}$$

where $\theta_d(n)$ is the dynamic AM/PM conversion, M_{PM} is the memory depth, and $f(k)$ is the AM/PM filter impulse response. A least-squares method is used to calculate the FIR filter coefficients

$$\mathbf{f} = (\boldsymbol{\psi}^T\boldsymbol{\psi})^{-1}\boldsymbol{\psi}^T\boldsymbol{\theta}_d \tag{4.59}$$

where $\mathbf{f}$ is a vector of the FIR filter coefficients, $\boldsymbol{\theta_d}$ is a vector of the measured ET PA phase, and $\boldsymbol{\psi}$ is a matrix composed from the extended Saleh model output phase. The total number of model coefficients (N_{PAR}) for the overall proposed model with all the extensions are as follows:

$$N_{PAR} = N_A + N_B + P_a + P_b + (M_{AM}+1) + (M_{PM}+1) \tag{4.60}$$

The parameters N_A, N_B, and M_{AM} are the orders of the dynamic extended Saleh AM/AM model, and the parameters P_a, P_b and M_{PM} are the orders of the dynamic extended Saleh AM/PM model [27].

4.12.2 Model Evaluation

The experimental results for data acquisition is shown in Figure 4.24. The ET PA was built using OPA267 envelope modulator and RFPA380 RF main PA [27]. The rest of the experiment consist of two signal generators at the ET PA input and one signal analyzer on the ET PA output. The gain and phase conversions of the measured, the original Saleh model, and the proposed ET PA dynamic modeling results are shown in Figure 4.25. Clear

accuracy modeling improvements in both the AM/AM and AM/PM conversions are obtained when comparing the results with respect to the original Saleh model.

The modeling accuracy was evaluated in the time domain using NMSE and in the frequency domain using ACEPR. The model accuracy using NMSE results shown in Figure 4.26 are calculated for different maximum nonlinear orders N_A, N_B, P_a, and P_b. The model NMSE for a swept memory depth M_{AM} in AM/AM and M_{PM} in AM/PM are shown in Figure 4.27. Finally, the accuracy results of the dynamic Saleh model are compared to the state-of-the-art 2D-MPM and MBM for different number of model coefficients as shown in Table (4.5). The compared accuracy results of the ET PA models are depicted in Figure 4.28. These results show that the dynamic Saleh model achieves NMSE and ACEPR performance values below -42 dB and -51 dB ACEPR, respectively, at the maximum model accuracy using 20 coefficients, whereas the 2D-MPM and MBM require about 30 coefficients to reach the same accuracy in terms of NMSE and ACEPR results.
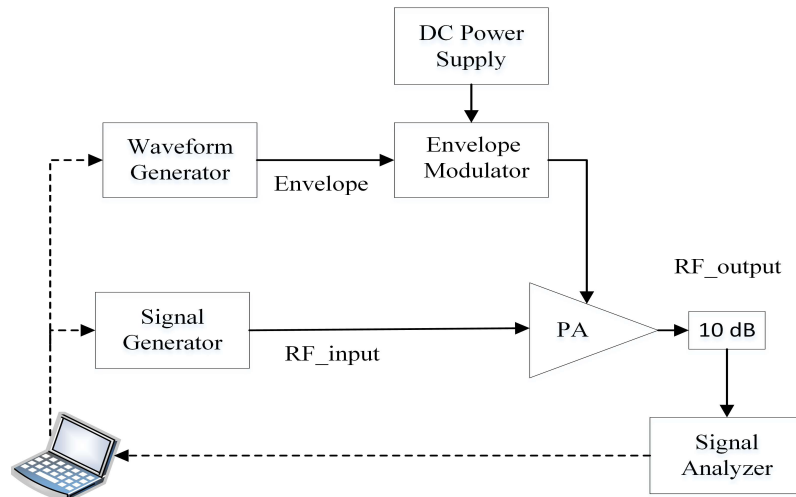
Figure 4.24 Measurement set-up used for the envelope tracking power amplifier.
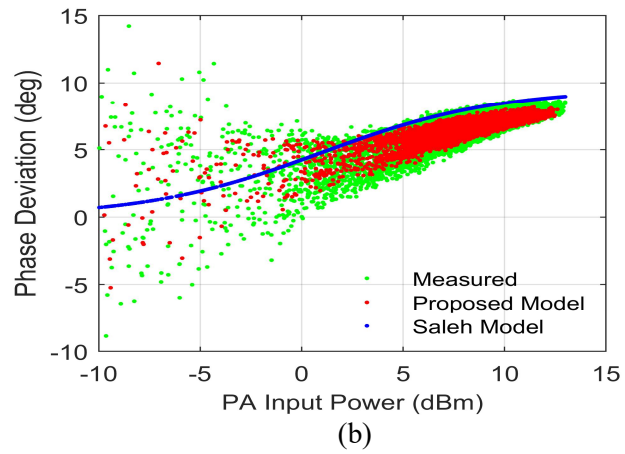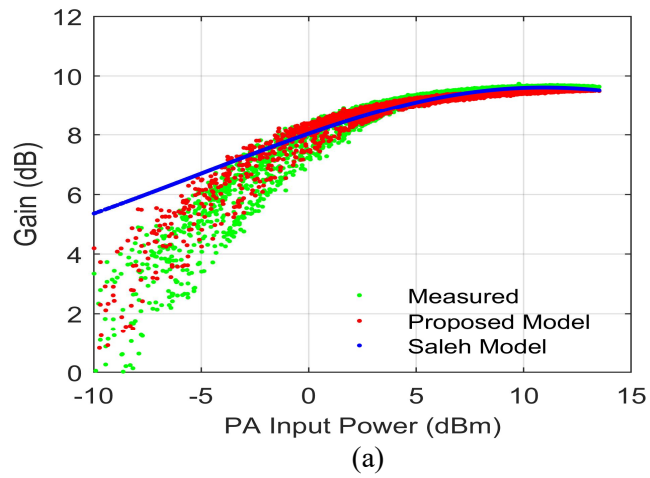
Figure 4.25 Gain and phase results of the Saleh model and dynamic Saleh model. (a) Gain. (b) Phase deviation.
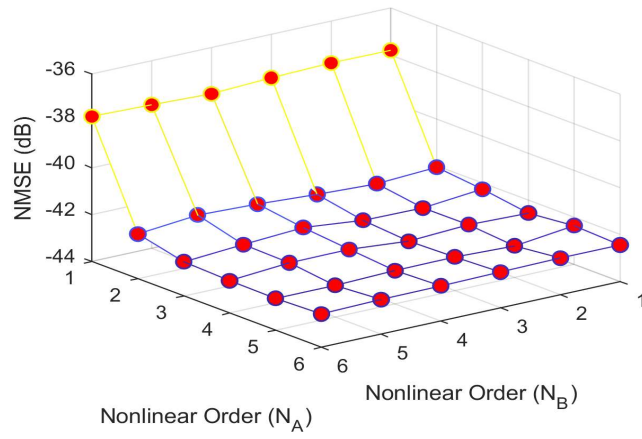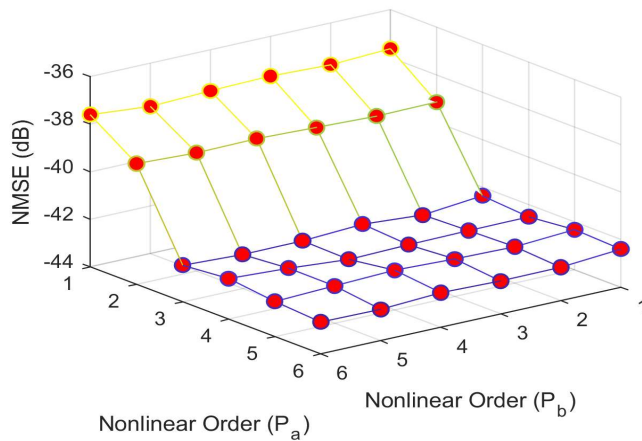
Figure 4.26 Accuracy evaluation in NMSE of the extended Saleh model for different nonlinear orders N_A, N_B, Pa, and Pb. (a) NMSE versus N_A and N_B. (b) NMSE versus P_a and P_b.
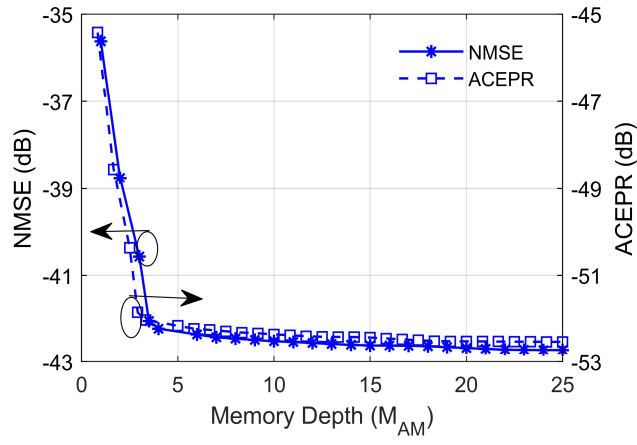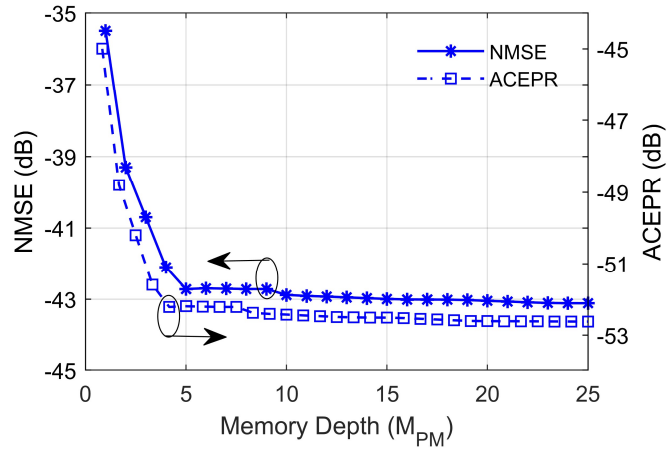
Figure 4.27 NMSE and ACEPR accuracy performance of the extended Saleh model versus a swept memory depth. (a) NMSE and ACEPR in terms of memory depth, M_{AM} and M_{PM} are set to 5. (b) NMSE and ACEPR in terms of memory depth, M_{PM} and M_{AM} is set to 5.
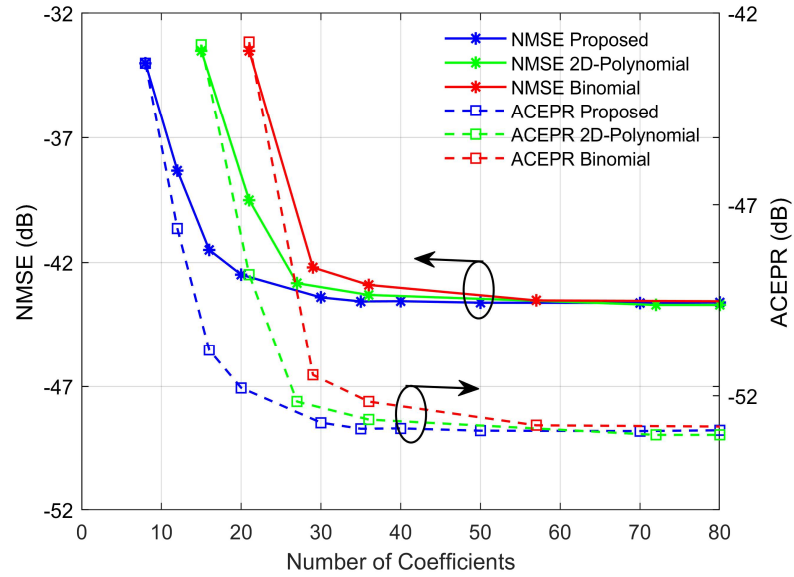
Figure 4.28 Comparison of models' accuracies in NMSE and ACEPR versus a swept model number of coefficients.

Table (4.5) Comparison results of different 2D-behavioral models for envelope tracking power amplifiers.

Model	Number of Coefficients	Nonlinear Order	Memory Depth	NMSE (dB)	ACEPR (dB)
Dynamic Saleh Model	12	$N_A=2$, $N_B=1$, $P_a=2$, $P_b=1$	$M_{AM}=2$, $M_{PM}=2$	-38.75	-49.23
	20	$N_A=3$, $N_B=2$, $P_a=2$, $P_b=3$	$M_{AM}=4$, $M_{PM}=4$	-42.48	-51.80
2D-MPM	27	$K=2$, $N=3$	$M=2$	-42.81	-52.63
	36	$K=2$, $N=3$	$M=3$	-43.28	-53.22
	72	$K=3$, $N=3$	$M=5$	-43.52	-53.91
MBM	28	$N=3$	$M=2$	-43.23	-52.67
	57	$N=4$	$M=3$	-43.55	-53.94
	121	$N=5$	$M=5$	-43.56	-54.02

4.12.3 Evaluation of Model Complexity

Model properties in terms of accuracy and computational complexity are two main criteria for evaluating the model performance [58]. Model accuracy in terms of NMSE and ACEPR for different model nonlinear orders is presented in the previous sections. The model accuracy can also have an impact on the model complexity in terms of the computational cost. This is because the model number of coefficients controls the model computational cost. The required number of coefficients in the behavioral model varies from one PA to another depending on the nonlinearity effect [59]. The complexity of ET PAs depends on the PA circuit design, IC chip temperature variation, load, and the memory depth as a circuit dependent, as well as the ET design, such as the variation in the shaping function or ET system.

A model of many coefficients often requires a high number of mathematical operations, such as multipliers and summer blocks, when implementing the ET PA model in DSP. For example, the number of multiplier operations in Volterra-based models are equal to the model number of coefficients; therefore, the Volterra model is computationally expensive.

Various measures of model complexity are presented in the literature of complexity theory, such as implementation complexity, time complexity, and size complexity. The big $O(.)$ (order of function) and Float Point Operation (FLOP) is a widely used measure in numerical analysis for algorithm computational complexity. The big $O(.)$ is a simple notation that describes the growth rate of the function in terms of its arguments. Furthermore, the big $O(.)$ is an indirect measure of the algorithm time-complexity in terms

of the number of input elements. The FLOP is a measure of the floating-point computation per second.

4.12.3.1 Models Size Complexity

The complexity in model size denotes the storage space (memory size) for model computation. The complexity of a model size is not a major implementation challenges in a small size model structure, but it consumes additional resources. The Volterra series and MPMs require a large memory size to store all the model coefficients, in addition to the memory units for the delayed polynomial terms, such as $\{$ $x(n-1)|x(n-1)|^N, x(n-2)|x(n-2)|^N, ..., x(n-M)|x(n-M)|^N\}$ in the subsequent iterative calculations.

The Dynamic Saleh model exhibits lower model size complexity, because of a lower number of model coefficients as discussed in the results section. In addition, the Hammerstein approach for both the AM/AM and AM/PM conversions reduces the required memory coefficients in the memory part (i.e. lower order FIR filler in the proposed model). This is because the MPM requires (M×N) delay terms, while the proposed model requires only ($M_{AM}+M_{PM}$) delay terms.

4.12.3.2 Complexity of Model Estimation

The least-squares is a commonly used approach in model estimation for ET PAs. The least-squares method is considered a simpler approach in estimating the polynomial models. The other models such as Cann and Rapp require complicated iterative estimation

approaches [29]. The high computational cost and the problem of convergence are two main drawbacks of the iterative methods.

The type of model coefficients (e.g. real or complex) is another important aspect in the model computational cost. The type of the model coefficients depends on the model structure and applications (e.g. memoryless polynomial models use real numbers and quasi-memory polynomial models use complex numbers). In addition, this also depends on the applied approximated functions for the PA circuit characteristics. For instance, the Taylor model of real coefficients is widely used to model only the AM/AM conversion under assumption that the impact of the AM/PM conversion is negligible, because it is minor for a low memory model.

The Taylor model of complex-type coefficients is used to model both the AM/AM and AM/PM conversions, simultaneously. Similarly, the state-of-the-art binomial and 2D-Polynomial models for ET PA have complex-type coefficients, as described in the previous sections. Thus, a least-squares calculation on a complex number is required when estimating the model parameters.

The computational cost of a complex mathematical operation is double or higher than the computational cost of a real operation [58]. For instance, the mathematical operation of multiplying any two real numbers costs 2 FLOPs, whereas the product of multiplying two complex numbers costs 6 FLOPs as illustrated

$$(a + jb) \times (c + jd) = ac - bd + jbc + jad \qquad (4.61)$$

where (a, b, c, d) is a set of any integer numbers. This shows that four multipliers $(a \times c), (b \times d), (b \times c), (a \times d)$, and two sum operations $(ac - bd), (jbc + jad)$ are required

when calculating the multiplication of any complex numbers. Hence, a total number of 6

operations (i.e. 6 FLOPs) is the model implementational cost.

Dimensions of the model matrix in least-squares is another factor that controls the

model complexity, because matrix inversion exhibits higher computational cost (i.e.

multiplication, addition, and division operations).

The advantage of the dynamic Saleh model is that all the coefficients are real.

Hence, this property can simplify the model computational cost when identifying the model

coefficients. On the other hand, the Hammerstein approach in the proposed model reduces

the required number of coefficients for modeling the ET PA, since the static nonlinearity

and memory effect are both modeled independently.

The estimation complexity of the proposed model in terms of $O(.)$ is an adequate

and important measure for the model computational cost. Different model structures can

be evaluated using the $O(.)$ as follows:

1. BM and 2D-MPM models:

The calculation of the least-squares for estimating the BM and 2D-MPM is described

using the following matrix operations:

$$\mathbf{j} = (\mathbf{Z}^H \mathbf{Z})^{-1} \mathbf{Z}^H \mathbf{y} \qquad (4.62)$$

where $\mathbf{Z}$ is the model matrix of $(n \times k)$ complex elements, $\mathbf{y}$ is a vector of complex output

measured data, and $\mathbf{j}$ is a vector of $(k \times 1)$ model coefficients.

Table (4.6) Computational cost of the least-squares calculation on complex numbers.

Matrix Operation	Complexity in big $O(.)$
$\mathbf{A} = \mathbf{Z}^{*(k\times n)}\mathbf{Z}^{(n\times k)}$	$O(8nk^2)$
$\mathbf{B} = (\mathbf{A})^{-1}$	$O(8k^3)$
$\mathbf{C} = \mathbf{B}^{(k\times k)}\mathbf{Z}^{(k\times n)}$	$O(8nk^2)$
$\mathbf{j} = \mathbf{C}^{(k\times n)}\mathbf{y}^{(n\times 1)}$	$O(8nk)$

Equation 4.62 can be re-written using matrix dimensions

$$\mathbf{j} = (\mathbf{Z}^{*(k\times n)}\mathbf{Z}^{(n\times k)})^{-1}\mathbf{Z}^{(k\times n)}\mathbf{y}^{(n\times 1)} \tag{4.63}$$

where $\mathbf{Z}^*$ denotes the complex conjugate operation on $\mathbf{Z}$. The complexity of each

operation in Equation 4.63 are calculated as in Table (4.6).

The total complexity of Equation 4.63 is a summation of the sub-operations in Table (4.6)

$$O_T = O(8nk^2) + O(8nk^2) + O(8k^3) + O(8nk) \tag{4.64}$$

where O_T is the total model complexity. Equation 4.64 can be simplified using the big

$O(.)$ notation property $O(g_1) + O(g_2) = O(g_1 + g_2)$. Hence, this leads to

$$O_T = O(16nk^2 + 8k^3 + 8nk) \tag{4.65}$$

Equation 4.65 shows that complexity grows at very high rate ($8\,k^3$) in terms of the model

number of coefficients specified by the matrix dimension (k). Therefore, reducing the

model number of coefficients can significantly reduce the identification complexity as

verified by Equation 4.65. This also illustrates that complexity grows linearly in terms of the data sample size (n).

2. Dynamic Saleh Model

The extended dynamic Saleh model consists of the following 4 modeling blocks: extended Saleh AM/AM model, extended Saleh AM/PM model, and two FIR filters. Thus, a least-squares method is used to identify each modeling block. Since the model coefficients are real, the computational cost of the matrix pseudo-inverse is lower than the presented complexity for the complex numbers. Table (4.7) shows that the order of each operation and the total complexity is

$$O_T = O_{Ex\_AM}(4nk_s^2 + 2k_s^3 + 2nk_s) + O_{Ex\_PM}(4nk_s^2 + 2k_s^3 + 2nk_s) +$$
$$O_{FIR\_AM}(4nk_s^2 + 2k_s^3 + 2nk_s) + O_{FIR\_PM}(4nk_s^2 + 2k_s^3 + 2nk_s) \tag{4.66}$$

where $O_{EX\_AM}(.)$ is the operation order of the extended Saleh AM/AM model, $O_{EX\_PM}(.)$ is the operation order of the extended Saleh AM/PM model, $O_{FIR\_AM}(.)$ is the operation order for the AM/AM FIR filter, and $O_{FIR\_PM}(.)$ is the operation order for the AM/PM FIR filter. Equation 4.66 can be simplified as

$$O_T = O(16nk_s^2 + 8k_s^3 + 8nk_s) \tag{4.67}$$

The variable k_s denotes the total number of coefficients in the dynamic Saleh model. The estimation complexity in Equation 4.67 shows a sharp increasing rate in terms of the model number of coefficients, and a lower increasing rate in terms of the data size as shown in Figure 4.29. When comparing Equation 4.65 and Equation 4.67, the complexity is equivalent for the same parameters n and k_s.

114

However, the estimation complexity of the dynamic Saleh model is lower than the complexity of MPM and MBM under the same accuracy in NMSE, due to the lower number of model coefficients. The complexity comparison in the number of FLOPs is illustrated in Table (4.8) for a model accuracy of around -42.81dB in NMSE and the number of data samples is 10,000. The compared complexity results in Table (4.8) illustrate that the identification complexity of the dynamic Saleh model is a round half the identification complexity of MPM and MBM. In addition to the obtained enhancement in the computational cost, the Saleh dynamic model can be implemented efficiently using parallel computational approach when estimating the model coefficients.

Table (4.7) Computational cost of the least-squares' calculations on real numbers

Operation No.	Matrix Operation	Order of Operation
1	$\mathbf{A} = \mathbf{Z}^{*(k \times n)}.\mathbf{Z}^{(n \times k)}$	$O(2nk^2)$
2	$\mathbf{B} = (\mathbf{A})^{-1}$	$O(2k^3)$
3	$\mathbf{C} = \mathbf{B}^{(k \times k)}.\mathbf{Z}^{(k \times n)}$	$O(2nk^2)$
4	$\mathbf{j} = \mathbf{C}^{(k \times n)}\mathbf{y}^{(n \times 1)}$	$O(2nk)$

Table (4.8) Complexity comparison in FLOPs for different behavioral models.

Model Type	Number of FLOPs
Dynamic Saleh Model	65,664,000
2D-MPM	118,957,464
Memory Binomial	127,855,616

115

Inversion instability is another common issue in a matrix of a large number of elements. This is another drawback in estimating the MPM and MBM, which require inversion and multiplying large size matrices.
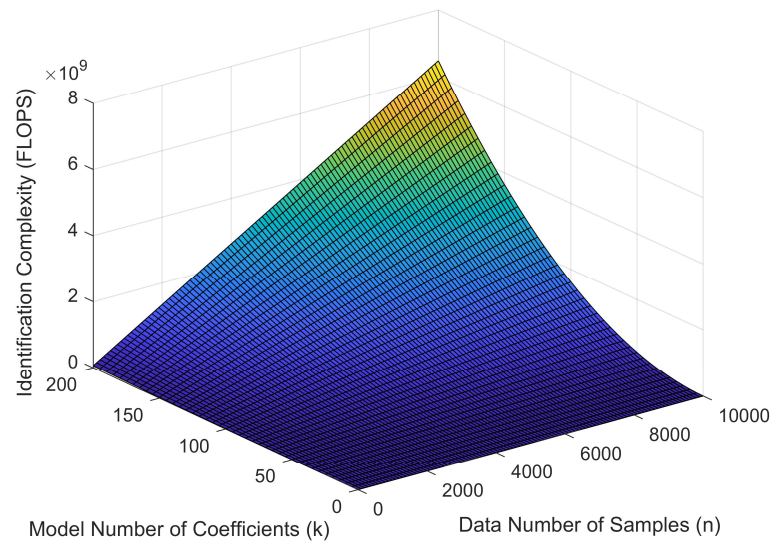
Figure 4.29 Complexity of models' estimation in terms of coefficients and modeling data size in number of samples.

Chapter 5

Power Amplifiers Linearization Techniques

5.1   Introduction

Signal approaches in linearizing PAs have become important aspects in modern wireless communications for improving the overall system signal-to-noise ratio and bit-error-rate [31]. Circuit-based linearization techniques such as analog feedback linearizers were developed in the literature to cancel-out a specific order of nonlinear distortion in RF PAs [60]-[78]. However, analog-based approaches are often insufficient because analog linearizers exhibit several drawbacks, such as high sensitivity to the variation of frequency and signal bandwidth. In addition, most of the PA design elements are frequency-dependent components. System level linearizers using digital signal processing techniques (e.g. DPD or shaping functions in ET PAs) exhibit more accuracy and implementation flexibility for wideband and multi-band wireless communications [80]-[85].

DPD models can be identified using either open-loop or closed-loop approaches. Adaptive modeling of DPD is a common example of a close-loop approach because the PA output signal is continuously acquired in the feedback branch for DPD model identification [65]. In other words, closed-loop DPDs are time-varying approaches, which exhibit better linearization performance, but the implementation complexity, bandwidth limitations, and stability are common design drawbacks [85]. However, open-loop DPD systems exhibit lower complexity and simpler implementation structure. In addition, open-loop DPDs are simpler nonlinear functions, which are placed on the baseband branch of the PA [70].

Open-loop DPD models are typically calculated from the PA behavioral model, because DPD models are mathematical inverse operations of the PA nonlinearity as depicted in Figure 5.1. Open-loop DPD model exhibits gain expansion property to compensate for the gain compression effect in PAs.

Two different modeling structures of the DPD approaches are presented in this chapter, the first approach is a SISO model that uses the PA manufacturing parameters, gain and third-order intercept point. Furthermore, a novel open-loop DISO digital predistortion is calculated for the PA with the ET system using a least-squares method. The linearity evaluation of the DPD models are compared with both the 2D-polynomial and binomial models.
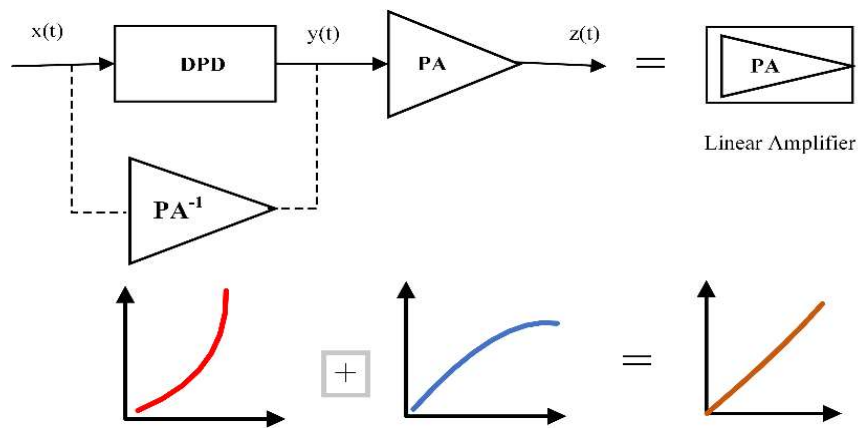
Figure 5.1 Block diagram illustrating the operation concept of DPD technique for PA linearization.

5.2 SISO-DPD Modeling Using IP₃

SISO-DPD models are extensively used approaches for linearizing constant-supply PAs in the signal digital baseband path, as illustrated in Figure 5.2. In addition, SISO-DPDs are deployed for ET PA, when the effect of dynamic supply is considered minor and negligible. The least-squares method is the typical modeling technique widely employed in the literature for PA modeling. Although the least-squares method is mathematically straightforward, an extensive data measurement is often required for model estimation, in addition to the complexity of inverting a large size matrix for coefficients computation. In this section, we derive a new approach for modeling DPD using gain and IP₃ parameters of the PA [78]. The DPD model can be mathematically written

$$x(t) = H^{-1}[u(t)] \qquad (5.1)$$

where u(t) and x(t) are the DPD input and output signals, respectively. The inverse function is calculated by exchanging the input and output variables in the Saleh AM/AM model H[.], and re-arranging the equation as

$$u\beta x^2 - \alpha x + u = 0 \qquad (5.2)$$

where α and β are the same parameters of the Saleh model. The inversion of the Saleh model is calculated by solving the quadratic Equation 5.2 with respect to the variable x.
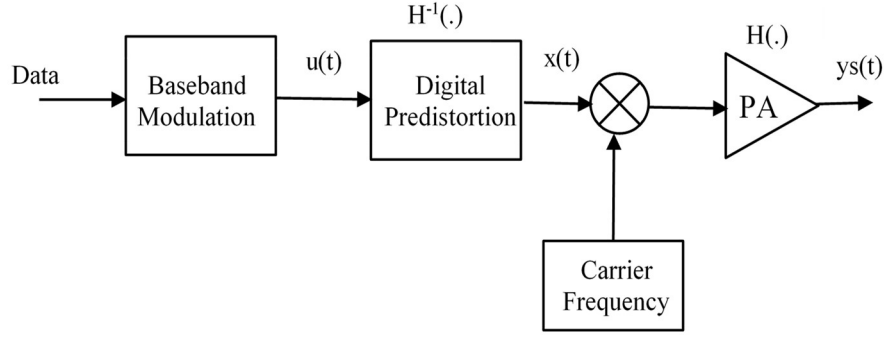
Figure 5.2 Block diagram of a transmitter system with DPD in the baseband branch.

$$H^{-1}[u] = \frac{\alpha - \sqrt{\alpha^2 - 4\beta u^2}}{2\beta u} \qquad (5.3)$$

The output of Equation 5.3 must be a real value for modeling the AM/AM DPD. Thus, the

signal magnitude (u) should satisfy the following constraint:

$$0 \le u < \sqrt{\frac{\alpha^2}{4\beta}} \qquad (5.4)$$

The parameters α and β are calculated from the PA gain and IP$_3$, as derived in Section

2.2.2. Substituting Equation 2.23 and Equation 2.25 into Equation 5.3, results in the

following SISO-DPD model [24]:

$$H^{-1}[u] = \frac{1 - \sqrt{1 - 3.012\, u^2 10^{\left(\frac{-IP_3}{10}\right)}}}{1.512\, u\, 10^{\left(\frac{-IP_3}{10} + \frac{G}{20}\right)}} \qquad (5.5)$$

Equation 5.5 is a simple expression of two parameters (G and IP$_3$) for a specific PA device.

The DPD input amplitude u must be limited by the condition in Equation 5.6 to satisfy a

real value of the DPD output signal [24].

$$0 \leq u < \sqrt{0.331 \times 10^{\left(\frac{IP_3}{10}\right)}} \tag{5.6}$$

Equation 5.6 represents a signal limiter function, which is required to maintain a specific signal level on the input port of the predistortion as shown in Figure 5.3 [24]. This equation shows that, the higher the IP_3, the larger the amplitude range of the DPD input signal. In fact, the DPD input amplitude range is significantly large, because IP_3 is a fictional point in PAs (e.g. around 10 dB higher than the 1dB compression point). A baseband WCDMA signal of 3.84 MHz bandwidth is used for evaluating the presented DPD model in the frequency and time domains. The results of the power spectrum density in Figure 5.4 illustrates a clear improvement in the upper and lower adjacent channels due to DPD linearization. The obtained spectrum enhancement in the ACPR is around 13.01 dBc. The time domain evaluation of the DPD model is shown in Figure 5.5 using the 16-QAM baseband signal, which illustrates a significant improvement in mapping the symbols' constellation on the output of PA. Finally, the results of both ACPR and NMSE between the PA input signal and PA output with DPD are illustrated in Table (5.1). The ACPR is calculated in the upper and lower adjacent channels (+/-2 MHz) of the WCDMA signal.
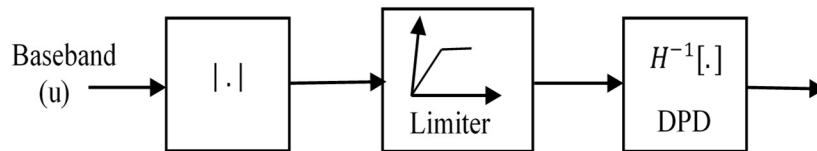
Figure 5.3 Block diagram of the AM/AM DPD model with magnitude limiter operation.

Table (5.1) DPD model performance in ACPR and NMSE results for power amplifier linearization.

Case	ACPR (dBc) +/- 2 MHz	NMSE (dB)
PA input	-36.05 / -36.55	*
PA output without linearization	-20.04 / -21.85	*
PA output with linearization	-33.05 / -33.97	-13.27
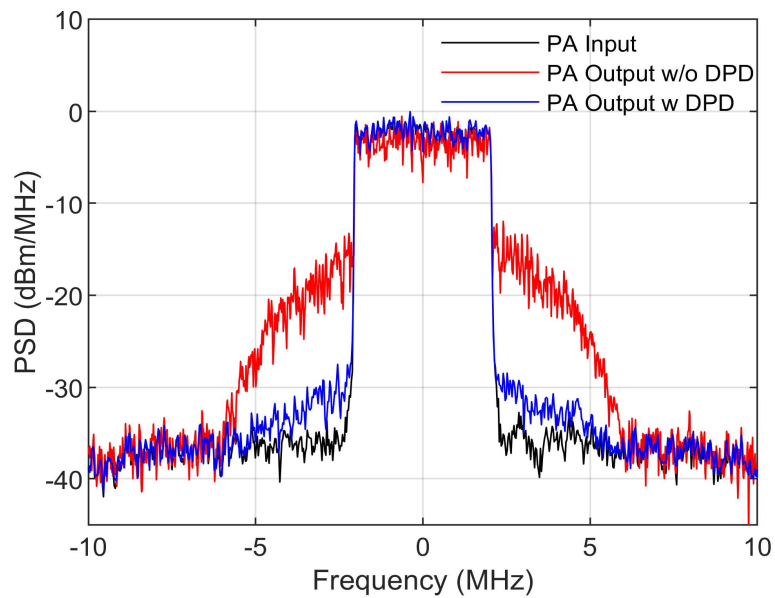
Figure 5.4 Spectrum of WCDMA signals at the input and output of the PA with and without DPD model.
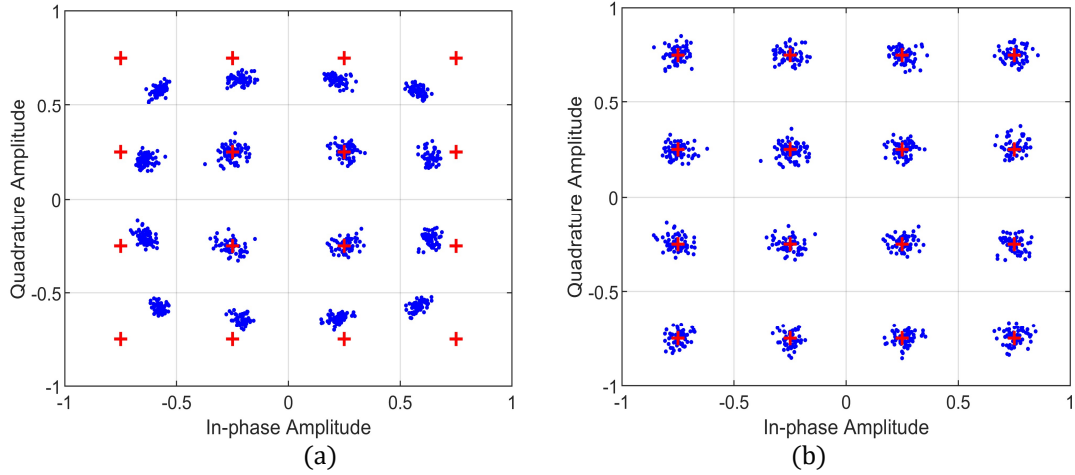
Figure 5.5 Constellation diagram of the 16-QAM signal on the output of the PA. (a) without DPD. (b) with DPD.

5.3 SISO-DPD Modeling Using 1dB Compression

DPD modeling using the 1dB compression point is extended from the previous approach of the DPD modeling using the IP_3 in Section 5.2 [25]. In this section, an additional linearization improvement is obtained compared to the previous modeling approach using the IP_3. This approach is derived directly from modeling the PA using the 1dB compression point in Section 2.2.2.2. By substituting the model parameters ε and μ in terms of gain, IP_3, and 1dB compression point in Equation 5.7, results in an expression of the derived DPD model as depicted in Equation 5.8. The dynamic range of the DPD amplitude is expressed as in Equation 5.9 [25]. Finally, the DPD model assessment in a frequency domain is shown in Figure 5.6 in terms of power spectral density. In addition, Table (5.2) reports the numerical results in ACPR evaluation of the linearization technique [25].

$$D[h] = \frac{\varepsilon - \sqrt{\varepsilon^2 - 4\mu h^2}}{2\mu h} \tag{5.7}$$

$$D[h] = \frac{1 - \sqrt{1 - 4h^2 \times 10^{\left(\frac{-5G}{24} + \frac{IP_3}{15} + \frac{157}{1500}\right)} \left(0.48 \times 10^{\left(\frac{3G}{20} + \frac{-IP_3}{10} + \frac{-P_{1dB}}{10}\right)} - 0.048 \times 10^{\left(\frac{G}{20} + \frac{-P_{1dB}}{5}\right)}\right)^{\frac{5}{6}}}}{2h \times 10^{\left(\frac{-7G}{60} + \frac{IP_3}{30} + \frac{4}{75}\right)} \left(0.48 \times 10^{\left(\frac{3G}{20} + \frac{-IP_3}{10} + \frac{-P_{1dB}}{10}\right)} - 0.048 \times 10^{\left(\frac{G}{20} + \frac{-P_{1dB}}{5}\right)}\right)^{\frac{2}{3}}} \tag{5.8}$$

$$0 < h < \frac{1}{2} \frac{10^{\left(\frac{5G}{48} + \frac{-IP_3}{30} + \frac{-157}{3000}\right)}}{\left(0.48 \times 10^{\left(\frac{3G}{20} + \frac{-IP_3}{10} + \frac{-P_{1dB}}{10}\right)} - 0.048 \times 10^{\left(\frac{G}{20} + \frac{-P_{1dB}}{5}\right)}\right)^{\frac{5}{12}}} \tag{5.9}$$
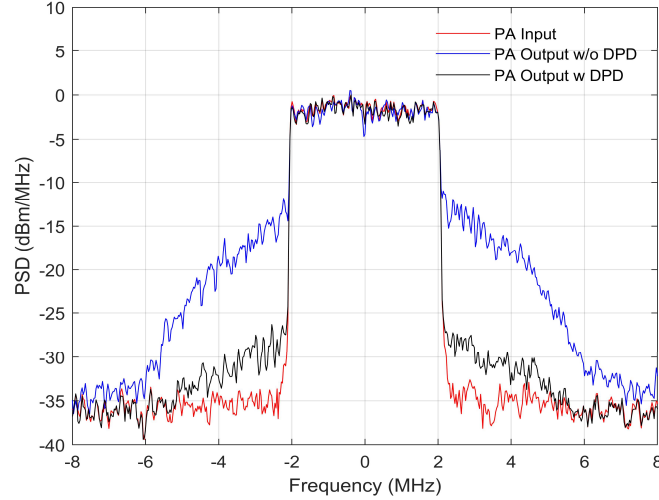
Figure 5.6 Input and output power spectrum for the cases of a PA without DPD and a PA with DPD.

Table (5.2) The linearization capability in ACPR of the digital predistortion model.

WCDMA Band	Without Linearization (dBc)	With Linearization (dBc)
Upper Band	-18.42	-31.23
Lower Band	-19.59	-32.12

5.4 Enhanced SISO-DPD Modeling

Polynomial-based DPD models are popular linearization techniques widely used to compensate for a weak-nonlinear distortion in PAs [1]. However, model dynamic range and system stability are common drawbacks of high order polynomials. In this section, a new linearization approach is derived for PAs from the enhanced Saleh model for SSPAs (Enhanced Saleh model is presented in 2.2.2.3). The DPD model in this work consists of 3 parameters and can be deployed for strong-nonlinearity PAs. The mathematical representation of the DPD model is

$$u(t) = F_{es}^{-1}(d(t)) \tag{5.10}$$

where $d(t)$ and $u(t)$ are the envelope signals of the DPD model input and output, respectively. $F_{es}^{-1}[.]$ denotes the DPD model. The inverse function of the enhanced Saleh model can be expressed as

$$d = \frac{\alpha\, u + \lambda\, u^2}{1 + \beta\, u^2} \tag{5.11}$$

The quadratic form of Equation 5.11 is

$$(d\beta - \lambda)u^2 - \alpha\, u + d = 0 \tag{5.12}$$

125

The solution of Equation 5.12 is computed using the following quadratic formula, and by considering the negative sign in the root term for real and normalized output amplitude

$$F_{es}^{-1}(d) = \frac{\alpha - \sqrt{\alpha^2 - 4\beta d^2 + 4d\lambda}}{2(d\beta - \lambda)} \tag{5.13}$$

The following constraint on the DPD input amplitude is required to meet the condition of real amplitude value.

$$|d| \leq \frac{\lambda + \sqrt{\lambda^2 + \beta\alpha^2}}{2\beta} \tag{5.14}$$

The signal clipping constraint in Equation 5.14 can be used in a combination with other clipping approaches for power efficiency enhancement in OFDM signals. This is because OFDM signals exhibit high-peak to average power ratio.

The evaluation results of the DPD model are illustrated using the AM/AM conversion for the PA and DPD model as depicted in Figure 5.7.

The DPD model evaluation using a 16-QAM OFDM signal is depicted in Figure 5.8, which shows a signal constellation diagram consisting of the reference symbols as well as the amplified symbols. The presented DPD model in this work is numerically more stable than the higher-order Taylor model, and it can be deployed for strong nonlinearity PAs over an adequate amplitude range.
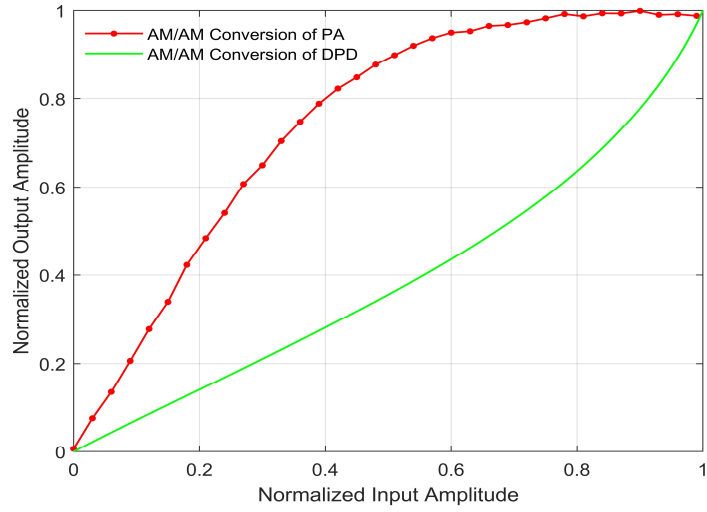
Figure 5.7 The AM/AM characteristics of the PA and DPD model.

(a)   (b)
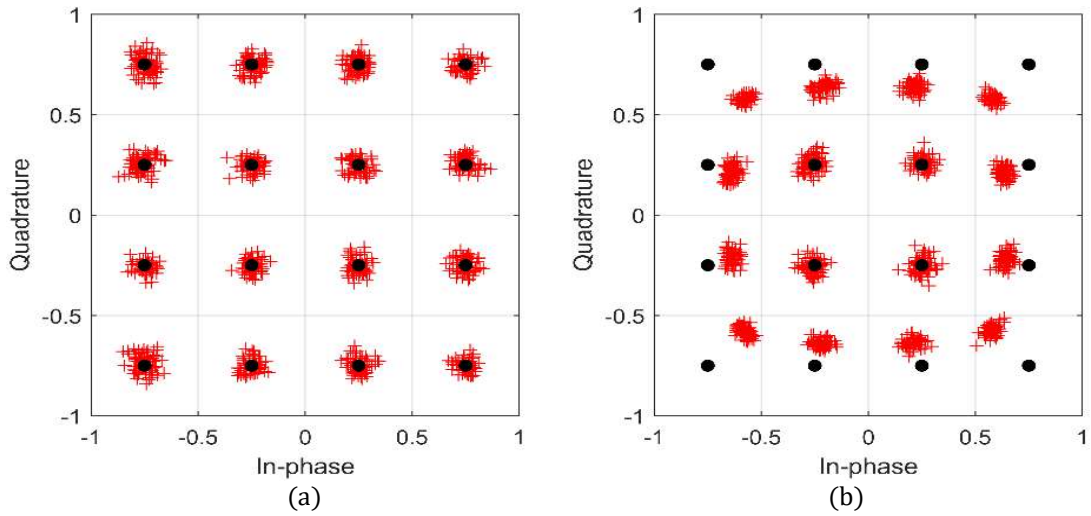
Figure 5.8 Constellation of 16-QAM OFDM baseband output signal. (a) PA with DPD. (b) PA without DPD.

5.5 DISO-DPD Modeling for ET PA

The time-varying supply voltage exhibits significant effects on the model accuracy and nonlinear distortion of ET PAs as discussed in the literature [18], [19], [27]. A dual-input open-loop digital predistorter model is derived in this work by inverting the extended Saleh model [27]. The DPD model based on the extension of the Saleh model considers the supply voltage as an additional independent input variable to account for the dynamic nonlinear distortion in both AM/AM and AM/PM conversions.

The extended AM/AM and AM/PM models of DPD are combined using complex polar operation, as illustrated in Equation 5.15. The amplitude linearizer (AM/AM DPD) is calculated by inverting the ET PA AM/AM function, and the phase linearizer (AM/PM DPD) is calculated by inverting the ET PA AM/PM function [27]. The estimation of the $PA_{AM}(.)$ and $PA_{PM}(.)$ functions are described in Chapter 4 to model the ET PA

$$z(x, v_{en}) = PA_{AM}\left(x, v_{en}\right)e^{j\left(PA_{PM}\left(x, v_{en}\right)\right)} \tag{5.15}$$

where z is the ET PA complex baseband output signal, x and v_{en} are the ET PA complex baseband input and the dynamic supply voltage, respectively.

5.5.1   Predistortion of the AM/AM Conversion

The AM/AM digital predistortion function $D_A(.)$ is expressed as

$$D_A\left(u, v_{en}\right) = PA_{AM}^{-1}\left(x, v_{en}\right) \tag{5.16}$$

where u is the DPD complex baseband input signal and $PA_{AM}(.)$ is the ET PA static AM/AM function, which was derived in Section 4.7, and can be re-expressed [27]

$$PA_{AM}\left(x, v_{en}\right) = \frac{\boldsymbol{\alpha} \mathbf{v}_{\alpha}^{\mathrm{T}} |x|}{1 + \boldsymbol{\beta} \mathbf{v}_{\beta}^{\mathrm{T}} |x|^2} \tag{5.17}$$

where $\boldsymbol{\alpha} = \left[\alpha_1, \alpha_2, \ldots \alpha_{N_A}\right]$ and $\boldsymbol{\beta} = \left[\beta_1, \beta_2, \ldots \beta_{N_B}\right]$ are two vectors consisting of the ET PA model coefficients. $\mathbf{v}_\alpha$ and $\mathbf{v}_\beta$ are the vectors of the envelope voltages as expressed in Equation 4.32 and Equation 4.33, respectively. The output signal of the AM/AM-DPD function represents the input signal of the ET PA, because the PA and DPD are connected in-series as shown in Figure 5.1. Thus, the $D_{AM}(.)$ function is

$$D_{AM}(u, v_{en}) = |x| \tag{5.18}$$

The modeling objective of the $D_{AM}(.)$ function is to compensate for static AM/AM nonlinear distortion in the ET PA. Therefore, the condition to be satisfied by a linearized ET PA AM/AM is expressed

$$PA_{AM}(D_{AM}(u, v_{en})) = |u| \tag{5.19}$$

Substituting Equation 5.18 and Equation 5.19 into Equation 5.20, results in the following:

$$\frac{\boldsymbol{\alpha} \mathbf{v}_{\alpha}^{\mathrm{T}} |x|}{1 + \boldsymbol{\beta} \mathbf{v}_{\beta}^{\mathrm{T}} |x|^2} = |u| \tag{5.20}$$

$$u\,\boldsymbol{\beta} \mathbf{v}_{\beta}^{\mathrm{T}} |x|^2 - \boldsymbol{\alpha} \mathbf{v}_{\alpha}^{\mathrm{T}} |x| + u = 0 \tag{5.21}$$

The solution of the quadratic formula in Equation 5.21 is [27]

$$|x| = \frac{\boldsymbol{\alpha} \mathbf{v}_{\alpha}^{\mathrm{T}} - \sqrt{(\boldsymbol{\alpha} \mathbf{v}_{\alpha}^{\mathrm{T}})^2 - 4\boldsymbol{\beta} \mathbf{v}_{\beta}^{\mathrm{T}} |u|^2}}{2\boldsymbol{\beta} \mathbf{v}_{\beta}^{T} |u|} \tag{5.22}$$

A negative sign is considered in the root-square term, because the variable $|x|$ is real and normalized in this work. Equation 5.22 is valid on the following magnitude interval [27]

$$0 \leq |u| \leq \sqrt{\frac{(\boldsymbol{\alpha}\mathbf{v}_\alpha^\mathrm{T})^2}{4\boldsymbol{\beta}\mathbf{v}_\beta^\mathrm{T}}} \qquad (5.23)$$

The DPD coefficients $\boldsymbol{\alpha}$ and $\boldsymbol{\beta}$ in Equation 5.22 are calculated from the ET PA modeling described earlier in Section 4.7.1. A simulation result of Equation 5.22 is shown in Figure 5.9 of the output amplitude $|x|$ with respect to the input amplitude $|u|$ and the envelope signal (v_{en}). The implementation of the AM/AM-DPD model in Equation 5.22 is represented in a simplified block diagram consisting of mathematical operations as in Figure 5.10.
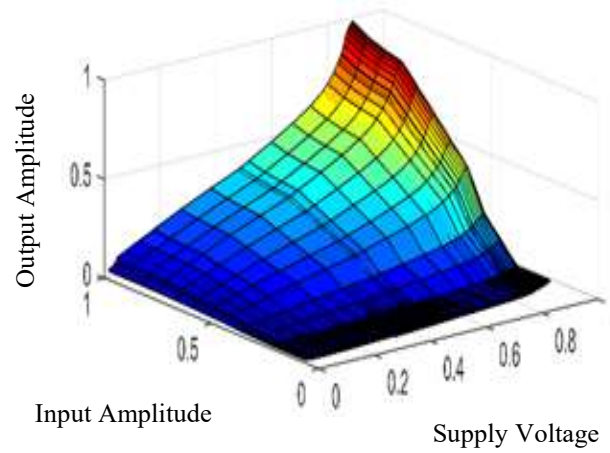
Figure 5.9   AM/AM DPD model versus the input amplitude and supply voltage.
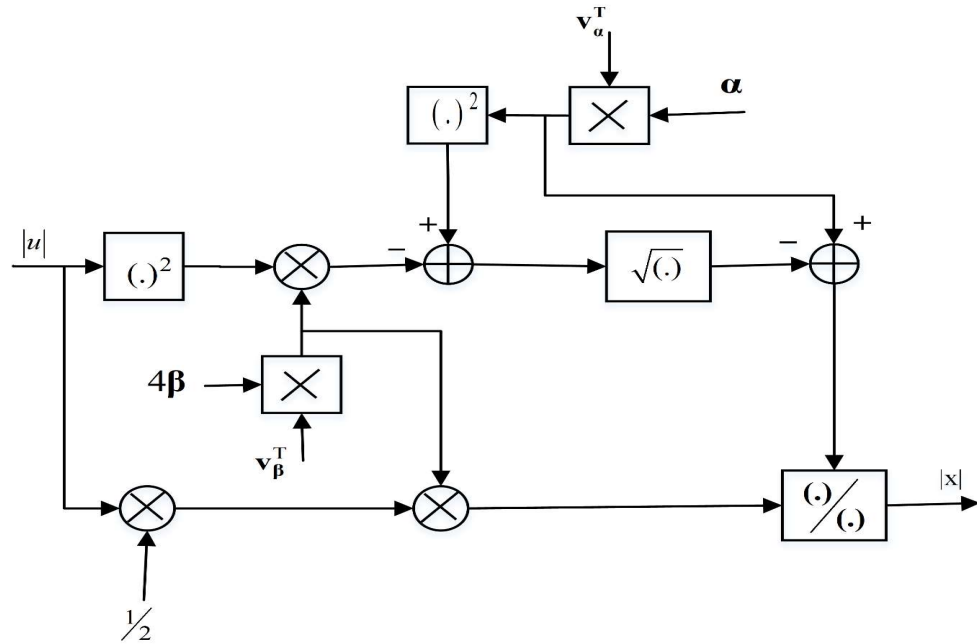
Figure 5.10 Mathematical operation structure of the AM/AM DPD.

5.5.2 Predistortion of the AM/PM Conversion

The AM/PM modeling of the DPD is calculated from the PA phase function using a complex system domain. In general, the overall phase of two complex systems in series represents a sum operation of the two functions. Hence, the AM/PM DPD model is calculated directly from the ET PA AM/PM function, because the DPD model is typically followed by the ET PA.

The AM/PM DPD function $D_P(.)$ is used in this dissertation to eliminate the ET PA AM/PM nonlinearity [27], which is mathematically satisfied by the following condition:

$$e^{j(D_P(u,v_{en}))} \cdot e^{j(\theta(x,v_{en}))} = 1 \qquad (5.24)$$

where $\theta(.)$ is the ET PA AM/PM function, which was derived earlier in Section 4.12 and

is expressed

$$\theta(x, v_{en}) = \frac{|x|^2 \lambda \mathbf{v}_\lambda^{\mathrm{T}}}{1 + |x|^2 \gamma \mathbf{v}_\gamma^{\mathrm{T}}} \tag{5.25}$$

Substituting Equation 5.17 into Equation 5.24, results in the following $D_P(.)$ function [27].

$$D_p(u, v_{en}) = \frac{-|u|^2 \lambda \mathbf{v}_\lambda^{\mathrm{T}}}{1 + |u|^2 \gamma \mathbf{v}_\gamma^{\mathrm{T}}} \tag{5.26}$$

where λ and γ are the ET PA coefficient vectors, which were derived earlier in Section 4.12.1. Figure 5.11 depicts the expansion curvature of the $D_p(.)$ phase function with respect to the magnitude of the input amplitude $|u|$ and envelope signal (v_{en}) using the same ET PA coefficients estimated from the least-squares method [27].

Finally, the combined DPD model of the AM/AM function D_A (.) and the AM/PM function D_P (.) in a complex notation are represented as follows:

$$x(u, v_{en}) = D_A(u, v_{en}) e^{j(D_P(u, v_{en}) + \angle u)} \tag{5.27}$$

A block diagram of a complete DPD architecture in Equation 5.27 with the ET PA is shown in Figure 5.12 using two independent blocks of magnitude and a phase linearizer model.

The calculated DPD expressions in Equations 5.22 and Equation 5.26 exhibit simple AM/AM and AM/PM DPD models. Furthermore, the proposed DPD model uses the same coefficients of the proposed ET PA model. This is another advantage that can significantly reduce the computational cost of the DPD identification [27].
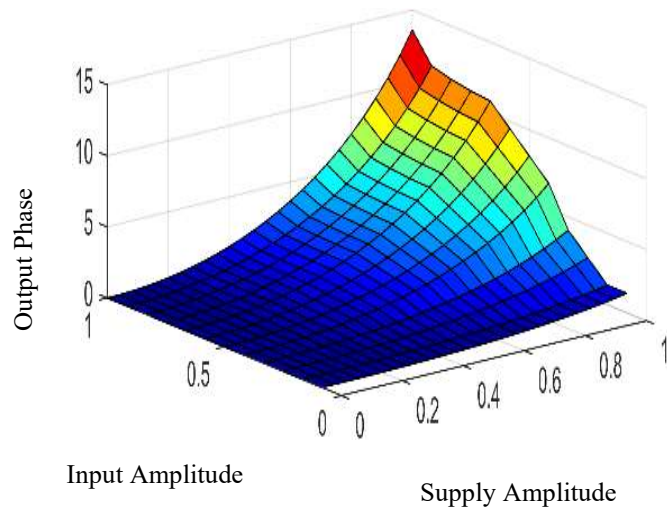
Figure 5.11   The AM/PM predistortion function in terms of the input amplitude and supply voltage
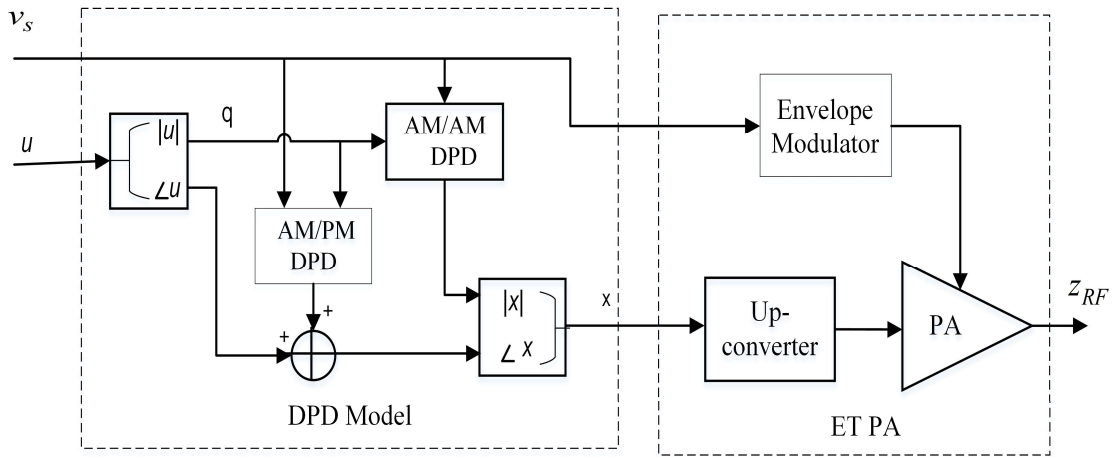
Figure 5.12   Block diagram of the AM/AM and AM/PM DPD functions in cascade with the envelope tracking power amplifier.

133

5.6   Evaluation of the DPD Model

All DPD models exhibit limitations in practical applications for mitigating the nonlinear distortion of PAs. This is because the hysteresis nonlinearity in PAs is difficult to characterize and it results from many different independent and dependent sources. In addition, phase and memory effect in PAs are changeable and difficult to quantify precisely. Therefore, DPD performance is often limited to cancel-out all the nonlinear distortions in RF PAs. The DPD linearization capability is evaluated in time domain and frequency domain. The NMSE evaluation in time domain and ACPR evaluation in frequency domain are two most widely used figures-of-merit for evaluating the linearization performance [55]. NMSE and ACPR are defined, respectively as follows:

$$NMSE_{dB} = 10 \ \log_{10}\left(\frac{\sum\limits_{n=1}^{N} |u(n) - z(n)|^2}{\sum\limits_{n=1}^{N} |u(n)|^2} \right)$$

(5.28)

where u is the DPD input signal and z is the PA output signal with DPD model in-series. N is total number of symbols in each signal. ACPR is a figure-of-merit specifying the power spectral emission in the nearby channels of the baseband signal due to the RF PA nonlinear distortion. ACPR is a power ratio in a frequency domain between the adjacent channel power and the desired channel power, which is calculated using [27]

$$ACPR_{dB} = 10\log_{10}\left(\frac{\displaystyle\int_{\left(f_c + f_{ofs} + \frac{-B_{adj}}{2}\right)}^{\left(f_c + f_{ofs} + \frac{B_{adj}}{2}\right)} P_o(f)\,df}{\displaystyle\int_{\left(f_c + \frac{-B_{ds}}{2}\right)}^{\left(f_c + \frac{B_{ds}}{2}\right)} P_o(f)\,df}\right) \tag{5.29}$$

where $P_o(f)$ is the output power spectral density, f_c is the center frequency, B_{ds} is the

bandwidth of the desired signal, B_{adj} is the bandwidth of the adjacent channel, and f_{ofs} is the

offset frequency. The parameters of the ACPR (f_c, B_{adj}, f_{ofs}) are clearly illustrated in Figure

5.13 on the graphical baseband PSD wireless baseband signal.
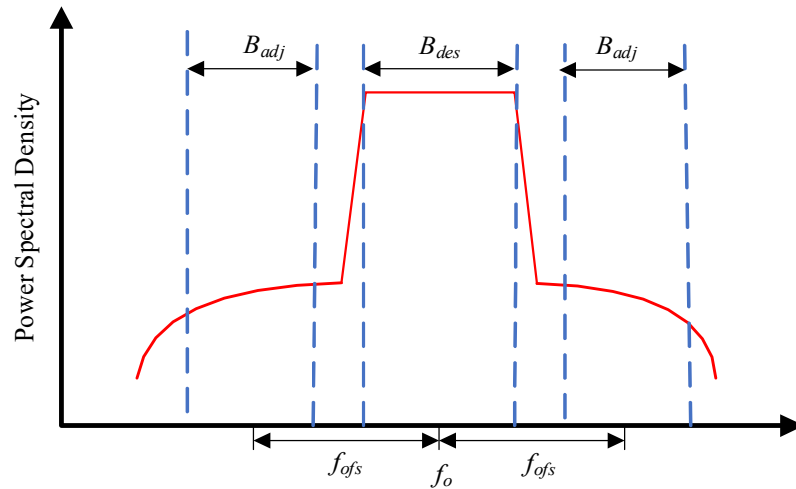
Figure 5.13 ACPR parameters representation depicted on the spectrum of baseband signal.

5.6.1 Modeling Results of the Digital Predistortion

The DPD model in this work is evaluated using the baseband WCDMA signal. The DPD evaluation in a time domain using both the AM/AM and AM/PM conversions of the PA is depicted in Figure 5.14 for the RF PA with and without DPD model [27]. This illustrates a clear linearity improvement in the AM/AM conversion as depicted in Figure 5.14 (a), in addition to phase enhancement in Figure 5.14 (b).

The performance of the DPD linearization in a frequency domain using the PSD is illustrated in Figure 5.15 [27]. A spectrum improvement of -17.11/-16.75 dB in ACPR is obtained due to the DPD linearization [47].

The model complexity in number of coefficients and linearization efficiency in ACPR are illustrated in Table (5.3), as compared with the state-of-the-art dual-input polynomial and binomial DPD models [27]. Finally, the ET PA with DPD is evaluated using the 16-QAM signal as shown in the signal constellation diagram of Figure 5.16. The scattering effect due to the nonlinear distortion of the ET PA without DPD is depicted in Figure 5.16 (a) and the improvement in symbols constellation diagram is in Figure 5.16 (b).
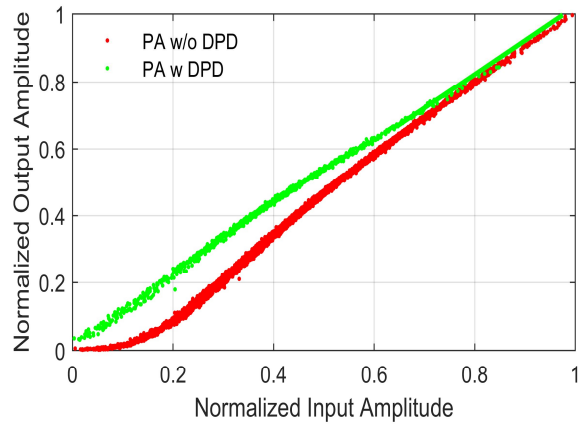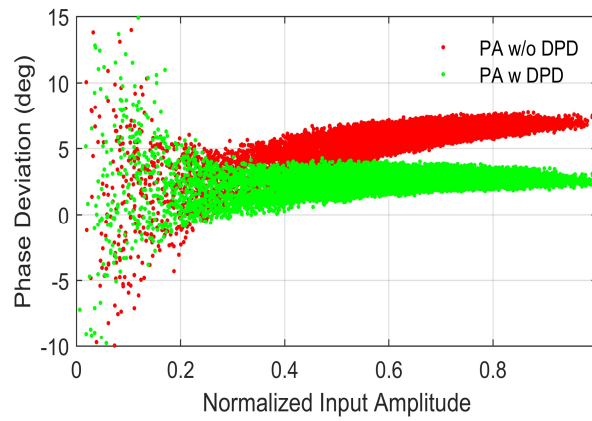
Figure 5.14 Nonlinear memory conversions of the ET PA, before and after linearization (a) AM/AM conversion (b) AM/PM conversion.
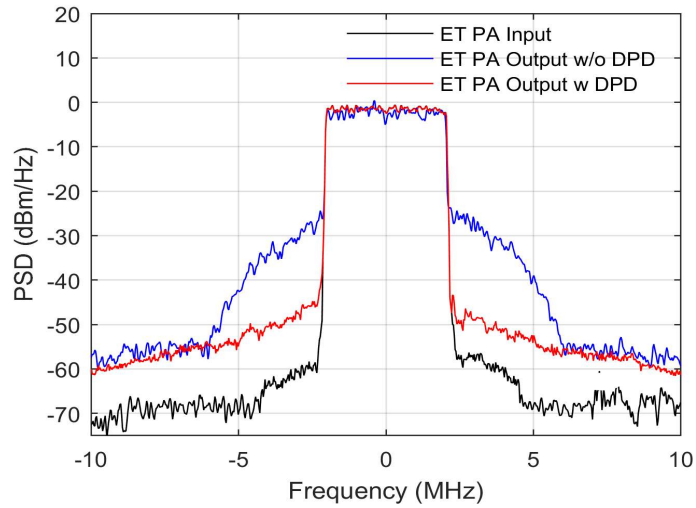
Figure 5.15 Power spectrum density of the ET PA output with and without digital predistortion.

Table (5.3) Model evaluation of the ET PA linearization using different digital predistortion models.

Case	Nonlinear Order	Number of Coefficients	ACPR (dBc) -/+4 MHz
PA Input	*	*	-65.85/-64.32
PA Output	*	*	-35.22/-34.56
Classical Saleh DPD	*	4	-38.03/-36.82
Extended Saleh DPD	$N_A=2$, $N_B=4$, $P_a=2$, $P_b=3$	11	-51.28/-50.25
	$N_A=6$, $N_B=5$, $P_a=5$, $P_b=2$	18	-52.33/-51.31
Dual-Input DPD Polynomial	K=2, N=5	15	-51.15/-50.20
	K=3, N=9	36	-52.78/-51.69
Binomial DPD	Q=5	21	-50.81/-49.78
	Q=7	36	-52.35/-51.37
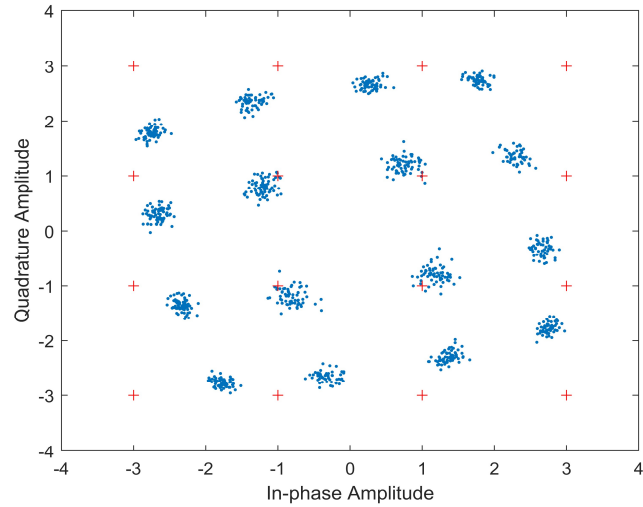
(a)
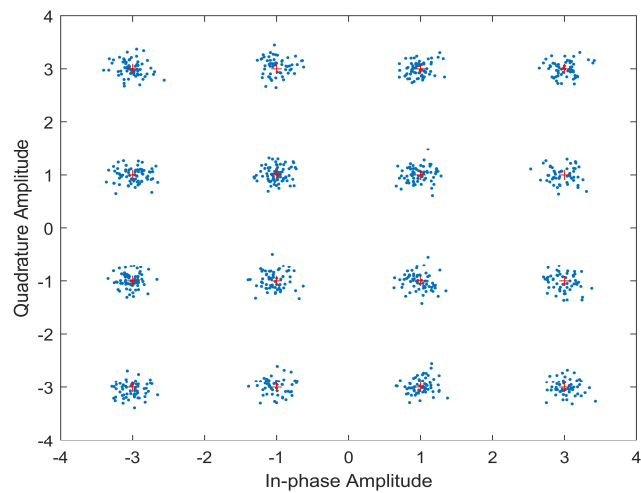
(b)

Figure 5.16 Measured 16-QAM signal constellation on the output of the PA.

5.6.2   Complexity of the Digital Predistortion

Two popular approaches are typically employed for modeling DPDs, direct-learning and indirect-learning. In the indirect-learning approach, the PA and DPD are modeled independently. On the other hand, the direct-learning approach requires a direct mathematical operation (e.g. P-inverse) when inverting the ET PA function, using the same

model coefficients of the ET PA [50]. Most of the DPD models for ET PA are estimated using the indirect-learning approach, because it is mathematically difficult to invert dual-input behavioral models of ET PAs, especially when the model consists of many coefficients.

The modeling complexity of the DPD model using the inversion of the extended Saleh model is lower than the modeling complexity of MPM and MBM. This is because the parameters' extraction of the dynamic Saleh model requires around half the computational cost of the 2D-MPM and MBM models, as demonstrated in Section 4.12.3, and the 2D-DPD model uses the same coefficients of the ET PA model. The proposed DPD functions can be used with any ET system.

Chapter 6

Conclusions and Future Work

6.1   Conclusions

This dissertation has presented new behavioral modeling and linearization techniques for ET PAs and constant-supply RF PAs in communication systems. The static nonlinearity in the RF PA was estimated in this work using the technical design parameters of the constant-supply PA such as gain, IP_3 and P_{1dB}. In addition, a DPD model was calculated by using the inversion of the Saleh behavioral model from the PA parameters, gain, IP_3, and P_{1dB}. This approach facilitates both the modeling and DPD of RF PAs, since the gain, IP_3, and P_{1dB} are easily provided from the manufacturing data sheets.

The Hammerstein model was used in this dissertation to quantify the dynamic nonlinearity in the AM/AM conversion of ET PAs. In addition, two different approaches were used to model the dynamic nonlinearity in the AM/PM conversion, the 2D-MPM and the Hammerstein model architecture. In the Hammerstein approach, the dynamic nonlinearity was decomposed into a static model in series with a FIR digital filter.

The static nonlinearities in AM/AM and AM/PM modeling were calculated using the proposed extensions of the Saleh model for dynamic-supply PAs. The evaluation results showed that the accuracy of the Saleh empirical model is significantly improved when including the effect of the dynamic supply voltage.

The dynamic Saleh model was developed to predict with adequate accuracy the AM/AM, AM/PM, and long-term memory effects in the ET PA. The long-term memory effect in AM/AM and AM/PM conversions is a specific challenge in the ET PA because of time-varying supply voltages, in addition to the effect of the energy storage elements

(e.g. capacitors and inductors) in ET PA circuits. The long-term memory effect was modeled using two digital FIR filters, one filter for the AM/AM conversion and another filter for the AM/PM conversion.

All the model coefficients (static and memory models) were calculated by solving normal equations using the least-squares method. Distortion effects in the ET PAs were mathematically analyzed using the proposed model and compared to the state-of-the-art ET PA models, such as the memory binomial and memory polynomial models.

The modeling accuracy performance was evaluated in the time and frequency domains using NMSE and ACEPR. The optimal NMSE and ACEPR were calculated by sweeping the model parameters such as the nonlinear orders of the extended Saleh model and the memory-depth of the FIR filters. The optimal accuracy obtained for the proposed behavioral model is -42.48 dB in NMSE and -51.80 in ACEPR using 20 coefficients. All the model coefficients are real numbers. Therefore, a reduction in the complexity (number of FLOPs) of the model estimation was observed and compared to the state-of-the-art models of complex type coefficients.

DPD models for linearizing ET PAs were calculated mathematically by inverting the extended static AM/AM and AM/PM conversions. Hence, this approach compensated for nonlinear distortion due to both amplitude variation and phase deviation.

The capability to improve the linearity of the PA was evaluated using NMSE and ACPR with respect to the swept model's nonlinear orders. The optimal results of the DPD model with the ET PA in NMSE and ACPR are -30.58 dB and -52.33/-51.31 dBc, respectively, using a WCDMA signal. The DPD model results showed a significant

reduction of the spectrum regrowth in the power spectrum density and time domain AM/AM and AM/PM distortions.

6.2 List of Publications

[1] H. Al-kanan, F. Tafuri, and F. Li, "Hysteresis Nonlinearity Modeling and Linearization Approach for Envelope Tracking Power Amplifiers in Wireless Systems," Microelectronics Journal, vol 82, pp.101-107, Dec. 2018.

[2] H. Al-kanan, F. Li, and F. Tafuri "Extended Saleh model for behavioral modeling of envelope tracking power amplifiers," Proceedings of IEEE 18th Wireless and Microwave Technology Conference, FL, pp. 1-4, 2017.

[3] H. Al-kanan, X. Yang, and F. Li "Saleh Model and Digital Predistortion for Power Amplifiers in Wireless Communications Using the Third-Order Intercept Point," Journal of Electronic Testing: Theory and Applications, vol. 35, no. 3, pp. 359-365, 2019.

[4] H. Al-Kanan, F. Li, and F. Tafuri, "Comparison of 2-D Behavioral Models for Modeling and Digital Predistortion of Envelope Tracking Power Amplifiers," Proceedings of IEEE Asia-Pacific Microwave Conference, Kuala Lumpar, pp. 999-1002, 2017.

[5] H. Al-kanan, X. Yang, and F. Li, "Improved estimation for Saleh model and predistortion of power amplifiers using 1dB compression point," IET Journal of Engineering, vol. 2020, no.1, pp.13-18, 2020.

6.3 Future Work

The performance of RF PAs exhibits a dominant impact on the overall communication transceivers, in particular for massive Multi-Input Multi-Output (MIMO) systems and fifth-generation (5G) wireless communications. The 5G systems will require more integrated PAs in RF chains. Thus, the power efficiency and linearity of multiple

PAs have become more challenging and critical than 3G/4G systems. The ET and DPDs are more attractive approaches for power efficiency and linearity enhancements to overcome the challenges and reliability of MIMO and beamforming systems. In addition, the higher bandwidth, data rate and the complex modulation schemes in future communications will require a complicated modeling and linearization approach to address such effects on ET PAs. Hence, we suggest the following future work:

1. Implementing and evaluating the proposed model using multi-band wireless signals.

2. Compensating for the long-term memory distortion effect in the ET PA.

3. Using an IIR filter instead of a FIR filter for the dynamic AM/AM and AM/PM conversion which might lower the number of coefficients and computational costs.

4. Implementing an adaptive DPD using the extended Saleh model.

References

[1] S. C. Cripps, "Advanced techniques in RF power amplifiers design," Nonvood, MA: Anech House, 2002.

[2] A. A. M. Saleh and D. C. Cox, "Improving the power added efficiency of FET amplifiers operating with varying-envelope signals," IEEE Trans. on Microwave Theory and Techniques, vol. 31, no. 1, pp. 51–56, 1983.

[3] P. Asbeck and Z. Popovic, "ET comes of age: envelope tracking for higher-efficiency power amplifiers," IEEE Microwave Magazine, vol. 17, no. 3, pp. 16–25, 2016.

[4] S. Hara and R. Prasad, "Multicarrier techniques for 4G Mobile communications," Artech House, Boston, 2003.

[5] A. R. Kaye, D. A. George, and. M. J. Eric, "Analysis and compensation, of bandpass nonlinearities for communications," IEEE Trans. on Communications, vol. 20, pp. 965-972, 1972.

[6] X.Li, C. M. Liu, and F. Li, "Statistical analysis of CDMA and 3G signal models," Proceedings of IEEE 11th International Conference on Signal Processing, Beijing, 2012.

[7] X. Li, C. M. Liu, H. Xiao, and F. Li, "Nonlinearity analysis of RF power amplified TD-SCDMA signal," Proceedings of IEEE 10th International Conference on Signal Processing, Beijing, 2010.

[8] Z. Wang, "Envelope tracking power amplifiers for wireless communications," Norwood, US: Artech House, 2014.

[9] H. Ochiai, and H. Imai, "On the distribution of the peak-to-average power ratio in OFDM signals," Proceedings of IEEE International Conference on Signal Processing, Beijing, 2012.

[10] G. Hanington, P. Chen, P. M. Asbeck, and L. E. Larson, "High efficiency power amplifier using dynamic power-supply voltage for CDMA applications," IEEE Trans. on Microwave Theory and Techniques, vol. 47, no. 8, pp.1471–1476, 1999.

[11] J. Heiskala and J. Terry, "OFDM wireless LANs : A theoretical and practical guide," SAMS, 2002.

[12] M. Iwamoto, A. Williams, P. Chen, A. G. Metgzer, L. E. Larson, and P. M. Asbeck, "An extended doherty amplifier with high efficiency over a wide power range," IEEE Trans. on Microwave Theory and Techniques, vol. 49, no. 12, pp. 2472–2479, 2001.

[13] H. Chireix, "High power outphasing modulation," Proceedings of IRE, vol. 23, no. 11, pp. 1370 –1392, 1935.

[14] P.N. Landin, J. Fritzin, W. Van Moer, M. Isaksson, and A. Alvand-pour, "Modeling and digital predistortion of class-D outphasing RF power amplifiers," IEEE Trans. on Microwave Theory and Techniques, vol. 60, no. 6, pp. 1907–1915, 2012.

[15] D. R. Anderson and W. H. Cantrell, "High efficiency high level modulator for use in dynamic envelope tracking CDMA RF power amplifiers," Proceedings of IEEE Microwave Symposuim and Digest, pp. 1509–1512, 2001.

[16] J. Staudinger, B. Gilsdorf, D. Newman, G. Norris, G. Sadowniczak, R. Sherman, and T. Quach, "High efficiency CDMA power amplifier using dynamic envelope tracking technique," Proceedings of IEEE Microwave Symposuim and Digest, pp. 873–976, 2000.

[17] M. Olavsbråten and D. Gecan, "Bandwidth reduction for supply modulated RF PAs using power envelope tracking," IEEE Microwave and Wireless Component Letters, vol. 27, no. 4, pp. 374-376, 2017.

[18] G. P. Gibiino, G. Avolio, D. M. Schreurs, A. Santarelli and F. Filicori, "A three-port nonlinear dynamic behavioral model for supply-modulated RF PAs," IEEE Trans. on Microwave Theory and Techniques, vol. 64, no. 1, pp. 133-147, 2016.

146

[19] K. Moon, Y. Cho, J. Kim, S. Jin, B. Park, and D. Kim, "Investigation of intermodulation distortion of envelope tracking power amplifier for linearity improvement," IEEE Trans. on Microwave Theory and Techniques, vol. 63, no. 4, pp. 1324-1333, 2015.

[20] A. Zhu, P. J. Draxler, C. Hsia, T. J. Brazil, D. F. Kimball, P. M. Asbeck, "Digital predistortion for envelope-tracking power amplifiers using decomposed piecewise volterra series," IEEE Trans. on Microwave Theory and Techniques, vol. 56, no. 10, pp. 2237-2247, 2008.

[21] F. F. Tafuri, D. Sira, T. S. Nielsen, "Memory models for behavioral modeling and digital predistortion of envelope tracking power amplifiers", Microprocessors and Microsystems, vol. 39, no. 8, , pp. 879-888, 2015.

[22] O. Hammi, F.M. Ghannouchi, and B. Vassilakis, "A compact envelope-memory polynomial for RF transmitters modeling with application to baseband and RF-digital predistortion," IEEE Microwave and Wireless Components Letters, vol. 18, no. 5, pp. 359 –361, 2008.

[23] D. Mirri, G. Iuculano, F. Filicori, G. A. Vannini, G. Pasini, and G. A. Pellegrini, "A modified Volterra series approach for the characterization of nonlinear dynamic systems," Proceedings of IEEE Instrumentation and Measurement Technology Conference, Brussels, Belguim, pp. 710–715, 1996.

[24] H. Al-kanan, X. Yang, and F. Li, "Saleh model and digital predistortion for power amplifiers in wireless communications using the third-order intercept point," Journal of Electronic Testing: Theory and Applications, vol. 35, no. 3, pp. 359-365, 2019.

[25] H. Al-kanan, X. Yang, and F. Li, "Improved estimation for Saleh model and predistortion of power amplifiers using 1dB compression point," IET Journal of Engineering, vol. 2020, no.1, pp.13-18, 2020.

[26] H. Al-kanan, F. Li and F. F. Tafuri, "Extended Saleh model for behavioral modeling of envelope tracking power amplifiers," Proceedings of IEEE 18th Wireless Microwave Technology Conference, Florida, pp. 1-4, 2017.

[27] H. Al-kanan, F. Tafuri, and F. Li, " Hystersis nonlinearity modeling and linearization approach for envelope tracking power amplifiers in wireless systems", Microelectronics Journal, vol 82, pp. 101-107, Dec. 2018.

[28] J. Jeong, D. F. Kimball, M. Kwak, C. Hsia, P. Draxler and P. M. Asbeck, "Wideband envelope tracking power amplifiers with reduced bandwidth power supply waveforms and adaptive digital predistortion techniques," IEEE Trans. on Microwave Theory and Techniques, vol. 57, no. 12, pp. 3307- 3314, 2009.

[29] F. Wang, A. Yang, D.F. Kimball, "Design of wide-bandwidth envelope-tracking power amplifiers for OFDM applications," IEEE Trans. on Microwave Theory and Techniques, vol. 53, no. 4, 2005.

[30] H. Xiao, "Spectrum modeling for linear RF power design for digital cellular communication signals," Ph.D. dissertation, Portland State University, 1999.

[31] J. Wood, "System-level design considerations for digital pre-distortion of wireless base station transmitters," IEEE Trans. on Microwave Theory and Techniques, vol. 65, no. 5, pp. 1880-1890, 2017.

[32] C. M. Liu, H. Xiao, Q. Wu, and F. Li, "Spectrum design of RF power amplifier for wireless communication systems," IEEE Trans. on Consumer Electronics, vol. 48,pp.72-80, 2002.

[33] X. Li and F. Li. "RF Power Amplifier's Nonlinear Modelling with Memory Effect." International Journal of Electronics Letters, vol 1, no. 1, pp. 44–49, 2013.

[34] C. Cho, W. Eisenstadt, and B. Stengel, "IIP3 estimation from the gain compression curve," IEEE Trans. on Microwave Theory and Techniques, vol. 53, no. 4, pp. 1197-1202, 2005.

[35] X. Li, B. S. Chen, C. M. Liu, X. R. Wang, K. R. Cho, and F. Li, " Spectrum Modeling and Regrowth for 4G Wireless Signals, " IET Electronics Letters, vol. 48,no. 4, p. 244-245, 2012.

[36] H. Ku, M. D. McKinley, and J. S. Kenney, "Quantifying memory effects in RF power amplifiers," IEEE Trans. on Microwave Theory and Techniques, vol. 50, no. 12, pp. 2843–2849, 2002.

[37] (Online) D. Talbot, "The Hottest Technology Not on Display at CES: Smart Radio Chips | MIT Technology Review". Technologyreview.com. Retrieved from https://www.technologyreview.com/s/523286/the-hottest-technology-not-on-display-at-ces-smart-radio-chips/.

[38] D. Kim, D. Kang, J. Choi, J. Kim, Y. Cho, and B. Kim, "Optimization for envelope shaped operation of envelope tracking power amplifier," IEEE Trans. on Microwave Theory and Techniques, vol. 59, no. 7, pp. 1787-1795, 2011.

[39] J. Kim, S. Member, D. Kim, Y. Cho, D. Kang, B. Park, "Analysis of envelope tracking power amplifier using mathematical modeling," IEEE Trans. on Microwave Theory and Techniques, vol. 62, no. 6, pp. 1352–1362, 2014.

[40] Y. Zhu, O. Klimashov, B. Jin, et al. "Novel shaping function for envelope tracking linearization," Proceedings of IEEE Asia Pacific Microwave Conference (APMC), Kuala Lumpar, pp. 402-405, 2017.

[41] J. Hoversten, S. Schafer, M. Roberg, M. Norris, D. Maksimovic, and Z. Popovic, "Codesign of PA supply signal processing for linear supply-modulated RF transmitters", IEEE Trans. on Microwave Theory and Techniques, vol. 60, no. 6, pp. 2010-2020, 2012.

[42] J. L. Woo, S. Park and Y. Kwon, "A wideband envelope-tracking CMOS linear transmitter without digital predistortion," Proceedings of IEEE Radio Frequency Integration Circuits Symposuim, Phoenix, AZ, pp. 367-370, 2015.

[43] J. J. Yan, C. Hsia, D. F. Kimball, Peter M. Asbeck, "Design of a 4-W Envelope Tracking Power Amplifier With More Than One Octave Carrier Bandwidth," IEEE Journal of Solid-State Circuits, vol. 47, no. 10, pp. 2298-2308, 2012.

[44] N. Wolff, W. Heinrich and O. Bengtsson, "100-MHz GaN-HEMT class-G supply modulator for high-power envelope-tracking applications," IEEE Trans. on Microwave Theory and Techniques, vol. 65, no. 3, pp. 872-880, 2017.

[45] C. Crespo-Cadenas, J. Reina-Tosina, and M. J. Madero-Ayora, "An equivalent circuit-based approach to behavioral modeling of long-term memory effects in wideband amplifiers," Microwave and Optical Technology Letters, vol. 53, no. 10, pp. 2278–2281, 2011.

[46] N. Benvenuto, F. Piazza, and A. Uncini, "A neural network approach to data predistortion with memory in digital radio systems," Proceedings of IEEE International Conference on Communications, pp. 232-236, 1993.

[47] H. Jang, A. Zai, T. Reveyrand, P. Roblin, Z. Popovic, and D. E. Root, "Simulation and measurement-based X-parameter models for power amplifiers with envelope tracking," IEEE Microwave Symposuim Digest, Seattle, WA, pp. 1-4, 2013.

[48] L. Gilabert and G. Montoro, "Look-up table implementation of a slow envelope dependent digital predistorter for envelope tracking power amplifiers," IEEE Microwave and Wireless Components Letters, vol. 22, no. 2, pp. 97-99, 2012.

[49] H. Al-Kanan, F. Li, and F. F. Tafuri , "Comparison of 2-D behavioral models for modeling and digital predistortion of envelope tracking power amplifiers," Proceedings of IEEE Asia-Pacific Microwave Conference, Kuala Lumpar, pp. 999-1002, 2017.

[50] H. Paaso and A. Mammela, "Comparison of direct learning and indirect learning predistortion architectures," IEEE Interenational Symposuim on Wireless Communications, Reykjavik, pp. 309-313, 2008.

[51] A. A. M. Saleh, "Frequency independent and frequency dependent nonlinear model of TWT amplifiers," IEEE Trans. on Communications, vol. COM-29, pp. 1715-1720, 1981.

[52] H. Ku and J. S. Kenney, "Behavioral modeling of nonlinear RF power amplifiers considering memory effects," IEEE Trans. on Microwave Theory and Techniques, vol. 51, no. 12, pp. 2495–2504, 2003.

[53] J. C. Pedro and S. A. Maas, "A comparative overview of microwave and wireless power-amplifier behavioral modeling approaches," IEEE Trans. on Microwave Theory and Techniques, vol. 53, no. 4, pp. 1150–1163, 2005.

[54] C. E. Shannon, "A mathematical theory of communication," The Bell System Technical Journal, vol. 27, pp. 379–423 and 623–656, 1948.

[55] P. Landin, M. Isaksson, and P. Handel, "Comparison of evaluation criteria for power amplifier behavioral modeling," Proceedings of IEEE Microwave Symposuim Digest, Atlanta, pp. 1441–1444, 2008.

[56] J. Wood, "Behavioral modeling and linearization of RF power amplifiers," Artech House, USA, 2014.

[57] J. Wood, D. E. Root, and N. B. Tufillaro, "A behavioral modeling approach to nonlinear model-order reduction for RF/microwave and systems," IEEE Trans. on Microwave Theory and Techniques, vol. 52, no. 9, pp. 2274–2284, 2004.

[58] A. S. Tehrani, H. Cao, S. Afsardoost, T. Eriksson, M. Isaksson, and C. Fager, "A comparative analysis of the complexity/accuracy tradeoff in power amplifier behavioral

models," IEEE Trans. on Microwave Theory and Techniques, vol. 58, no. 6, pp. 1510 – 1520, 2010.

[59] M. Isaksson, D. Wisell, and D. Ronnow, "A comparative analysis of behavioral models for RF power amplifiers," IEEE Trans. on Microwave Theory and Techniques, vol. 54, no. 1, pp. 348–359, 2006.

[60] T. Wang, "Compensation of nonlinear effects with memory in digital transmitters using a frequency domain identification method," M.S. Thesis, Dalhousie University, 2004.

[61] G. Baudoin, and P. Jardin, "Adaptive polynomial pre-distortion for linearization of power amplifiers in wireless communications and WLAN," Processdings of International Conference on Trends in Communications, pp. 157-160, Slovakia, 2001.

[62] S. Chang, J. Edward, and J. Chung, "A compensation scheme for nonlinear distortion in OFDM systems," Proceedings of IEEE Global Telecommunications Conference, San Francisco, pp. 736-740, 2000.

[63] A. Saleh and J. Salz, "Adaptive linearization of power amplifiers in digital radio systems," The Bell System Technical Journal, vol. 62, no.4 , pp. 1019-1033, 1983.

[64] F. Wang, A. Ojo, D. Kimball, P. M. Asbeck, and L. E. Larson, "Envelope tracking power amplifier with pre-distortion for WLAN 802.11 g," IEEE Microwave Symposuim Digest, pp. 1543–1546, 2004.

[65] J. Kim, C. Park, J. Moon, and B. Kim, "Analysis of adaptive digital feedback linearization techniques," IEEE Trans. on Circuits and Systems I: Regular Papers", vol.57, no. 2, pp. 345 –354, 2010.

[66] D. R. Morgan, Z. Ma, J. Kim, M. G. Zierdt, and J. Pastalan, "A generalized memory polynomial model for digital predistortion of RF power amplifiers," IEEE Trans. in Signal Processing, vol. 54, no. 10, pp.3852–3860, 2006.

[67] J. Kim and K. Konstantinou, "Digital predistortion of wideband signals based on power amplifier model with memory," Electronic Letters, vol. 37, no. 23, pp. 1417–1418, 2001.

[68] O. Hammi, S. Boumaiza, and F.M. Ghannouchi, "On the robustness of digital predistortion function synthesis and average power tracking for highly nonlinear power amplifiers," IEEE Trans. on Microwave Theory and Techniques, vol. 55, no. 6, pp. 1382 – 1389, 2007.

[69] C. Eun and E.J. Powers, "A new volterra predistorter based on the indirect learning architecture," IEEE Trans. on Signal Processing, vol. 45, no. 1, pp. 223 –227, 1997.

[70] A. Zhu, P. J. Draxler, H. Chin, T. J. Brazil, D. F. Kimball, and P. M. Asbeck, "Digital predistortion for envelope-tracking power amplifiers using decomposed piecewise Volterra series," IEEE Trans. on Microwave Theory and Techniques, vol. 56, no. 10, pp. 2237–2247, 2008.

[71] M. Schetzen, "Theory of pth-order inverses of nonlinear systems," IEEE Trans. on Circuits and Systems, vol. 23, no. 5, pp. 285 – 291, 1976.

[72] A. Zhu, P. J. Draxler, J. J. Yan, T. J. Brazil, D. F. Kimball, and P. M.Asbeck, "Open-loop digital predistorter for RF power amplifiers using dynamic deviation reduction-based Volterra series," IEEE Trans. on Microwave Theory and Techniques, vol. 56, no. 7, pp. 1524–1534, 2008.

[73] W. J. Jung, W. R. Kim, K. M. Kim, and K. B. Lee, "Digital predistorter using multiple lookup tables," Electronics Letters, vol. 39, no.19, pp. 1386–1388, 2003.

[74] G. Lazzarin, S. Pupolin and A. Sari, "Nonlinear compensation in digital radio systems," IEEE Trans. on Communications, vol. 42, pp. 988-999, 1994.

[75] G. Karam and H. Sari, "Data predistortion technique using interpolation," IEEE Trans. on Communications, vol. 38, pp. 1716-1723, 1990.

[76] H. Cao, H. M. Nemati, A. Soltani Tehrani, T. Eriksson, and C. Fager, "Digital predistortion for high efficiency power amplifier architectures using a dual-input modeling approach," IEEE Trans. on Microwave Theory and Techniques, vol. 60, no. 2, pp. 361–369, 2012.

[77] O. Hammi, M. Khalifa, A. Abdulahfiz, A. Kwan, A. Zerguine, and M. Sharawi, "A dual-input two-box model for digital predistortion of envelope tracking power amplifiers," IEEE Microwave and Wireless Components Letters, vol. 26, no. 5, pp. 361-363, 2016.

[78] D. Schreurs, M. O'Droma, A. A. Goacher, and M. Gadringer, "RF power amplifier behavioral modeling," Cambridge University Press, 2008.

[79] F. Ghannouchi, O. Hammi, and M. Helaoui, "Behavioral modeling and predistortion of wideband wireless transmitters", John Wiley, USA, 2015.

[80] Z. Ren, and H. Chen," Distortion-characteristic estimation predistorter for high efficiency power amplifiers," IET Signal Processing, vol. 10, no. 9, pp. 1024-1030, 2016.

[81] R. Marsalek, P. Jardin, and G. Baudoin, "From post-distortion to pre-distortion for power amplifiers linearization," IEEE Communications Letters, vol. 7, no. 7, pp. 308-310, 2003.

[82] T. M. Nguyen, J. Yoh, and C. H. Lee, "Modeling of HPA and HPA linearization through a predistorter: Global Broadcasting Service Applications," IEEE Trans. on Broadcasting, vol. 49, no. 2, pp. 132-141, 2003.

[83] K. Jang, H. Ryu, and S. Ryu, "Spectrum characteristics and predistortion gain in the nonlinear high-power amplifier (HPA)," Proceedings of International Conference on Information and Communication Technology Convergence, Jeju, pp. 931-934, 2017.

[84] L. Ding and G. T. Zhou, "Effects of even-order nonlinear terms on power amplifier modeling and predistortion linearization," IEEE Trans. on Vehicular Techniques, vol. 53, no. 1, pp. 156-162, 2004.

[85] G. P. White, A. G. Burr and T. Javornik, "Modelling of nonlinear distortion in broadband fixed wireless access systems," Electronics Letters, vol. 39, no. 8, pp. 686-687, 2003.